
[All ETDs from UAB](#)

[UAB Theses & Dissertations](#)

2009

Comparisons Between Behavioral and Electrophysiological Measures of Visual Function in Rodent Models of Retinal Degeneration

Glen R. Rubin
University Of Alabama At Birmingham

Follow this and additional works at: <https://digitalcommons.library.uab.edu/etd-collection>



Part of the [Optometry Commons](#)

Recommended Citation

Rubin, Glen R., "Comparisons Between Behavioral and Electrophysiological Measures of Visual Function in Rodent Models of Retinal Degeneration" (2009). *All ETDs from UAB*. 216.
<https://digitalcommons.library.uab.edu/etd-collection/216>

This content has been accepted for inclusion by an authorized administrator of the UAB Digital Commons, and is provided as a free open access item. All inquiries regarding this item or the UAB Digital Commons should be directed to the [UAB Libraries Office of Scholarly Communication](#).

COMPARISONS BETWEEN BEHAVIORAL AND ELECTROPHYSIOLOGICAL
MEASURES OF VISUAL FUNCTION IN RODENT MODELS OF RETINAL
DEGENERATION

by

Glen R Rubin

Timothy W Kraft, PhD, CHAIR
Clyde Guidry, PhD
Michael S Loop, PhD
Steven Pittler, PhD
Leo Semes, OD

A DISSERTATION

Submitted to the graduate faculty of The University of Alabama at Birmingham,
in partial fulfillment of the requirements for the degree of
Doctor of Philosophy

BIRMINGHAM, ALABAMA

2009

Comparisons Between Behavioral and Electrophysiological Measures of Visual Function in Rodent Models of Retinal Degeneration

Glen R Rubin

Vision Sciences Graduate Program

ABSTRACT

The critical flicker frequency (CFF) is the lowest frequency for which a flickering light appears steady. Measuring CFF indicates rod- and cone-driven function relative to light intensity. CFF can be measured by both electroretinogram (ERG) and behavior. We measured CFF in several rodent models of retinal degeneration in order to better characterize retinal degeneration and understand the functional implications of electrophysiological changes.

We measured ERG CFF in RCS dystrophic (RCS- p^+) and wild type (WT) rats at PN23, PN44, and PN64. ERG CFF data in RCS rats show significant early degeneration of the rods followed by cones. CFF was significantly lower at PN23. However, rod-driven CFF was more severely reduced. At PN44 there was no longer a discernable rod-cone break. By PN64 the rod driven CFF was immeasurable in the RCS rats. We measured a- and b-wave amplitudes to bright white flashes and ERG CFF in a β subunit GARP knockout (KO) mouse model (*Cngb1-x1*). At 1-month old KO mice exhibit a diminished dark-adapted b-wave and normal light-adapted b-wave compared to WT mice. Over the next 3 months, both dark- and light-adapted b-wave amplitudes declined, and the decline was greater for dark-adapted b-wave amplitudes. ERG CFF was lower for the KO mice at scotopic intensities, but normal at photopic intensities at one month of age. CFF values remained stable in the KO mice as the b-wave amplitudes

decreased with age. We measured a- and b-wave amplitudes to bright white flashes and CFF before and after a 10-day period of low-intensity (280 lux) light-damage in albino rats. Dark- and light adapted ERG responses were significantly reduced after light damage. The a-wave was permanently reduced, while b-wave amplitude recovered over 80% by R20. There was a small, but significant dip in scotopic ERG CFF at R6. Photopic behavioral CFF was slightly lower following light damage.

Retinal degeneration did not consistently reduce CFF. In general, ERG thresholds were better preserved than ERG maximum amplitudes. We found that CFF measured by ERG agreed with behavioral measures. The preservation of threshold responses that mediate behavior has positive implications for the clinic.

DEDICATION

To my family for their love and unfaltering support.

ACKNOWLEDGMENTS

I am grateful to Dr. Timothy Kraft for his mentoring and friendship. Thank you for teaching me to work and live by a higher standard. I would like to thank Dr. Loop for his co-mentoring and inspiring example of speaking truth to power. I want to thank my committee members, Dr. Clyde Guidry, Dr. Steven Pittler, Dr. Leo Semes for their input and careful proofing of this manuscript. I wish to thank Youwen Zhang for his friendship and collaboration. I thank YuQuan Wen for his prudent opinion on everything and all of his hard work on the light damage histology project. I want to thank Kristen Bowles for joining our lab and pursuing flicker research in human. Thank you Shanta Sarfare for our collaboration and stimulating scientific discussions. I thank Jerri Millican for building the water maze. Thank you Abi Yildirim for helping design the flicker electronics. Thank you Mark Bolding for providing all of the software fixes and consultation. Thank you Michael Risner for your short, but significant presence in our lab. Thanks to Ramona Hart for being a gem of a lady. And thank you Clifford Kennon whom I trusted instantly and always will.

TABLE OF CONTENTS

	<i>Page</i>
ABSTRACT	ii
DEDICATION	iv
ACKNOWLEDGMENTS	v
LIST OF TABLES	ix
LIST OF FIGURES	x
LIST OF ABBREVIATIONS	xii
INTRODUCTION	1
Retina	1
Overview.....	1
Phototransduction.....	1
Retinal Pigment Epithelium.....	5
Retinitis Pigmentosa.....	6
Electroretinogram	9
Components of the Electroretinogram	9
Isolated Rod or Cone ERG	12
Flicker ERG	15
Retinal Origins of the High Frequency Flicker Response.....	16
Psychophysics.....	19
Psychophysical Response to Flicker	19
Rodent Models of Retinal Degeneration.....	22
Royal College of Surgeon's Rat.....	22
Light Damage	26
Cngb1 Knockout Mouse.....	31
Hypothesis.....	35

MANUSCRIPT PREFACE.....	36
Manuscript 1: Flicker Assessment of Rod and Cone Function in a Model of Retinal Degeneration.....	37
Title Page	37
Abstract	38
Introduction	40
Materials and Methods	43
Results	47
Discussion	49
References	53
Figures.....	57
Tables.....	61
Manuscript 2: Age-Related ERG Changes in Cngb1-X1 Knockout Mice: Cone Survival.....	62
Title Page	62
Abstract	63
Introduction	65
Materials and Methods	68
Results	73
Discussion	77
References	80
Figures.....	84
Tables.....	91
Manuscript 3: Comparisons Between ERG and Behavioral CFF in a Light-Damaged Albino Rat.....	95
Title Page	95
Abstract	96
Introduction	98
Materials and Methods	101
Results	111
Discussion	115
References	120
Figures.....	125
Tables.....	133

DISCUSSION	134
Rod- Versus Cone-driven Flicker Response	134
Aim	134
Retinal Function in RCS Rat.....	134
Retinal Function in Cngb1 GARP Knockout Mouse.....	136
Retinal Function in A Light Damaged Albino Rat.....	139
Summary of ERG Findings.....	141
Behavioral Versus ERG CFF.....	142
 LIST OF REFERENCES	 146
 APPENDICES	
A PERMISSION LETTERS.....	165
B INSTITUTIONAL ANIMAL CARE AND USE COMMITTEE APPROVAL FORM	172

LIST OF TABLES

<i>Table</i>		<i>Page</i>
1	Photopic Versus Scotopic CFF.....	61
2	ERG Analysis PN30 Cngb Mice.....	91
3	$I_{1/2}$ Cngb1 b-wave amplitude.....	92
4	1- to 4-Month-Old Dark-Adapted b-wave.....	93
5	1- to 5-Month-Old Light-Adapted b-wave.....	94
6	Dark-Adapted ERG WT Versus LD.....	133

LIST OF FIGURES

<i>Figure</i>		<i>Page</i>
1	Diagram of the Eye.....	2
2	Illustration of the Retina.....	3
3	The Phototransduction Cascade.....	4
4	Retinal Pigment Epithelium.....	6
5	ERG Flash Response.....	9
6	Generators of the ERG.....	10
7	ERG Step Response.....	11
8	ERG Flicker Response.....	15
9	CFF Versus Wavelength.....	19
10	CNGC Channel Structure.....	33
11	ERG CFF Method.....	57
12	RCS Rat ERG CFF.....	58
13	RCS Rat Mean ERG CFF.....	59
14	Dodt and Echte CFF.....	60
15	Cngb1 Mouse Intensity-Response.....	84
16	Cngb1 Mouse b-wave.....	86
17	Cngb1 Mouse b-wave Ratio.....	87
18	Cngb1 Mouse b-wave Recovery.....	88

19	Cngb1 Mouse ERG CFF.....	90
20	Albino Rat Light Damaged Dark-Adapted ERG.....	125
21	Albino Rat Light Damaged Light-Adapted ERG.....	127
22	Albino Rat Light Damaged Intensity Response.....	128
23	Albino Rat Light Damaged OP Power.....	129
24	Albino Rat Light Damaged CFF.....	130
25	Albino Rat Light Damaged Histology.....	131
26	Albino Rat Light Damaged Retinal Thickness.....	132

LIST OF ABBREVIATIONS

APB	2-amino-4-phosphonobutyric acid
AIF	apoptosis-inducing factor
AAV	adeno-associated virus
AMD	age related macular degeneration
bFGF	basic fibroblast growth factor
cAMP	cyclic adenosine monophosphate
CaM	calmodulin
CFF	critical flicker frequency
CNTF	ciliary neurotrophic factor
CNG	cyclic nucleotide gated
Cngb1	cyclic nucleotide gated β subunit
CNGC	cyclic nucleotide gated cation channel
CRD	cone rod dystrophies
cGMP	cyclic guanosine monophosphate
DBC	depolarizing bipolar cells
ERG	electroretinogram
GARP	glutamic-acid-rich protein
Gas6	growth arrest-specific 6
GC	ganglion cell layer
GDNF	glial derived neurotrophic factor

Gnat1	guanine nucleotide binding protein, alpha transducing 1
HBC	hyperpolarizing bipolar cells
hFGF	human fibroblast growth factor
HT	heterozygote
I	intensity
INL	inner nuclear layer
IPL	inner plexiform layer
IR	intensity response
IS	inner segment
ISI	inter-stimulus interval
KO	knockout
LD	light damage
MERTK	c-met proto-oncogene tyrosine kinase
ND	neutral density
NMDA	N-methyl-D-aspartate
ONL	outer nuclear layer
OP	oscillatory potential
OPL	outer plexiform layer
OS	outer segment
PDA	piperidinedicarboxylic acid
PDE	phosphodiesterase
PDE*	activated phosphodiesterase
PEDF	pigment epithelium-derived factor

PN	post-natal day
R*	activated rhodopsin
R	recovery day
R _{max}	maximum response
RdCVF	rod-derived cone viability factor
RCS	royal college of surgeons
RCS-p ⁺	royal college of surgeons pigmented dystrophic
RK	rhodopsin kinase
RP	retinitis pigmentosa
RPE	retinal pigment epithelium
s	second
scot	scotopic
T	transducin
T*	activated transducin
td	trolland
TTX	tetrodotoxin
WT	wild type

INTRODUCTION

Retina

Overview

The neural process of seeing begins when light focused from the cornea and lens strikes the retina (Figure 1). The retina is a thin piece of neural tissue lining the back of the eye (Figure 2), remarkable for its highly ordered architecture and stratification. Mammalian retina measures in the range of several hundred microns thick varying by species and vasculature ¹. The retina contains 6 major neuronal cell classes: Photoreceptor, Horizontal, Bipolar, Amacrine, Ganglion, and interplexiform cells ². Each class consists of numerous types and subtypes ³. Cell bodies typically reside in the outer nuclear layer (ONL), inner nuclear layer (INL), or ganglion cell layer (GC). Chemical signaling between cells occurs in either the outer (OPL) or inner plexiform (IPL) layers. Cells also communicate by direct electrical coupling through gap junctions ⁴.

Phototransduction

Photoreceptor cell bodies reside in the outer nuclear layer (ONL). As their name photoreceptor implies, they are a class of receptor activated by light.

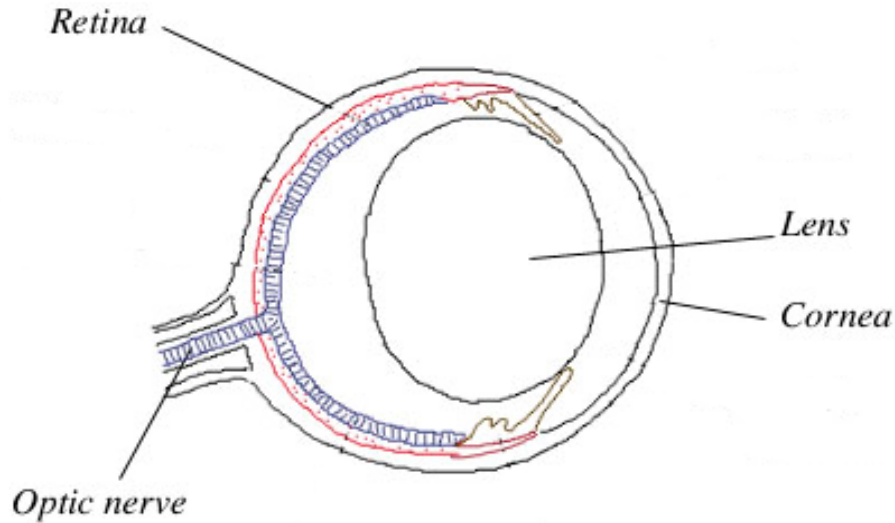


Figure 1. Annotated diagram of the rat eye. Entering light is focused by the transparent cornea and lens onto the retina. The retinal pigment epithelium forms a functional unit with the photoreceptors. Visual signals are transmitted along the optic nerve.

Note: From "The Rat's Eye's" by A. Hanson, <http://www.ratbehavior.org> Copyright 2003, 2004 Anne's Rat Page. Reprinted with permission.

Photoreceptors transduce the electromagnetic energy spectrum of visible light into electro-chemical nerve impulses of the retina, which are propagated to and understood by the brain as visual phenomena.

There are two types of photoreceptors, rods and cones. Rod and cones differ in morphology, visual pigment, response kinetics, and sensitivity⁵⁻⁸. These differences translate to a functional specialization. Rods are optimized for vision under dim or scotopic lighting. Cones mediate our high-acuity vision under bright

light and are also responsible for color vision. The phototransduction process has been studied extensively in rods.

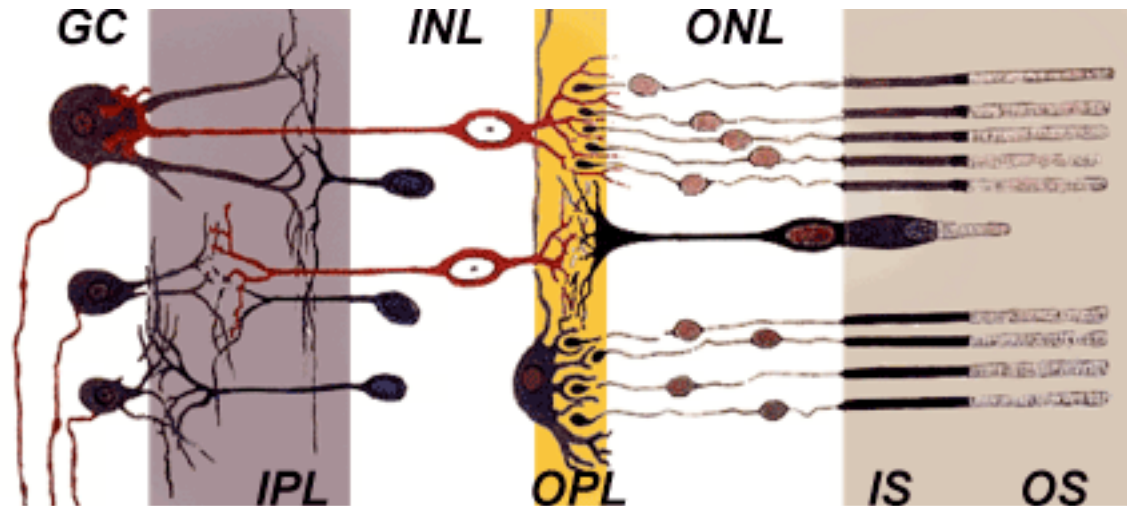


Figure 2. Illustration of the retinal layers. There are three nerve cell body layers and two synaptic layers. The photoreceptor cell bodies reside in the outer nuclear layer (ONL). Opsin molecules are manufactured in their inner segments (IS) and transported to the outer segments (OS), the site of phototransduction. Horizontal and bipolar cells in the inner nuclear layer (INL) communicate with photoreceptors in the outer plexiform layer. The visual signal is further processed by amacrine cells in the INL and ganglion cells in the ganglion cell layer (GC) before being transmitted along the optic nerve to the brain

Note: Adapted from a drawing by Ramon y Cajal⁹, 1911 Public Domain.

Phototransduction is initiated when a photon of light is absorbed by photosensitive visual pigment rhodopsin (Figure 3), embedded in the stacked membraneous disks of the rod photoreceptor's outer segments (OS). Rhodopsin consists of an opsin protein moiety covalently bound to 11-cis retinal via a Schiff base linkage¹⁰. The absorbed energy of a photon can produce a conformational change of 11-cis-retinal to the all-trans configuration. Activated rhodopsin (R*) catalyzes the exchange of bound GDP for cytosolic GTP on the alpha subunit of

the heterotrimeric $T\alpha\beta\gamma$ complex, releasing an active G Protein transducin^{11,12}. Activated transducin $T\alpha$ (T^*) in turn activates phosphodiesterase (PDE^*) by relieving inhibition from its $PDE\gamma$ subunit¹³. Activated phosphodiesterase (PDE^*) hydrolyzes cGMP to 5'-GMP¹⁴.

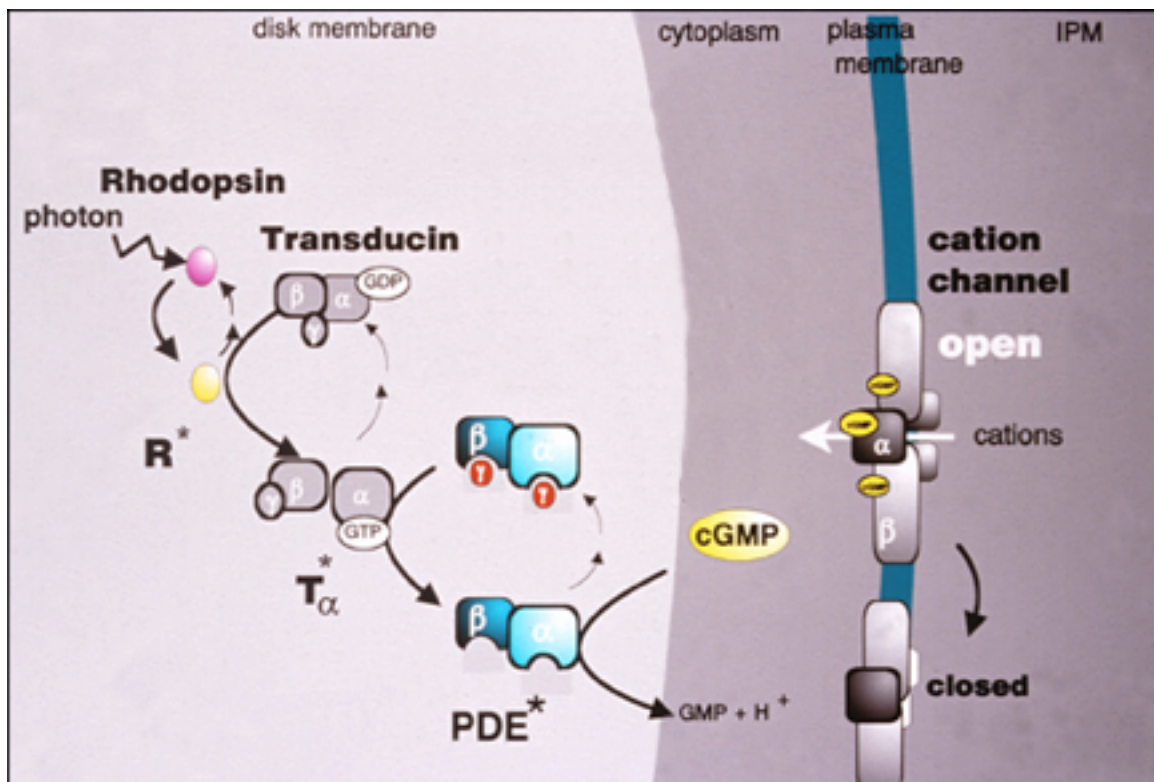


Figure 3 Photons of light initiate the phototransduction cascade. Activated Rhodopsin (R^*) turns on Transducin (T^*), which relieves the inhibition on Phosphodiesterase (PDE^*). PDE^* hydrolyzes cGMP leading to a closure of cyclic nucleotide gated ion channels

Note: From "Turned on by Ca^{2+} " by A. Polans, W. Baehr, & K. Palczewski¹⁵, Trends in Neurosciences, p. 549. Copyright 1996 Elsevier Limited. Reprinted with permission.

A decrease in cGMP concentration results in closure of cGMP-gated ion channels. Closing cGMP channels interrupts the inward flowing 'Dark Current', resulting in a hyperpolarization of the photoreceptors. This change in electrical potential spreads passively to the synaptic terminal, where it decreases glutamate release^{16, 17}. The visual signal is further processed by bipolar and ganglion cells in the retina before traveling out along the optic nerve to visual cortex in the brain.

Retinal Pigment Epithelium

Retina is arranged counter-intuitively with photoreceptor outer segments furthest away from incoming light, nestled next to the retinal pigment epithelium (RPE) and the choroidal vasculature. This seemingly inverted organization of the retina may be explained by the retina's high metabolic demands¹⁸. RPE plays an integral role in the visual process, forming a functional unit with the photoreceptors (Figure 4)¹⁹. RPE is a cuboidal monolayer of polar epithelium cells, which forms the blood-brain barrier between retina and choroid. The RPE shuttles ions and nutrients basally from the choroid to the photoreceptors through its apical processes. RPE removes photoreceptor waste including shed rod outer segments²⁰. Also of key importance is the recycling of all-trans-retinol into the photosensitive 11-cis configuration²¹. Mutations to RPE and or photoreceptors are primary causes of retinal degeneration (e.g. Retinitis Pigmentosa) and subsequent blindness.

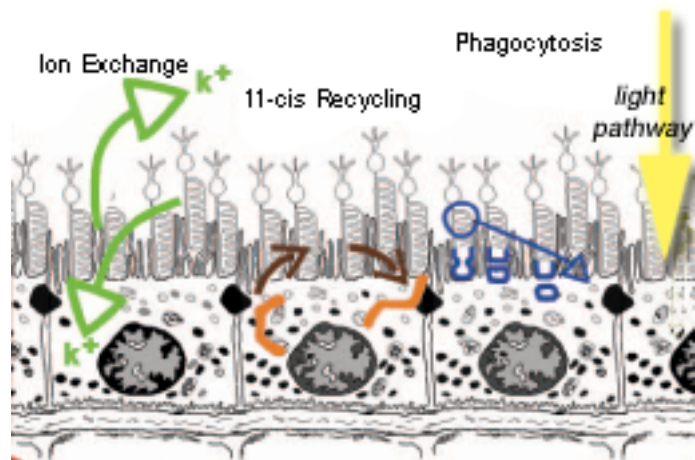


Figure 4 Retinal Pigment Epithelium (RPE) plays several key roles ensuring photoreceptor function. RPE helps maintain homeostatic ion balance, recycles 11-cis retinal, and phagocytosis shed rod outer segments

Note: Adapted from “The Retinal Pigment Epithelium in Visual Function” by O. Strauss¹⁹, *Physiological Reviews*, p. 846. Copyright 2005 by the American Physiological Society. Adapted with permission.

Retinitis Pigmentosa

Retinitis Pigmentosa (RP) is a heterogeneous group of inherited retinal degenerations affecting one in every 4000 individuals world-wide²². Over 100 genes have been implicated in the etiology of RP²²⁻²⁴, including mutations to choriocapilaris²⁵, RPE²⁶, and photoreceptor proteins²⁷. Although the causes of typical RP are diverse, degeneration follows a stereotyped pattern in which rods degenerate first; then cones. In RP it is highly unusual for cone degeneration to precede rod degeneration²⁸. Cone Rod Dystrophies (CRD) in which there is a primary or concomitant cone degeneration have an estimated prevalence of only

1 in 40,000²⁹. Cone degeneration impairs our important daytime visual function and eventually leads to blindness due to the cone photoreceptor's critical role in high acuity vision. A worthy goal that is being actively pursued is to prevent secondary cone degeneration in RP.

The precise mechanism leading to cone death during RP degeneration is unclear. There is evidence supporting a primary role for structural and biochemical changes in the degenerating retina^{27, 30-32}. Foremost, is the idea that rods secrete cone viability factors (Rod-derived Cone Viability Factors (RdCVFs))^{33, 34}. Studies have demonstrated increased cone survival when rod photoreceptors were transplanted³⁵ or co-cultured³⁶ alongside degenerate rd1 mouse retina.

Several endogenous factors that prevent photoreceptor degeneration have been isolated^{37, 38}. Pigment epithelium-derived factor (PEDF) inhibits retinal degeneration in rodents by inhibiting the nuclear translocation of apoptosis-inducing factor (AIF)³⁹. PEDF works in synergy when administered or co-expressed with human Fibroblast Growth Factor (hFGF)^{40, 41}. Intravitreal injections of fibroblast growth factor (bFGF) delays the onset of photoreceptor degeneration in RCS rats⁴². Adenovirus-mediated (AAV) gene transfer of Ciliary Neurotrophic Factor (CNTF) prevents morphological deterioration in rodent models⁴³⁻⁴⁶. Subretinal injections or AAV delivered Glial Derived Neurotrophic Factor (GDNF) also inhibits photoreceptor degeneration in rodent models^{47, 48}. Native rod factors RdCVF1 and RdCVF2 of the thioredoxin super family

demonstrate trophic cone cell activity^{38, 49}. Cone survival was significantly decreased in retinal explants deprived of either RdCVF1 or RdCVF2.

Trophic factors do not always produce a clear benefit. Administration of bFGF is implicated in the formation of dose dependent cataracts⁴². CNTF may impair ERG and visual function^{45, 46, 50-53}. Generally, it is not clear whether morphological and or electrophysiological improvements will yield real gains to vision. Comparisons between rod and cone based measures of electrophysiology, histology, and behavior may aid our understanding and our ability to assess the benefits of treatment.

Electroretinogram

Components of the Electroretinogram

The electroretinogram (ERG) represents the massed electrical activity of retinal neurons in response to light stimuli. ERG recordings to bright flashes of light (Figure 5) results in a waveform composed of an initial negative inflection (a-wave) followed by a positive deflection (b-wave).

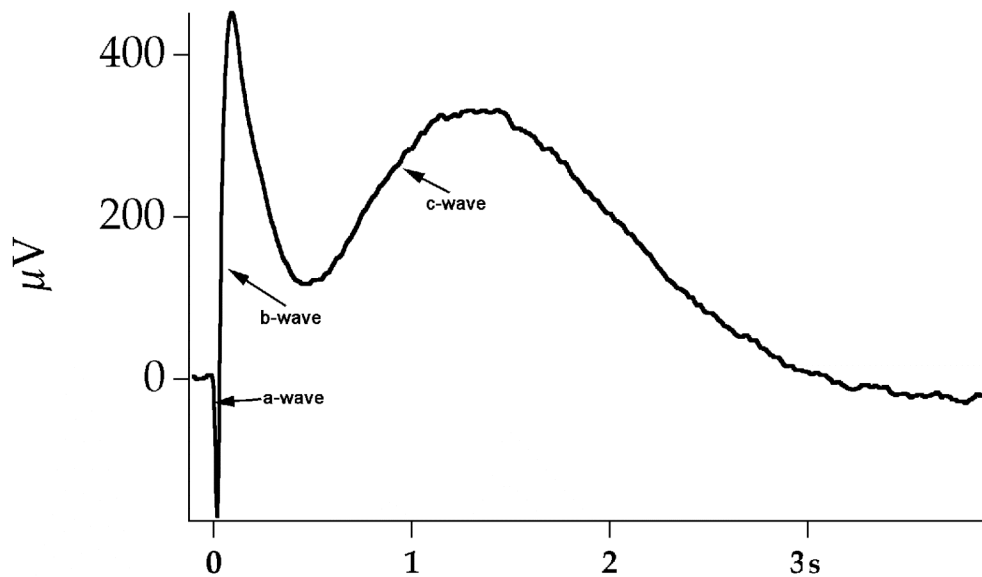


Figure 5 ERG recording in mouse. A bright 505 nm flash of 10 ms duration was delivered at 0s. The initial negative inflection known as the a-wave is followed by positive b- and c-waves.

Granit was first to attribute the appearance of standard features (a-wave, b-wave, etc...) in the ERG waveform to underlying physiological processes (PI – PIII) in the retina (Figure 6) ^{54, 55}.

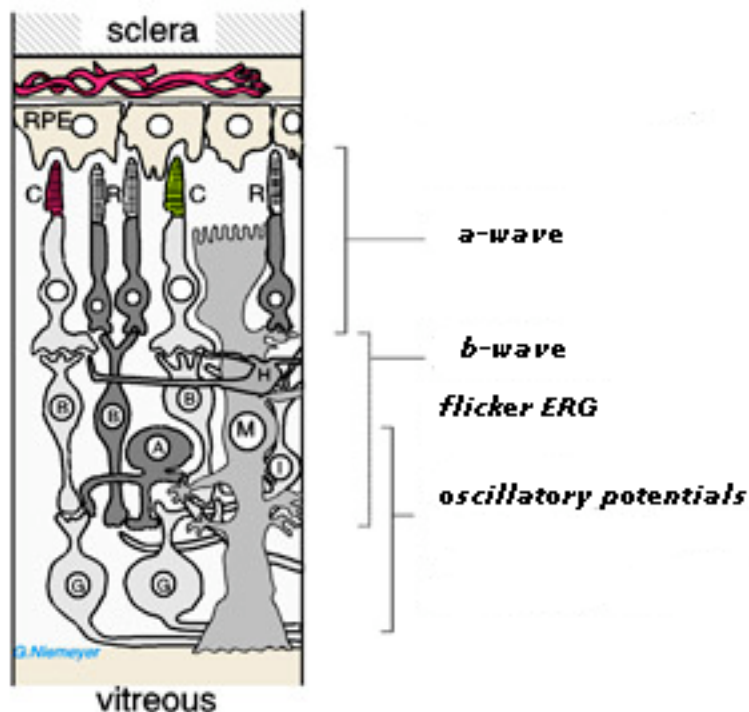


Figure 6. Generators of the ERG signal have been located at different retinal layers. The a-wave mainly reflects photoreceptor activity. The b-wave and flicker response is thought to come mostly from ON-bipolar cells. Oscillatory potentials come from inner retina.

Note: From “Making Diagnostic Use of the Electrical Events in the Retina” by G. Niemeyer, <http://www.thebalticeye.com> Copyright 2008 The Baltic Eye. Reprinted with permission.

Our contemporary understanding of the ERG waveform and its physiological significance has grown considerably. A negative PIII process underlying the ERG has been proposed to originate from photoreceptors and singularly contribute to the leading edge of the a-wave ⁵⁶⁻⁵⁹. Pharmacological

isolation of the positive PII process with analogs of glutamate reveals the principal responsibility of depolarizing ON-bipolar cells (DBC) for the b-wave ^{60,}

⁶¹. Similar pharmacological blocking demonstrates the Hyperpolarizing

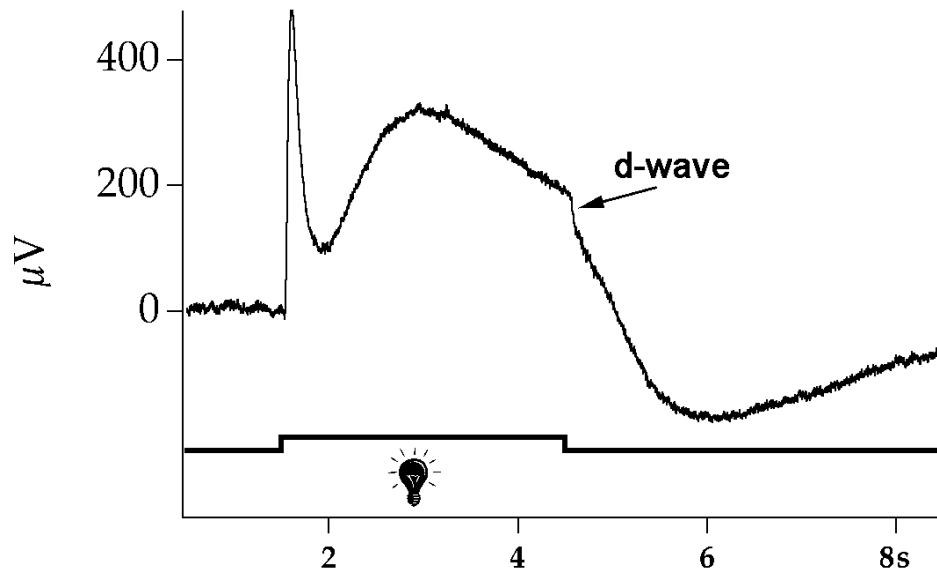


Figure 7 An ERG recording in mouse to a 3 second step of light shows the OFF response or d-wave. The d-wave is generated by OFF bipolar cells.

OFF-bipolar Cells (HBC) role in mediating an OFF response or d-wave (Figure 7) ^{62, 63}. Non-neuronal slow potentials elicited from RPE and Müller Glial cells are reflected in a positive going c-wave (figure 5), which follows the b-wave. The c-wave arises as a direct result of changes in the extracellular ion concentration of potassium due to phototransduction ⁶⁴⁻⁶⁷.

Oscillatory Potentials (OPs) are high frequency wavelets riding the ascending limb of the b-wave; they are a less obvious, but important component

of the ERG. The cellular origins of the OPs are unclear. They are thought to be generated by activity of the inner retina^{68, 69}. Intra-retinal ERG recordings in mudpuppy retina showed that the generators of individual OP wavelets are located increasingly distal to inner retina with respect to their timing⁷⁰. OP generators are believed distinct from the physiological processes giving rise to the b-wave⁷¹. However, their superimposition on the b-wave's leading edge affects the peak time and the amplitude of the b-wave⁷². Retinal degeneration can adversely affect OP timing and amplitude⁷³⁻⁷⁷. Oscillatory Potential analysis has been used in human studies to characterize damage to inner retina^{78, 79}.

Isolated Rod or Cone ERG

There are several commonly used techniques in electroretinography for generating isolated rod or cone pathway responses. The red minus blue subtraction^{80, 81} technique takes advantage of the differences between the spectral sensitivities of rod and cone photo-pigments in humans. Responses from spectral flashes are photopically matched and then subtracted in order to yield a pure rod or cone response. Rods have a spectral sensitivity peak at around 498 nm^{80, 82}, and are most sensitive to blue light. Dim blue flashes less than .85 log scot td s⁸³, only activate rod receptors. A longer wavelength red flash will yield a mixed rod and cone response. Middle and long wavelength cone receptor peak spectral sensitivity is between 521-575 nm⁸⁰ in primates including humans. The red flash intensity can be manipulated respective to rod spectral sensitivity so as to elicit a rod response equal to that of the shorter wavelength

dim blue flash. The two flashes arranged thus are defined as scotopically⁸¹ matched, since they differ in wavelength and intensity, yet elicit the same rod response. Computationally subtracting the rod only response from the mixed rod and cone response yields an isolated cone response. Similarly, an isolated rod response can be computed by subtracting the derived cone response from a photopically matched blue flash⁸¹. There are several drawbacks to deriving pure rod or cone responses from spectrally matched flashes. Degenerative changes to spectral sensitivity and response amplitude may alter the intensities required for generating scotopically and photopically matched flashes^{84,85}. Moreover, in rat the close proximity of maximum wavelength of absorption (λ_{\max}) between photo-pigments of the rods and cones⁸⁶ prohibits the procedure from being effectively employed. Finally, the spectral flash technique is limited over the intensity range in which a blue flash evokes a rod only response.

Photoreceptor activity can be independently measured with the ERG a-wave. Computational models predict the bio-kinetics of receptor response $R(j, t)$ as a function of time t after the presentation of a flash of energy I ^{57, 58}. Fitting these models to the leading edge of the a-wave demonstrates its receptor origins. While medium intensity scotopic flashes are effective for generating isolated rod activity, pure cone recordings must be obtained using photopically matched spectral flashes or a rod-desensitizing adapting field^{56, 87}. Theoretically an adapting stimulus should saturate the rods while minimally activating cones. Subsequent flashes will primarily reflect cone responses. Unfortunately, the a-

wave's leading edge embodies only a small portion, ca. 20 ms, of the total photoreceptor response.

The paired-flash technique is another method for generating isolated photoreceptor responses⁸⁸. In this paradigm, the recovery kinetics of the photoreceptors are analyzed by presenting an initial test flash followed by a higher intensity probe flash. Response amplitude at the time of the probe flash indicates the remaining photoreceptor current. By varying the inter-stimulus interval between these two flashes the remaining photoreceptor current can be determined at different times. This technique also allows for the faithful reconstruction of the single cell rod response. Isolated cone function can be ascertained using a similar protocol, but in conjunction with a rod adapting field⁸⁹.

These aforementioned techniques suffer from several drawbacks when attempting to measure the cone response. First, rod saturation cannot be complete without some activation of cone receptors as well. Second, the effects of rod adaptation upon the cones is unclear, in rat for example the photopic ERG grows with light adaptation⁹⁰. Finally, post receptor activity occurs far earlier after activation of cones than for rods⁸⁹.

An alternative double flash protocol generates pure cone responses by taking advantage of the differing temporal resolution of rods and cones^{91, 92}. Rod receptors are specialized for maximum sensitivity, responding with high gain. Part of the trade off for this high sensitivity is a low temporal resolution. When the inter-stimulus interval between two flashes is brief (1 s), the faster cone response

will have recovered while the relatively slower rods will still be saturated. The second probe flash will then mainly reflect cone pathway activity. Similarly, rod and cone response can be resolved by the flicker response.

Flicker ERG

ERG recordings to flicker yield a modulated response. As flicker frequency increases response amplitude decreases. The International Standard for Clinical Electrophysiology recommends using 30 Hz photopic flicker in humans in order to isolate cone function⁹³, since the rods are unable to follow flicker at this relatively high frequency⁹⁴.

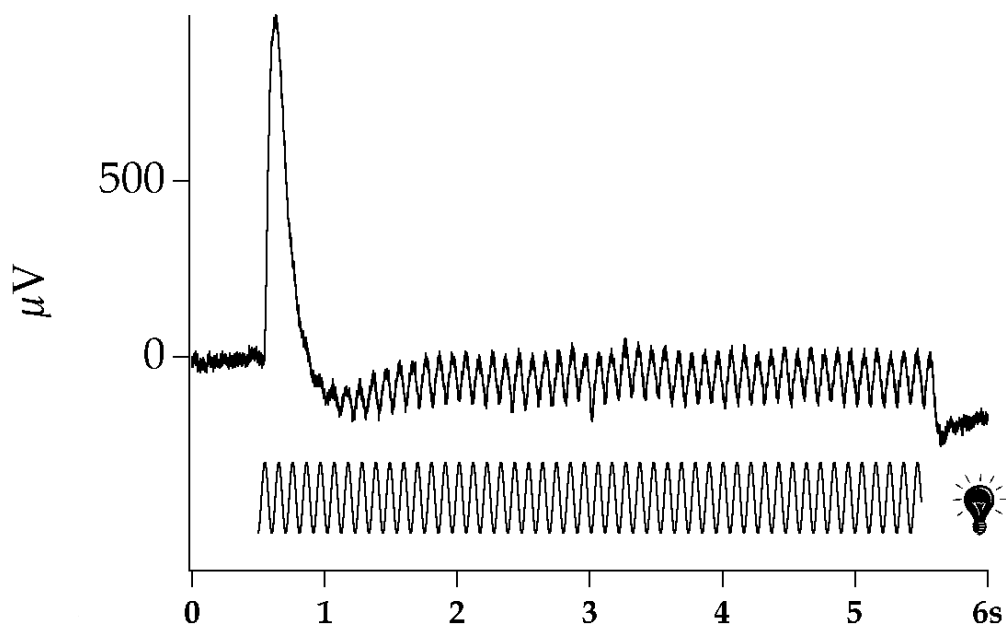


Figure 8 ERG recording in rat to 10 Hz flicker.

The threshold frequency at which a flickering light appears steady is known as the critical flicker frequency (CFF). Similarly, the stimulus frequency which causes a just detectable modulated response on the ERG is also known as the critical flicker frequency (CFF). The biochemical and biophysical kinetics of the photoreceptor response forms a ceiling of maximum temporal resolution. Since, cone receptors and their pathways have a greater temporal resolution than rods^{91, 92}, CFF is higher at photopic intensities. This yields a branched CFF curve for both psychophysical and electrophysiological measures of CFF as a function of light intensity.

Retinal Origins of the High Frequency Flicker Response

Early studies led researchers to believe in an outer retinal locus as the origin of the fast (high frequency) flicker ERG signal⁹⁵⁻¹⁰². Recent pharmacological studies in primate have called this idea into question, demonstrating a relatively minor photoreceptor contribution to the fast photopic flicker ERG. 2-amino-4-phosphonobutyric acid (APB) is a competitive agonist of sign-inverting glutamate receptors. APB is capable of blocking signal transmission to the depolarizing bipolar cell (DBC) ON-pathway¹⁰³. cis-2,3-Piperidinedicarboxylic acid (PDA) suppresses OFF-pathway responses by acting as an antagonist at sign conserving glutamate receptors on hyperpolarizing bipolar cells (HBC)¹⁰⁴. Using these glutamate analogs (APB & PDA) Bush and Sieving⁹⁴ were able to isolate the photoreceptor component of the ERG by selectively suppressing ON or OFF post-receptoral pathways. Their experiments

executed at photopic intensities revealed that the pharmacologically isolated cone photoreceptor response to 33 Hz flicker is relatively small. Rather, the majority of the response originated from ON/OFF bipolar pathways represented in the ERG b and d waves, respectively.

Expanding on this research, Kondo and Sieving¹⁰⁵ selectively suppressed ON/OFF pathways and recorded the flicker ERG at multiple temporal frequencies. Vector analysis of the flicker ERG fundamental confirmed a relatively small contribution of the isolated cone receptors for frequencies greater than 24 Hz. Furthermore, demonstrable differences in the phase response of ON and OFF pathways could be shown to determine the amplitude of the overall ERG. Interestingly, total destructive interference of ON and OFF pathways was seen at 10 Hz, revealing a signal equal in amplitude to that of the isolated cone response.

The relative contributions of HBC and DBC to the flicker ERG in murine retina are less clear. Krishna et al.¹⁰⁶ analyzed flicker ERG recordings in wild type and nob (no b-wave) knockout mice. The b-wave, which is purported to originate from the DBC^{60,61}, contributed less to high frequency flicker ERG recordings in mice than in primates.

Viswanathan, Frishman, and Robson¹⁰⁷ studied the contribution of spiking retinal neurons (ganglion, amacrine, and interplexiform layer cells) in macaque to the ERG. A series of experiments were conducted administering pharmacological block of action potentials with either tetrodotoxin (TTX) or N-methyl-D-aspartate (NMDA) alongside partial, full, or no blockage of ON/OFF

pathways using APB and PDA. Subsequent analysis showed contributions of spiking neurons to both fundamental and second harmonic amplitudes across a frequency range from 0.5-120 Hz. The contribution to the fundamental was demonstrated to be irregular across the frequency range and therefore theorized to be generated from multiple mechanisms. A more continuous contribution to the second harmonic across frequencies likely represents a single mechanism from spiking neurons.

The scotopic flicker ERG has not been subject to such a detailed analysis concerning the origin of its components. However, the identification of a branched rod function representative of fast and slow rod pathways has been identified ¹⁰⁸. The slower π_0 rod pathway is optimized for sensitivity at the expense of its temporal resolving power. The faster π'_0 rod pathway is thought to contribute at higher mesopic intensities. Destructive interference between these two pathways may be evident in humans as a scotopic flicker null present at 15 Hz ¹⁰⁹. The π'_0 rod pathway is usually masked by faster cone signals, especially under rod saturating photopic conditions. However, out of phase rod and cone pathways will interfere destructively, as evidenced by a mesopic flicker null reported at 7.5 Hz in humans ¹¹⁰.

Psychophysics

Psychophysical Response to Flicker

CFF is the frequency at which a modulated light varies between appearing steady or flickering. This relationship between CFF and light intensity is probably the most well known CFF phenomenon and has been described mathematically

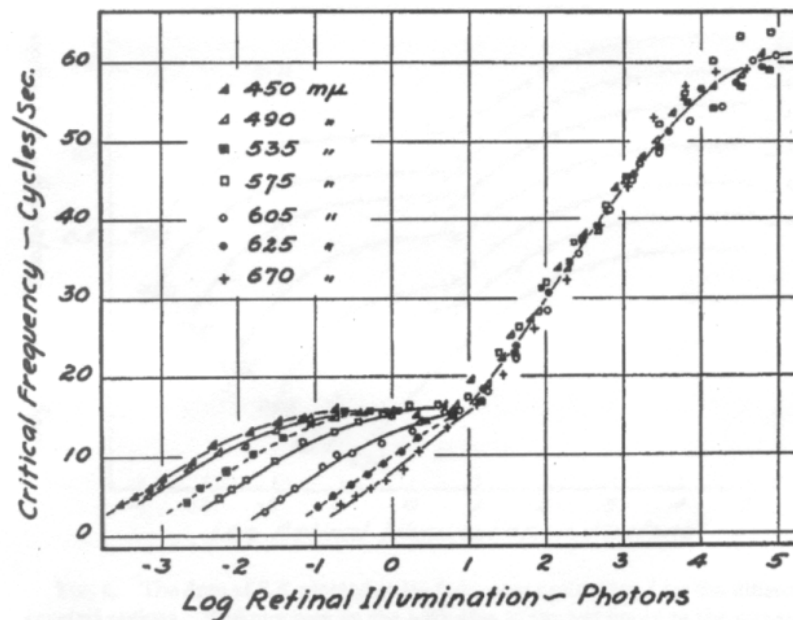


Figure 9 CFF as a function of intensity for various colors of light, Hecht and Schlaer (1936)¹¹¹

Note: From "Intermittent Stimulation by Light. VI." by S. Hecht and E. Smith, The Journal of General Physiology, p. 979-91. Copyright 1936 Hecht and Smith. Reprinted with permission.

by The Ferry-Porter Law ¹¹², which states that CFF increases directly with the logarithm of stimulus intensity.

The branched nature of the CFF curve reflects the retina's duplex nature and respective differences between rod and cone temporal resolution. Hecht and Schlaer ¹¹¹ demonstrated this intensity dependent function of rod and cone pathways in human by making psychophysical measurements of CFF (figure 9). In a first set of experiments the CFF curve was determined at increasing retinal eccentricities ¹¹¹. A flickering light confined to the fovea yields an unbranched sigmoidal curve. The retinal location and continuous nature of the data suggest a CFF curve mediated by only the cones. In order to confirm this, Hecht and Schlaer proceeded to determine the CFF curve for different wavelengths equated with respect to photopic spectral sensitivity ($V\lambda$). The results, seen in Figure 9, show a convergence of CFF curves at higher intensities, supporting the idea that cone receptors singularly mediate faster CFF values at higher intensities. Moreover, the disparate branches at lower intensities suggest that the rods, with a different spectral sensitivity, predominate to determine CFF at lower light intensities.

Factors such as color, size, and shape of a flickering stimulus also affect CFF values ¹¹³. Wavelength of the stimulus affects CFF due to the spectral sensitivities of the rod and cone receptors, as seen in figure 9. The shape of the stimulus waveform (square, sine, sawtooth, etc) has negligible affect with respect to the wave's fundamental fourier component. Psychophysical and electrophysiological experiments have found comparable results for both square

and sine waveforms of the same fundamental frequency upon which CFF is based^{114, 115}.

Detecting flicker or a change in light intensity ultimately depends on the temporal resolving power of the visual system. If the temporal frequency of a stimulus exceeds the ability of the visual system to integrate information over time, then rapid fluctuations of intensity will not be perceived. As such, CFF is a measure of temporal resolution informing us of the smallest perceivable temporal discrimination the visual system can make.

Rodent Models of Retinal Degeneration

Royal College of Surgeon's Rat

Animal models provide an important means for studying retinal degeneration. Rats are of great utility owing to their prolific nature and the availability of genetically homogeneous strains. Characterizing rat models of retinal degeneration is typically accomplished by monitoring both functional and morphological changes to the retina in comparison with normal development of wild type animals. This type of research has important implications for our understanding of the retinal machinery as well as possibly hastening the development of therapeutic treatments for degenerative conditions ²⁸.

The Royal College of Surgeon's (RCS) rat was the first known rat model to have an inherited retinal degeneration. The dystrophy was brought to the attention of Bourne et al. in 1938, due to the co-morbid presentation of a cataractous condition in the original pink-eyed piebald agouti strain (*Rattus Norvegicus*). Bourne et al. noted the "striking resemblance which the histologic picture in certain stages of the development of this lesion bears to the microscopic appearance described in certain cases of retinitis pigmentosa" ¹¹⁶.

The RCS rat is a model of choice for studying RP and has been extensively characterized. In RCS rat, degeneration is due to the failure of RPE to phagocytose shed outer segments ¹¹⁷⁻¹²⁰. The outer segments accumulate in

the subretinal space forming a cytotoxic debris zone¹²¹. Rod photoreceptors die by apoptosis¹²², however the exact events triggering cell death are unknown¹²³⁻¹²⁵. The debris zone may interfere¹²⁶ with diffusion of metabolites¹²⁷ or oxygen¹²⁸. As is typical in RP, cones degenerate secondarily to rods.

The inability of RPE to phagocytose outer segment material has been traced to a recessive mutation in c-mer proto-oncogene tyrosine kinase receptor gene (MERTK)^{129, 130}. Specifically, a frameshift mutation causes a truncation of the mer protein. This interferes with the recognition of the growth arrest-specific 6 (Gas 6) ligand, necessary for the phagocytosis signaling pathway¹³¹. An orthologous mutation in humans will manifest as RP, similarly arresting the RPE phagocytosis pathway²⁶ and ultimately resulting in blindness. The genotype and associated disorder is present in albino as well as pigmented rat strains^{127, 132}.

A seminal study in 1962 by Dowling and Sidman characterized the biochemical, functional, and histological changes in the degenerating RCS rat retina¹²¹. Starting as early as post-natal day (PN) 12 they noted an abnormally thick OS layer. At PN22 the inner segments begin to shrink up and photoreceptors start to degenerate. The OS layer continues to grow until PN27. At about this age rhodopsin content of the retina reaches a maximum, over twice that of control animals. By PN40 ONL is reduced to a couple of rows and inner segments are completely missing. At PN60 degeneration is nearly complete. Few photoreceptors remain and rhodopsin content has fallen precipitously. The pigment epithelium is disorganized and some of the cells have migrated from the monolayer.

In RCS rats, ERG recordings by Dowling and Sidman ¹²¹ show a slightly raised threshold as early as PN18, followed by depression of the a-wave at PN22, and reduced b-wave amplitudes by PN32. Other early ERG recordings ¹³³ showed a detectable difference in maximum b-wave amplitude as early as PN20. These early results are consistent with more recent findings ¹³⁴, which show a rapid decrease in a-wave and b-wave amplitude after PN35. Psychophysical experiments ¹³⁵ confirm an elevated threshold response for RCS rats between PN 35 to PN60.

Double Flash technique ¹³⁶, aimed at isolating rod or cone pathway responses, indicate that rod pathway function is impaired as early as PN18 with continuing degeneration after PN21 ¹³⁷. However, in the same study isolated response of the cone b-wave remains normal until PN42. Cone pathway function in RCS rats was also studied by recording ERG responses to flicker at one mean luminance ¹³⁸. In this flicker study, cone function exhibited signs of dysfunction as early as PN28.

A number of behavioral studies have investigated loss of visual function in the RCS rat. These studies show functional declines that depend on the type of visual processing demanded by the behavioral task. Visual function is better preserved for those tasks that require integration over large areas of the retina in contrast to an early loss of high resolution acuity. In this respect, even elder RCS rats appear to retain some rudimentary visual capacity. Conditioned suppression studies aimed at training RCS rats to detect a bright light signal using foot shock, found RCS rats competent to detect a light signal at as old as 2

years, a point at which only a few stray photoreceptors remain¹³⁹. Trejo and Cicerone¹⁴⁰ carried out similar conditioned suppression studies, which showed a decline in the RCS rat dark adapted threshold response of about 0.5 log units per month beginning 4 months postnatally. Water maze experiments have also been used to gauge the visual function of the RCS rat. In this type of experiment, the rat is trained to associate a light stimulus with an escape platform, taking advantage of the rat's aversion to drowning^{141, 142}. Performance time is used as an indicator of functional deficit. In water maze experiments RCS rats took significantly longer to find an escape platform than wild type. However, RCS rats' performance times were stable for the first six months after which they rapidly increased¹⁴³. Interestingly, this decrease in visual function in RCS rats is happening at a time in which there is little change in photoreceptor populations. Other behavioral evidence for a crude and lingering visual capacity in the RCS rat stems from pupilometric studies¹⁴⁴ as well as the rat's preserved photophobia¹⁴⁵.

Behavioral studies on younger RCS rats, confirm a reduced dark-adapted threshold, which remains stable between PN36 and PN103¹³⁵. Reflex modification studies however, show the failure of a pre-light stimulus to inhibit the RCS rat's startle reflex as early as PN100. Visual acuity studies show a similar precipitous early decline in visual function. RCS rats lose the ability to head-track gratings as large as 0.5 cyc/deg as early as 8 weeks of age¹⁴⁶. A separate water maze study determined RCS spatial resolution acuity to be 80% of wild type at 1 month with dramatic decreases thereafter¹⁴⁷.

Light Damage

Light inflicted damage is a commonly used method for studying retinal degeneration¹⁴⁸⁻¹⁵¹. There are many advantages to using this model. Genetic models like RCS may suffer from functional changes not associated with the primary defect. For example, RCS rats are generally smaller in weight and size. It is unknown what impact these changes to the body and possibly other unapparent corollary changes, stemming from loss of Merck function, might have on retinal degeneration. Similarly, mutations in other genetic models of retinal degeneration may have confounding variables such as synaptic remodeling¹⁵². In the light damage model however, by manipulating simple stimulus parameters such as stimulus intensity, wavelength, and duration of exposure we can precisely control the magnitude of the effect. Moreover, the extent of damage can be consistently reproduced.

Non-thermal photochemical damage of the retina can be broadly classified broadly into Class I or II type damage¹⁵³⁻¹⁵⁵. Our experiments will investigate the degenerative changes that result from Class I type damage. Briefly, however, Class II or Ham type damage from high intensity light was originally demonstrated in primate retina. Ham et al. found that by irradiating small patches of retina in anaesthetized monkey's they could preferentially damage photoreceptors or RPE^{156, 157} depending on wavelength. Gorgles and van Norren¹⁵³ confirmed Ham's spectral classification by examining the effect of wavelength on threshold intensity for light damage in albino rat¹⁵³. Rats

exposed to light in the (320-440) UV range suffered photoreceptor damage, while those exposed to light in the 470-550 nm range, suffered both photoreceptor and RPE damage.

Class I damage results from long exposures (> 12 hrs) at relatively moderate intensities over large areas of the retina in freely roaming animals. Photoreceptors are predominantly affected, however varying degrees of RPE damage will result depending on experimental conditions. Noell et al. discovered this class of retinal damage in albino rats after prolonged exposure to ordinary fluorescent light bulbs¹⁵⁸. In a series of experiments (for review see¹⁵⁹), Noell et al. exposed freely roaming albino rats to low intensity (130-270 lux) filtered green fluorescent light. The resemblance of the action spectrum of this light to rhodopsin's absorption spectrum suggested a role for rhodopsin or one of its bleach products in mediating photo-toxicity^{158, 160}. Grimm et al.¹⁶¹ demonstrated preservation of rod inner segments in young rhodopsin deficient mice after light damage confirming rhodopsin's primary role in mediating light-induced photoreceptor apoptosis.

The degenerative changes post-exposure noted by Noell et al.¹⁵⁹ affected photoreceptor and RPE cell layers. However, damage to photoreceptors compared with RPE could be enhanced by reductions in light intensity. Rapp and Williams¹⁶² confirmed this in experiments using only 65 lux. Additionally using filtered blue light appears to effectively target photoreceptors over RPE cells¹⁶³. Noell et al.¹⁵⁹ found they could maximize photoreceptor death with relative sparing of the RPE by using younger 20 day-old dark-reared albino rats.

These rats also exhibited an extended period of ERG recovery, which results in an abnormally high a-/b-wave ratio 2-3 months after light damage. Both the age and 'light history' of an animal have proved to be variables of consequence when implementing light damage.

Ballowitz and Dammrich ¹⁶⁴ determined that rats exposed to continuous fluorescent light from birth suffered less damage to their retinas than adult rats given equivalent exposures. O'Steen et al. ¹⁶⁵ compared the vulnerability of various aged groups of albino rats to high intensity (3,780 lux) brief duration (< 24 hrs) exposures. Adult rats (16-24 weeks) were the most susceptible to damage, in contrast to younger rats (< 5 weeks), which did not appear vulnerable. Organisciak et al. confirmed the greater vulnerability of older animals to light damage by exposing different aged groups of albino rats to 1500 lux for a 24 hour period. However, this disparity was eliminated if animals were dark-reared. Noell et al. also showed that rats reared or maintained in constant darkness prior to exposure exhibit greater vulnerability to light damage ¹⁶⁶. Animals raised in cyclic light are afforded greater protection from light damage due to the upregulation of several antioxidative agents ¹⁶⁷.

There is some controversy over whether rod or cone function is more severely impaired by light damage. Early studies found remaining visual function in rats apparently devoid of rods. In a series of light-dark discrimination studies, Bennett et al. exposed albino rats to fluorescent light between 200-400 lux, as measured from the cage floor, for up to 200 days ¹⁶⁸⁻¹⁷⁰. Typical performance on a task discriminating an illuminated from dark reward chamber was significantly

above chance, even in rats where rod photoreceptor loss was apparently complete. In concurrent studies O'Steen & Anderson had similar results regarding the spatial resolution of light damaged rats^{171, 172}. In this set of experiments albino rats were exposed to fluorescent light, which reflected from the cage floor measured 194 lux or 760 lux directly¹⁶⁸. Rod photoreceptors were undetectable after only 30 days of exposure. However, rats were unimpaired on their ability to make black-white and pattern discriminations.

Following this mantle of work led researchers to believe that a number of undetected and more resilient cone cells were mediating the remaining function. In a series of histological assays conducted to determine nuclear morphology and cell type by heterochromatin staining, La Vail showed a greater percentage of cones surviving light damage than rods¹⁷³. In one experiment, 7 week-old Fischer albino rats were exposed to 700 lux, measured from cage floor, for 54 days. The percentage of cones in posterior sections of the retina increased from 1.5 to 21.8%. In the peripheral retina the percentage of cones increased from 1.5 to 10.3%. The percentage of surviving cones increased to roughly 60% when the time of exposure was extended beyond 178 days.

Using the ERG, Cicerone measured the dark-adaptation curve in light damaged albino rats¹⁷⁴. Rats were first exposed to 1080 lux, measured at cage floor, for up to 24 hours and then dark adapted for 24 hours before ERG testing. She found the rod branch of the dark adaptation curve was significantly raised while the cone branch was relatively unaltered.

The characterization of the rods as more vulnerable than cones to light damage is not consistent throughout the literature. Experiments on pigeons by Marshall, et al. indicate the contrary^{175, 176}. Birds exposed to 3000 lux for a 24-hour period showed preferential cone degeneration. A lower threshold for cone damage has been confirmed in monkeys^{177, 178}. Skyes, et al. found the threshold for cone damage after 12 hours of exposure was in a range of 5,900 and 10,800 lux, whereas the threshold for rod damaged occurred between 10,800 and 19,400 lux. These alternative findings may be due the relatively high exposure intensities and inter-species variability. However, Williams et al. demonstrated a greater decline of photopic function in albino rats by determining their thresholds for seeing flicker¹⁷⁹. After learning to discriminate a flickering stimulus, adult rats were then exposed to 700 +/- 140 lux for 8 days. Plotting CFF as a function of light intensity for the light damaged rats yielded curves, which seemed to reflect rod driven activity.

In another ERG study detailing the changes to both rod and cone pathways 8 week old albino rats were exposed to between 1000-3000 lux for up to 48 hours¹⁸⁰. ERG measures taken one week post-exposure show significant reductions to light- and dark-adapted b-wave amplitudes as well as threshold responses.

There are several factors, which may account for the discrepancy between rod and cone vulnerability. Hao, et al. recently demonstrated at least two biochemically distinct apoptotic pathways active in light damage. After exposing guanine nucleotide binding protein, alpha transducing 1 (*Gnat1*^{-/-}) knockout mice

to bright light, 1700 lux, for seven days they were able to show damage that was independent of transducin activation or downstream events. In contrast, prolonged exposure to a dim light of 20 lux engendered degenerative changes that required transducin activity. The relative damage to rods or cones from these forms of apoptosis has not been quantified. Alternatively, ERG recordings may be detecting a relatively greater amplification of the cone signal. Comparisons between ERG and histology have been made on albino rats that were exposed to 2000 lux for up to 48 hours⁷³. This study indicated that photopic log b-wave amplitudes decline twice as much per cone lost than scotopic log b-wave amplitudes declines per rod lost. Finally, there is some evidence that the relative vulnerability of scotopic and photopic systems is dependent on an animals' history of exposure before damage¹⁸¹. Rod photoreceptors in dark reared animals are more vulnerable to light damage.

Cngb1 Knockout Mouse

The mouse has hugely benefited our understanding of vertebrate genetics. Extensive knowledge of the mouse genome enables “precise engineering of DNA sequence alterations that can be passed stably to offspring and analyzed genetically at the level of the whole organism”¹⁸². This is particularly useful in vision science research where single mutations are known to cause RP. Transgenic mice targeting proteins of the cyclic nucleotide gated (CNG) channel have been developed¹⁸³⁻¹⁸⁶.

CNG channels reside on the plasma membrane of photoreceptor outer segments (OS). Changes in CNG channel conductance triggered by concentration change in cGMP binding are essential to phototransduction. The rod photoreceptor cyclic nucleotide gated cation channel (CNGC1) is composed of α and β subunits (Figure 10) occurring with a stoichiometry of $3\alpha: 1\beta$ ¹⁸⁷. The gene locus of the β subunit (CNGB1) consists of 33 exons¹⁸⁸. The β subunit is distinguished by a glutamic-acid-rich protein (GARP) region at its N-terminal third¹⁸⁹. Alternative splicing of CNGB1 gives rise to two shorter soluble forms of GARP¹⁹⁰. GARP-1 encoded by exons 1-16 exists in extremely low concentrations. This has impeded investigations into GARP-1 function. A shorter GARP-2 encoded by exons 1-12 also exists. It has been determined that GARP-2 binds to phosphodiesterase (PDE6), possibly helping to stabilize the PDEy inhibitory complex in the dark¹⁹¹. The β subunit GARP region and the soluble GARP proteins both interact with peripherin-2 oligomers at the rim region of rod photoreceptor disk membranes. This interaction suggests a structural role for GARP in connecting OS disks and the CNGC channel to the plasma membrane¹⁹².

Two separate β subunit knockout mice with Retinitis Pigmentosa type degeneration were recently developed *Cngb1-x26* with exon 26 deletion¹⁸³ and *Cvgb1-x1* with promoter region and exons 1 and 2 deletion¹⁸⁶. In *Cngb1-x26* knockout expression of the soluble GARP proteins are unaffected.

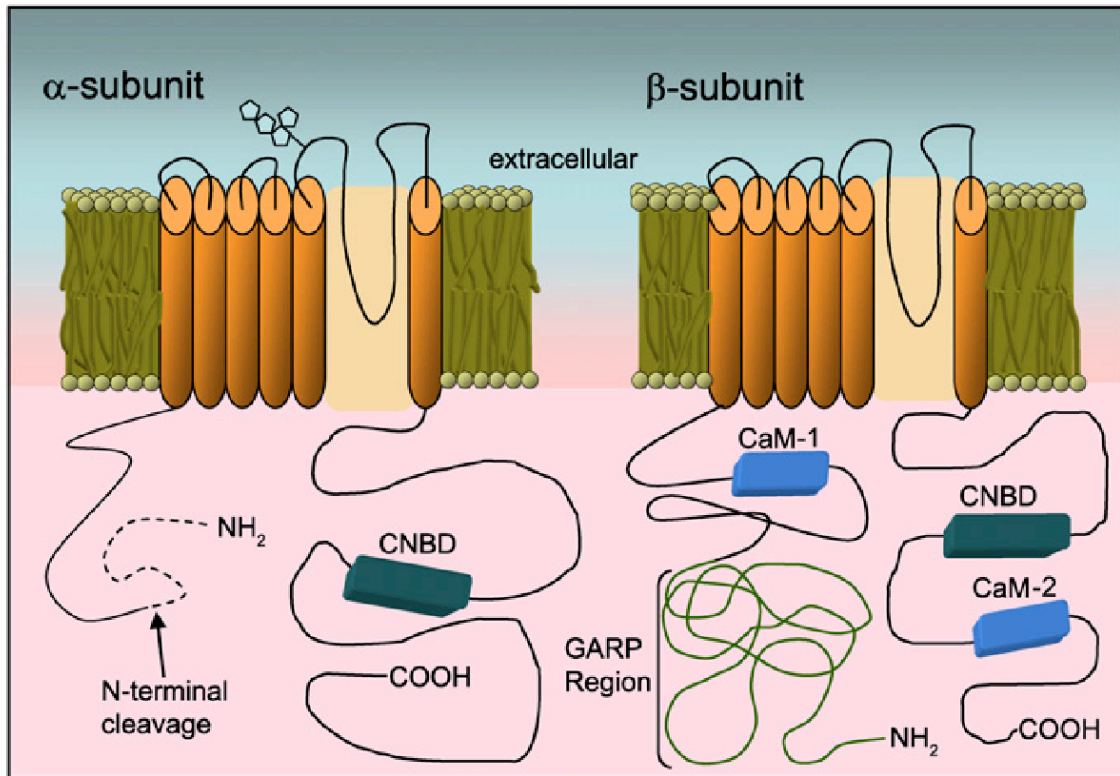


Figure 10 CNGC channels are composed of alpha and beta subunits. Both subunits consist of six trans-membrane spanning domains with a poor-loop region situated between domains 5 and 6. Cyclic nucleotide binding domain (CNBD) is also present in each subunit. The β subunit has an unusual bipartite structure consisting of N-terminal glutamic-acid-rich protein (GARP) region and a C-terminal channel like region. The modulatory Ca^{2+} /CaM binding domains are unique to the beta subunit.

Note: From “Focus on Molecules: Rod photoreceptor cGMP-gated cation channel” by S. Sarfare and S. Pittler¹⁹⁰, Experimental Eye Research, p. 174. Copyright 2007 Elsevier Limited. Reprinted with permission.

Homomeric α subunit ion channels form in heterologous expression systems. However α subunit expression is reduced in both knockout models. And the expression level of α subunits in *Cngb1-x26* mice is apparently much lower than that in *Cngb1-x1* mice. The morphology of one month-old rod photoreceptors is relatively more healthy in *Cngb1-x26* mice than that in *Cngb1-*

x1 mice, the single cell's response is more diminished in the former than in the latter, implying a distinctive role of GARPs in the photoresponse. A fuller characterization of the *Cngb1-x1* mouse will help to more clearly elucidate the role of GARP in disease pathogenesis and may provide a means to stabilize photoreceptor structural integrity.

Hypothesis

In typical RP there is primary rod degeneration followed by cone loss. Therapies aimed at stemming secondary cone degeneration have been considered an important alternative to outright cures. Such an approach requires an accurate assessment of rod- versus cone-driven visual function. Cone function can be isolated by using the 30 Hz photopic flicker response, since rods are unable to follow flicker at this frequency^{94, 95}. In this manner CFF should also isolate rod- versus cone-driven visual function. Our hypothesis is that rod- and cone-driven visual function can be accurately assessed by ERG or behavioral measures of CFF.

We tested this hypothesis by addressing the following questions:

1. Do these measures reflect rod and cone degeneration evident in traditional flash ERG measures in rodent models of retinal degeneration?
2. Will compensatory changes in b-wave response amplitude be reflected in CFF values?
3. What ERG criterion generates a CFF measure that corresponds to behavioral CFF?
4. How does the progression of retinal degeneration affect the relationship between ERG and behavioral CFF?

MANUSCRIPT PREFACE

The following chapters of this dissertation contain three separate manuscripts that together encompass our research into ERG and flicker evaluation of rod and cone function in degenerating retinas. In our first article, 'Flicker Assessment of Rod and Cone Function in a Model of Retinal Degeneration' ¹⁹³ (published 2007), we describe a method for measuring ERG CFF in the RCS rat, a model of inherited retinal degeneration. The second article, 'Age-Related ERG Changes in Cngb1-X1 Knockout Mouse: Cone Survival' (in submission), was a collaborative effort made with Drs. Steven Pittler and Youwen Zhang. In this study we applied our method for measuring ERG CFF to a new transgenic Cngb1 knockout mouse. Finally, in the third article, 'Comparisons Between ERG and Behavioral CFF in a Light-Damaged Albino Rat', we undertook a comparison of ERG CFF to psychophysically measured CFF in an albino rat light damage model of degeneration. We are making the final revision and it should be submitted prior to the defense. The reference collection for an individual manuscript is given following the text of that manuscript. And there is a global reference section at the end of the thesis whose numbering system refers to the numbers used in the introduction and discussion chapters.

Flicker Assessment of Rod and Cone Function in a Model of Retinal
Degeneration

by

GLEN R. RUBIN, TIMOTHY W. KRAFT

Documenta Ophthalmologica 2007;115:165-172

Copyright
2007
by
Springer

Used by permission

Format adapted for dissertation

Abstract

Critical flicker frequency (CFF) is the lowest frequency for which a flickering light is indistinguishable from a non-flickering light of the same mean luminance. CFF is related to light intensity, with cone photoreceptors capable of achieving higher CFF than rods. A contemporaneous measure of rod and cone function can facilitate characterization of a retinal degeneration. We used sinusoidal flicker ERG to obtain CFF values, over a wide range of light intensities, in RCS dystrophic (RCS-p⁺) and wild type rats. Recordings were made at PN23, PN44, and PN64. The CFF curve in control animals increased in proportion to the log of stimulus intensity, with a gentle slope over the lowest 4 log-unit intensity range. The slope of the CFF curve dramatically increased for higher intensities, indicating a rod-cone break. In the RCS rats the rod driven CFF was significantly lower in amplitude compared to normal rats at the earliest age tested (PN23). By PN64 the rod driven CFF was immeasurable in the RCS rats. The amplitude of the cone driven CFF approached normal values at PN23, but was greatly reduced by PN44. By PN64 the entire CFF function was greatly depressed and there was no longer a discernable rod-cone break. These CFF/ERG data show that RCS rats exhibit significant early degeneration of the rods, followed soon after by degeneration of the cones. Using this approach, rod and cone function

can be independently accessed using flicker ERG by testing at a few select intensities.

Introduction

Inherited retinal degeneration disorders, resulting from defects of the photoreceptors (retinitis pigmentosa / RP) or retinal pigment epithelium (age related macular degeneration / AMD), are a leading cause of blindness¹⁻⁴. Initial loss of rod function is subsequently followed by a more debilitating loss of cone function^{5,6}. This two staged loss of photoreceptors proceeds even when the precipitating defect is associated with only rod physiological processes, suggesting that cones need rods to survive.

The relationship between rod and cone function during retinal degeneration has been studied in Royal College of Surgeons (RCS) rats using a double flash technique⁷. Rod function was estimated by subtracting the cone based electroretinogram (ERG) response to the second flash from the mixed rod and cone response to the first flash. Cone function alone has also been studied in RCS rats,⁸ by using high frequency flicker leaving rod function to be inferred from other data. Obtaining isolated measures of rod or cone function in rat is challenging due to the proximity of their respective photopigments⁹. We have used a method that allows contemporaneous, and isolated, assessment of both rod and cone function using the ERG to better follow the functional relationship between rods and cones. We have applied this technique in the RCS rat, a widely used model of retinal degeneration^{10,11}.

Critical flicker frequency (CFF) is the lowest frequency at which a flickering light appears steady. The relationship between CFF responses and stimulus intensity has been described mathematically by the Ferry-Porter Law, the diffusion model, and the cascaded integrator model functions¹². The rise in CFF with increasing background light reflects underlying activity of the neural retina. The biochemical and biophysical kinetics of the photoreceptor response forms the envelope of temporal resolution.

Pharmacological studies in primate demonstrate a predominant bipolar cell contribution to flicker ERG recordings at high frequencies^{13, 14}. By selectively suppressing ON/OFF pathways, Kondo and Sieving¹⁴ showed a relatively minor contribution from the photoreceptors to the overall ERG at frequencies greater than 24 Hz; suggesting that the bipolar cell response kinetics may establish a new envelope (or ceiling) of maximum temporal resolution. Accordingly, ERG amplitudes at high frequencies could be accounted for by phase differences between depolarizing ON (DBC) and hyperpolarizing OFF (HBC) bipolar cell pathways. The relative contributions of HBC and DBC to the flicker ERG in murine retina are less clear. Krishna et al.¹⁵ analyzed flicker ERG recordings in wild type and nob (no b-wave) knockout mice. The b-wave, which is purported to originate from the DBC^{16, 17}, contributed less to high frequency flicker ERG recordings in mice than in primates.

ERG recordings to sinusoidal flicker yield a modulated response, which follows the stimulus. As flicker frequency increases the response amplitude decreases. CFF/ERG is considered to be the frequency at which the response is

unmodulated and comparable to that of the noise level for a light of the same mean intensity. Previous studies have shown sensitivity of phasic ganglion cells to luminance flicker in macaque that is comparable to results obtained from humans using psychophysical threshold measurements¹⁸. In humans, two studies found CFF/ERG to be higher than psychophysical CFF^{19,20}, however the reverse has been reported in dog²¹. Both psychophysical²² and ERG electrophysiological²³ measurements display a prominent rod/cone break, indicating the relationship between CFF and stimulus intensity. We have used these CFF/intensity functions to follow the degeneration of both rods and cones in RCS rats compared to very stable CFF/intensity functions in wild type rats measured over the same ages. While our studies have thoroughly investigated CFF versus intensity, one can easily imagine a much shorter test with limited stimulus intensities for quickly measuring rod- and cone- driven CFF.

Materials and Methods

All animals were handled according to the principles of the ARVO Statement for the Use of Animals in Ophthalmic and Vision Research. Pigmented RCS rats were studied as an RP model, in comparison to Long Evans wild type rats in order to assess rod and cone function. Animals were maintained under cyclic 12-hour light/dark conditions. Illumination was provided by fluorescent lighting (mean luminance = 140 lux). Throughout the paper wild type refers to normal Long Evans rats. ERG recordings were made postnatal (PN) at PN23 (n = 11), PN44 (n = 12), and PN64 (n = 12) (+/- 1 day).

Rats were dark-adapted for at least 4 hours prior to anesthesia. Rats were sedated with 3% isoflurane in a chamber and then anesthetized via intraperitoneal injection of xylazine (9.09 mg/kg) and ketamine (90.9 mg/kg). Corneas were anesthetized with proparacaine (0.5%) and pupils dilated with topical phenylephrine HCl (2.5%) and tropicamide (1%). Only the eye to receive light stimuli was dilated.

During recordings the rat was placed in a Faraday cage with head fixed by a bite-bar and body temperature maintained at 38°C by a heating pad (Braintree Scientific, Braintree, MA). The light source was a 100-W tungsten-halogen lamp focused onto one end of a fiber optic. A shutter with 6-mm aperture (Uniblitz; Vincent Associates, Rochester, NY) set stimulation duration for 6 seconds. A

second ferro-electric liquid crystal shutter (LV050; Displaytech, Longmont, CO) produced flicker by sinusoidally modulating the stimulus. An optical power meter (Graseby Optronics, Orlando, FL) was used to measure the energy output at the level of the cornea on every experimental day. Average Michelson contrast of the flicker stimulus was .86, Stdev = \pm .017

Full-field ERGs were recorded using one of two different diameter recording electrodes, 2 mm and 4 mm, depending on the size of the animal²⁴. These consisted of a platinum wire loop embedded in the tapered end of a Plexiglas rod that had been hollowed out to receive the fiber optic. This arrangement was designed to ensure a constant distance between the fiber optic and the eye. The tapered end also acted as a diffusing element, yielding an isotropic plane of illumination at the pupil²⁴. The reference electrode was a second platinum loop in contact with the non-stimulated eye. Methylcellulose (Goniosol, CIBA Vision Corp, Duluth, GA) was applied to both eyes as well as to the recording and reference corneal electrodes. The recording electrode was placed on the left eye and the reference electrode was affixed to the right eye. The amplifier (Astro-med CP122W; Grass Telefactor, W. Warwick, RI) was set to DC. Responses were amplified 2000X and low-pass filtered at 300 Hz. The ERG voltage and stimulus-monitor signals were digitized with hardware (MIO16) and software (LabView) from National Instruments (Austin, TX).

Stimulus strength was controlled by a set of calibrated inconel neutral-density filters that allowed attenuation in steps of approximately 0.3 log units up to a maximum of 6.9 log units attenuation. After CFF was determined for a given

attenuation, light intensity was incrementally raised. Minor variations in energy output between experimental days, due primarily to use of either the 4 mm or 2 mm electrode, was insignificant compared to the wide range of light intensities tested. A three-cavity interference filter (Andover Co., Salem, NH) set the wavelength of the stimulus at 505 nm (35 nm bandwidth).

IGOR PRO (Wavemetrics Inc, Lake Oswego, OR) was used for analyzing data and generating figures. Experimental runs for each temporal frequency contain a total of 24 000 points, representing 6 seconds of recording at a sampling rate of 0.25 ms/pt. The shutter was closed for the initial and final 500 ms, thus 5 seconds of light exposure containing between 5 and 200 repeated cycles of the sinusoidal stimulus drove the retinal response. The following stimulus frequencies were used: 1, 2, 4, 5, 10, 16, 20, 25, 32, and 40Hz. The response was approximately sinusoidal mirroring the stimulus (Fig 11a pg 57).

An average response wave of one or two cycles was generated from the repeated stimulus cycles. By using a constant stimulus duration of 5 seconds, the number of averaged cycles increased directly with frequency. The first 0.5 s was ignored to avoid the transient caused by the stimulus onset (Fig 11). So, for a 2 Hz stimulus frequency 9 cycles were averaged, while for a 20 Hz stimulus 90 cycles were averaged. Response amplitude remained stable throughout the presentation of the stimulus. For large amplitude responses, there was less than 5% difference between the response amplitude measured early (0-1 sec) or late (4-5 sec).

The average response was fitted with a sine wave in order to measure the

response amplitude (μV) (Fig 11b). Direct peak to trough amplitude measurements were occasionally made for the lowest frequency and highest intensity, since these responses did not always conform well to a sinusoid. A line was fitted to the \log_{10} of the response amplitudes starting from the peak of the monotonic decline, which typically occurred at 1 or 2 Hz. A $3\mu\text{V}$ criterion voltage point was used to define the electrophysiological CFF (Fig 11c).

Results

The shape of the CFF versus intensity curves obtained from 23-day-old PN23 Long-Evans (wild type, PN23) rats can be seen in Figure 12a (open circles pg 58).

CFF increased with a gentle slope over an intensity range from 1 to 40 000 photons/ μm^2 , while at higher light intensities the slope of the CFF curve increased dramatically. The general shape and position of the CFF curves did not vary greatly as the wild type rats matured (Fig 12b, c, open circles).

However, CFF curves of the oldest PN64 (Fig 12c, open circles) animals differed slightly with the development of a mesopic notch²⁵ around the rod-cone break, where CFF decreased slightly.

At the earliest age, PN23, the rod driven CFF values for all RCS rats were lower than all wild type (Fig 12a, filled circles). Across the lower 3 log units of stimulation CFF of RCS rats grew from 13 – 25 Hz, in contrast to wild type values, which ranged between 18 – 34 Hz over the same intensity range. CFF values of RCS rats were approximately 25% lower than wild type on average over this scotopic range of light intensities. The rod-cone break occurred at roughly the same mean light intensity of 40 000 photons/ μm^2 for both RCS and wild type. At this stimulus intensity, CFF values of RCS rats were on average 30% lower than wild type CFF. At the higher light intensities cone driven CFF

values for RCS differ less in magnitude and rose with a slope similar to wild type.

By PN44 RCS rats (Fig 12b, filled circles) suffered a loss of the lowest 1.5 log units of the rod response range. Also lacking was a clearly discernible rod-cone break. CFF values for cone driven light intensities were on average 45% lower in RCS at PN44. RCS rats of this age exhibited the greatest variability of CFF values. At PN64 (Fig 12c, filled circles), CFF values for RCS rats were generally the lowest at all light intensities, however there is some overlap between the best PN64 CFF values and the worst PN44 values. Figure 13 (pg 59) shows the range of values obtained for all ages of wild type rats (grey area = mean \pm STDEV) in comparison to the mean (\pm STDEV) for the RCS rats at PN23 (filled circles), PN44 (open triangles), and PN64 (filled squares).

Discussion

Several early ERG papers²⁶⁻²⁸ exploring the mechanisms of dark adaptation, evaluated rat CFF as a function of light intensity. These early rat studies established a typical branched CFF curve as a function of stimulus intensity. However, of these previous rat CFF studies, only Dodt and Echte's curves²⁶ were well defined, having numerous CFF values determined over a wide range of stimulus intensities. Their results are compared to our wild type PN64 rats' CFF curves in Figure 14 (pg 60). Our wild type rat's function has been shifted down by 17 Hz to align with Dodt and Echte's. The shapes of these two curves are in close agreement at mesopic and higher intensities. However, over the dimmest scotopic range of intensities there is a marked difference in curve shape, ours declining more. This difference is perhaps the result of the steady state recording conditions employed by Dodt and Echte. In their experiment separate lights were used for producing flicker and pre-adaptation to the mean luminance level. The higher CFF values achieved in our experiments may also be attributable to our use of an averaging program and/or lower criterion of response compared to Dodt and Echte's unspecified criterion.

In RCS rats, ERG recordings by Dowling and Sidman¹⁰ first revealed slight changes as early as PN18, followed by depression of the a-wave at PN22, and reduced b-wave amplitudes by PN32. Other early ERG recordings²⁹

showed a detectable difference in maximum b-wave amplitude as early as PN20. These early studies used pink-eyed or albino RCS rats ³⁰, which are known to deteriorate anatomically at a faster rate than black-eyed RCS rats ³¹.

Recent experiments with pigmented RCS also demonstrate early declines in the ERG; Bush et al. ³² found a rapid decrease in a- and b-wave amplitudes after PN35. Double Flash technique ³³, aimed at isolating rod or cone pathway responses, indicate that rod pathway function is impaired as early PN18 with marked degeneration after PN21 ⁷. However, in the same study isolated response of the cone b-wave remains normal until PN42. Cone pathway function in RCS rats was also studied by recording ERG responses to flicker at one mean luminance ⁸. In this flicker study, cone function exhibited signs of dysfunction as early as PN28. Our flicker results over a broad range of light intensities show abnormality in cone driven function of pigmented RCS rats as early as PN23. We did not follow maximum a- and b-wave amplitudes in our animals, in parallel with CFF measures.

Our CFF measures indicate rod and cone degeneration as early as PN23. As seen in Table 1 (pg 61), average CFF values for a scotopic range of intensities ($3.25 - 3.6 \times 10^4$ Photons/ μm^2) are significantly lower (66% of wild type) than wild type ($p < .001$; one-tailed two sample student's t-test assuming equal variance). While average CFF values approach normal (84% of wild type) for the photopic range ($1.79 - 1.98 \times 10^6$ Photons/ μm^2), values are still significantly lower ($p < .05$). The slight cone degeneration at PN23 is a novel finding, which lends weight to CFF as an extraordinarily sensitive measure of retinal function.

However, the CFF values of individual RCS rats and wild type animals did overlap at this age, suggesting variable degeneration in individual animals.

The degenerative condition of an individual could be quantified by comparisons to a baseline of normal performance from a normative database. For example, $\text{Baseline} = \text{Avg} - (2 * \text{STDEV})$; (e.g. $\text{Baseline} = 51.0 - 9.4 = 41.6$ Hz). Table 1 demonstrates the validity of obtaining CFF measures at singular scotopic and photopic intensities. This would suffice for the determination contemporaneous rod and cone function while simplifying the already easy CFF procedure. Moreover, scotopic values can be measured in dim light foregoing the need for a prolonged period in absolute darkness. In any event, our results showing considerable rod pathway degeneration as early as PN23 and considerable cone pathway degeneration at PN44 are comparable with those yielded by the double flash technique.

CFF is a measure of retinal function sensitive to differences in the temporal resolution of rods and cones and their postsynaptic pathways. Unlike the a-wave, which is a direct measure of photoreceptor activity, an altered flicker response may reflect changes postsynaptic to photoreceptors as has been demonstrated previously. Immunocytochemistry has shown differences between RCS rats and wild type when staining for horizontal and bipolar cell markers as early as PN 21³⁴. In vitro recordings from RCS rat horizontal cells have also indicated early abnormalities of the dopaminergic pathway³⁵.

Producing flicker requires specialized equipment, but flicker ERG can be compared to psychophysically obtained CFF. Maximum ERG responses do not

have a simple behavioral equivalent for comparison. Testing the ability of the retina to track a modulated stimulus may also serve to indicate if there are difficulties in sustained function due to biochemical changes in phototransduction or the postsynaptic circuitry. In the RCS rat for example, kinetics of rhodopsin regeneration is severely slowed³⁶ and could overtime alter scotopic flicker sensitivity.

Past ERG studies involving CFF have largely focused on isolating cone function. Pinilla et al.³⁷ examined the homozygous P23H RP model rat using photopic flicker produced by a xenon strobe flash. Changes to CFF were commensurate with decreases in maximum response amplitude and increases to the threshold of scotopic and photopic b-waves. In this model the a-wave is the most severely affected ERG parameter.

An increased threshold for detecting flicker at specific frequencies under mesopic conditions has been demonstrated by human psychophysics²⁵. This flicker null has been explained as the destructive interference between out of phase rod and cone signals. The development of a mesopic notch at PN64 in wild type rats may be attributable to similar mechanisms.

Our analysis demonstrates that CFF is an effective method for evaluating rod function as well. While phase was not determined in our study this information may yield other significant insights in to the underlying pathological dynamics of the disease process. Finally, knowing relative rod and cone function better informs us of the window of opportunity in which it is reasonable to perform a therapeutic intervention aimed at cone survival.

References

1. Boughman JA, Conneally PM, Nance WE. Population genetic studies of retinitis pigmentosa. *Am J Hum Genet* 1980;32:223-235.
2. Bourla DH, Young TA. Age-related macular degeneration: a practical approach to a challenging disease. *J Am Geriatr Soc* 2006;54:1130-1135.
3. Hartong DT, Berson EL, Dryja TP. Retinitis pigmentosa. *Lancet* 2006;368:1795-1809.
4. de Jong PT. Age-related macular degeneration. *N Engl J Med* 2006;355:1474-1485.
5. Chader GJ. Animal models in research on retinal degenerations: past progress and future hope. *Vision Res* 2002;42:393-399.
6. Delyfer MN, Leveillard T, Mohand-Said S, Hicks D, Picaud S, Sahel JA. Inherited retinal degenerations: therapeutic prospects. *Biol Cell* 2004;96:261-269.
7. Pinilla I, Lund RD, Sauve Y. Contribution of rod and cone pathways to the dark-adapted electroretinogram (ERG) b-wave following retinal degeneration in RCS rats. *Vision Res* 2004;44:2467-2474.
8. Pinilla I, Lund RD, Sauve Y. Cone function studied with flicker electroretinogram during progressive retinal degeneration in RCS rats. *Exp Eye Res* 2005;80:51-59.
9. Neitz J, Jacobs GH. Reexamination of spectral mechanisms in the rat (*Rattus norvegicus*). *J Comp Psychol* 1986;100:21-29.

10. Dowling JE, Sidman RL. Inherited retinal dystrophy in the rat. *J Cell Biol* 1962;14:73-109.
11. Arnhold S, Heiduschka P, Klein H, et al. Adenovirally Transduced Bone Marrow Stromal Cells Differentiate into Pigment Epithelial Cells and Induce Rescue Effects in RCS Rats. *Invest Ophthalmol Vis Sci* 2006;47:4121-4129.
12. Corwin TR, Dunlap WP. The shape of the high frequency flicker sensitivity curve. *Vision Res* 1987;27:2119-2123.
13. Bush RA, Sieving PA. Inner retinal contributions to the primate photopic fast flicker electroretinogram. *J Opt Soc Am A Opt Image Sci Vis* 1996;13:557-565.
14. Kondo M, Sieving PA. Primate photopic sine-wave flicker ERG: vector modeling analysis of component origins using glutamate analogs. *Invest Ophthalmol Vis Sci* 2001;42:305-312.
15. Krishna VR, Alexander KR, Peachey NS. Temporal properties of the mouse cone electroretinogram. *J Neurophysiol* 2002;87:42-48.
16. Robson JG, Frishman LJ. Response linearity and kinetics of the cat retina: the bipolar cell component of the dark-adapted electroretinogram. *Vis Neurosci* 1995;12:837-850.
17. Hood DC, Birch DG. Beta wave of the scotopic (rod) electroretinogram as a measure of the activity of human on-bipolar cells. *J Opt Soc Am A Opt Image Sci Vis* 1996;13:623-633.
18. Lee BB, Martin PR, Valberg A. Sensitivity of macaque retinal ganglion cells to chromatic and luminance flicker. *J Physiol* 1989;414:223-243.
19. Sokol S, Riggs LA. Electrical and psychophysical responses of the human visual system to periodic variation of luminance. *Invest Ophthalmol* 1971;10:171-180.

20. Van Der Tweel L. Relation between psychophysics and electrophysiology of flicker. *Documenta ophthalmologica* 1964;18:287-304.
21. Coile DC, Pollitz CH, Smith JC. Behavioral determination of critical flicker fusion in dogs. *Physiol Behav* 1989;45:1087-1092.
22. Hecht S, Smith EL. Intermittent stimulation by light. VI. Area and the relation between critical frequency and intensity. *J Gen Physiol* 1936;19:979-991.
23. Dodt E, Wirth A. Differentiation between rods and cones by flicker electroretinography in pigeon and guinea pig. *Acta Physiol Scand* 1953;30:80-89.
24. Lyubarsky AL, Pugh EN, Jr. Recovery phase of the murine rod photoresponse reconstructed from electroretinographic recordings. *J Neurosci* 1996;16:563-571.
25. Sharpe LT, Stockman A, MacLeod DI. Rod flicker perception: scotopic duality, phase lags and destructive interference. *Vision Res* 1989;29:1539-1559.
26. Dodt E, Echte K. Dark and light adaptation in pigmented and white rat as measured by electroretinogram threshold. *J Neurophysiol* 1961;24:427-445.
27. Dowling JE. Visual adaptation: its mechanism. *Science* 1967;157:584-585.
28. Green DG. Light adaptation in the rat retina: evidence for two receptor mechanisms. *Science* 1971;174:598-600.
29. Noell WK. Cellular Physiology of the Retina. *Journal of the Optical Society of America* 1963;53:36-48.
30. LaVail MM, Sidman RL, Gerhardt CO. Congenic strains of RCS rats with inherited retinal dystrophy. *J Hered* 1975;66:242-244.

31. LaVail MM, Battelle BA. Influence of eye pigmentation and light deprivation on inherited retinal dystrophy in the rat. *Exp Eye Res* 1975;21:167-192.
32. Bush RA, Hawks KW, Sieving PA. Preservation of inner retinal responses in the aged Royal College of Surgeons rat. Evidence against glutamate excitotoxicity in photoreceptor degeneration. *Invest Ophthalmol Vis Sci* 1995;36:2054-2062.
33. Birch DG, Hood DC, Nusinowitz S, Pepperberg DR. Abnormal activation and inactivation mechanisms of rod transduction in patients with autosomal dominant retinitis pigmentosa and the pro-23-his mutation. *Invest Ophthalmol Vis Sci* 1995;36:1603-1614.
34. Cuenca N, Pinilla I, Sauve Y, Lund R. Early changes in synaptic connectivity following progressive photoreceptor degeneration in RCS rats. *Eur J Neurosci* 2005;22:1057-1072.
35. Hankins M, Ikeda H. Early abnormalities of retinal dopamine pathways in rats with hereditary retinal dystrophy. *Doc Ophthalmol* 1994;86:325-334.
36. Perlman I. Kinetics of bleaching and regeneration of rhodopsin in abnormal (RCS) and normal albino rats in vivo. *J Physiol* 1978;278:141-159.
37. Pinilla I, Lund RD, Sauve Y. Enhanced cone dysfunction in rats homozygous for the P23H rhodopsin mutation. *Neurosci Lett* 2005;382:16-21.

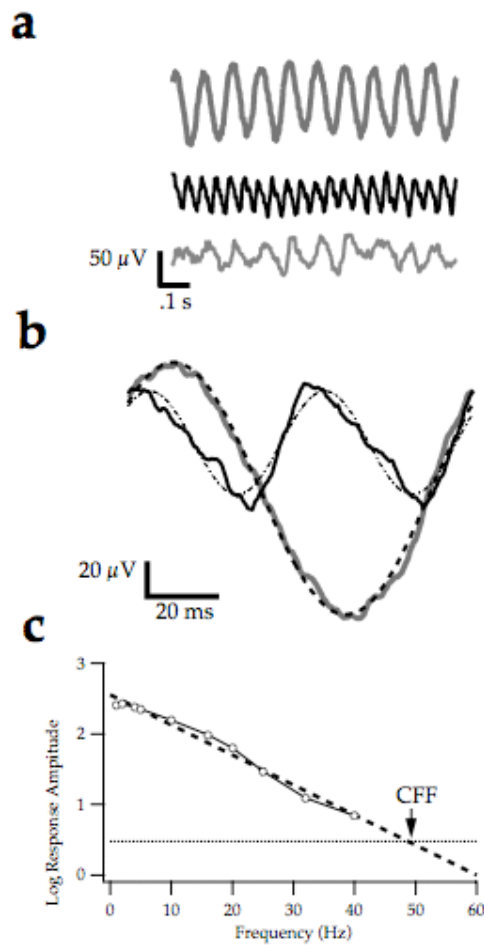


Figure 11. (a) One second of ERG data recorded in wild type rat to sinusoidal flicker at 10 Hz (top grey trace) and 20 Hz (black trace) and in RCS rat at 10 Hz (bottom grey trace) ($1.8\text{-}2.0 \times 10^6$ Photons/ μm^2). (b) A computer algorithm computes the averaged one or two cycle response. The best fit sine-wave (dotted lines) was used for quantifying the response amplitude. (c) Log of the response amplitudes are plotted and a best fitting line is used to determine CFF for a criterion response of $3 \mu\text{V}$ ($0.477 \log \mu\text{V}$).

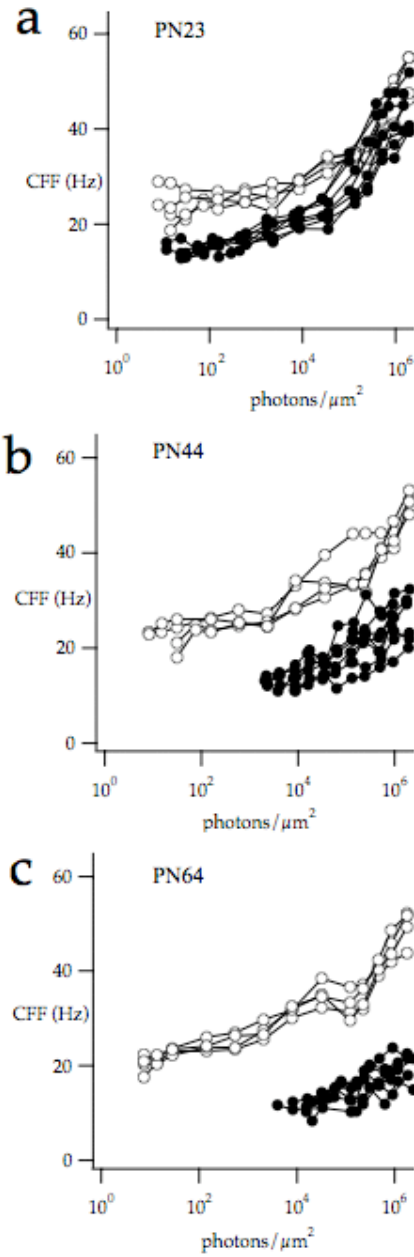


Figure 12. Comparison of CFF curves between wild type (open circles) and Royal College of Surgeons rats (filled circles). (a) PN23 (b) PN44 (c) PN64

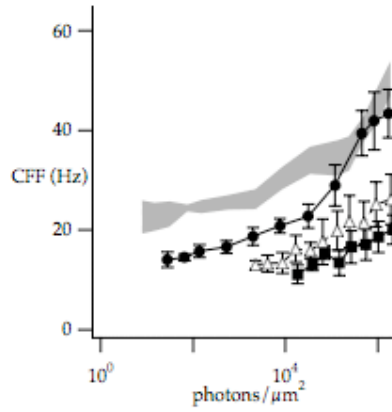


Figure 13. Comparison between RCS CFF at various ages versus wild type. Grey area gives the range based on the standard deviations for wild type CFF curves across all ages studied (n = 12). PN23 (n = 7, filled circles), PN44 (n = 8, open triangles), PN64 (n = 8, filled squares) [Error bars = STDEV].

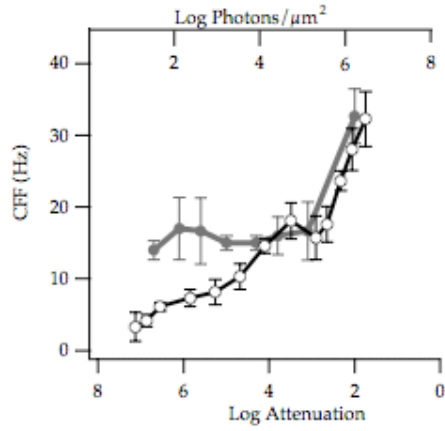


Figure 14. Average ($n = 3$) of CFF curves obtained by Dodt and Echte²⁶. Plotted in grey with filled circles. Our average curve for wild type PN64 is plotted in black with open circles. Our curve is aligned to Dodt and Echte's by shifting it down 17 Hz to match the higher, cone driven, CFF values [Error bars = STDEV].

Table 1

Animal	Scotopic CFF		Photopic CFF	
	WT	RCS	WT	RCS
PN23	32.7±1.6	21.8±2.3†† (66%)	51.0±4.7	42.9±6.0† (84%)
PN44	34.1±3.8	15.9*±2.0†† (47%)	50.8±2.1	26.1±4.2††(51%)
PN64	35.1±2.5	13.0±1.5†† (37%)	49.3±3.8	21.0±2.0††(43%)

Table 1. Comparison of scotopic and photopic CFF values for wild type and RCS rats. CFF values (Hz) reflect an average of n = 4, unless otherwise noted. Differences between groups of wild type and RCS were analyzed using a one-way independent t-test; assuming equal variance. Also indicated is the percentage ratio, RCS/WT for rats of the same age. Scotopic stimulus intensity ranged between (3.3-3.6 e+4 Photons/ μm^2). Photopic stimulus intensity ranged between (1.8-2.0 e+6 Photons/ μm^2).

* - n = 5

†† - p < 0.001

† - p < 0.05

Age-Related ERG Changes in *Cngb1-X1* Knockout Mice: Cone Survival

by

GLEN R. RUBIN, YOUWEN ZHANG, STEVEN J. PITTLER, TIMOTHY W.
KRAFT

Submitted to Investigative Ophthalmology and Visual Science

Format adapted for dissertation

Abstract

Purpose: The rod and cone function in a β subunit GARP knockout (KO) mouse model (*Cngb1-x1*) was evaluated using the full field corneal electroretinogram (ERG) and flicker ERG.

Methods: All animals were handled according to the principles of the ARVO Statement for the Use of Animals in Vision Research. We measured a- and b-wave amplitudes to bright white flashes under dark-adapted conditions and on a rod-saturating background. The ERG response to flicker was used for determining the critical flicker frequency (CFF) of KO mice.

Results: At 1-month old KO mice exhibit a diminished dark-adapted b-wave and normal light-adapted b-wave compared to wild type (WT) mice. Over the next 3 months, both dark- and light-adapted b-wave amplitudes declined, and the decline was greater for dark-adapted b-wave amplitudes. The intensity-response series of flashes showed a 26 fold lower sensitivity in one-month old KO mice. Recovery of the b-wave as a function of the inter-stimulus interval (ISI) between multiple flashes, demonstrated a greater b-wave recovery in KO mice for an ISI of 16 sec or less. The CFF was substantially lower for the KO mice at scotopic intensities, but normal at photopic intensities at one month of age. CFF values remained stable in the KO mice as the b-wave amplitudes decreased with age.

Conclusions: Rod function is reduced but detectable in Cngb1 KO mice.

Declining b-wave amplitudes confirm an RP phenotype of rod followed by cone degeneration. Flicker responses show that the cone circuits functional normally at threshold despite significant losses in the maximum light adapted b-wave amplitude. Thus, CFF may be a more sensitive measure of functional cone vision in animal models undergoing progressive rod-cone degeneration.

Introduction

Cyclic nucleotide gated (CNG) channels, residing on the plasma membrane of photoreceptor outer segments (OS) are critical to phototransduction^{1,2}. The binding of cGMP to CNG channel subunits keeps channels open in the dark. A circulating 'dark current' maintains the photoreceptors in a relatively depolarized state.³ When light activates rhodopsin, a series of biochemical events ensues that leads to the hydrolysis of cGMP and closure of cGMP gated channels. Closed channels interrupt the inward Na^+ and Ca^+ current causing a hyperpolarization of the photoreceptors, detectable as a corneal negative a-wave in ERG recordings^{4,5}. A positive reflecting b-wave that follows the a-wave mainly reflects on-bipolar cell responses⁶⁻⁸.

The rod photoreceptor cyclic nucleotide gated cation channel (CNGC1) is composed of α and β subunits with a stoichiometry of $3\alpha:1\beta$ ⁹⁻¹¹. While the α subunits can form functioning homomeric ion channels when expressed alone in heterologous systems, β subunits expressed individually do not form functioning channels. When α subunits are co-expressed with β subunits they form channels closely resembling the native rod channel¹²⁻¹⁵. Native and coexpressed channels relative to homomeric α channels display a flickery open state, are 100 times more sensitive to the Ca^{2+} channel blocker L-cis-diltiazem, have increased

permeability to divalent ions (Ca^{2+} blockage), exhibit greater ionic selectivity, are modulated by Ca^{2+} -CaM, and show greater fractional activation by cAMP^{12, 13, 16}.

The β subunit has an unusual bipartite structure consisting of N-terminal glutamic-acid-rich protein (GARP) region and a C-terminal channel like region¹². Two related soluble proteins, GARP1 and GARP2 are also expressed from the same gene encoding the β subunit. A β subunit knockout mouse that targeted only the channel like region has been reported¹⁷. This model designated here as *Cngb1-x26* is deleted for exon 26 and does not effect GARP 1 or 2 expression. Recently, we have created a *Cngb1-x1* mouse model with exon 1 and exon 2 deletion¹⁸. In this model, the β subunit and related GARP proteins are not expressed. Although *Cngb1-x1* and *Cngb1-x26* both exhibit degeneration typical of Retinitis Pigmentosa (RP), differences in phenotype suggest structural and functional roles for GARPs. Rod photoreceptor morphology is better preserved in one month-old GARP expressing *Cngb1-x26* knockout mice, yet the single cell's response is almost absent in this animal.

The larger electrical response in our *Cngb1-x1* mice is most likely due to the greater reduction of the channel α -subunit in the *Cngb1-x26* KO mice. Both models show reduced functional expression of the α subunit, however α subunit expression appears of lower abundance in *Cngb1-x26* mice. However it cannot be ruled out that the difference is due to GARPs interaction with proteins in the visual cycle that affect recovery. Arrestin, rhodopsin kinase (RK), retinal pigment epithelium (RPE), and other gene knockouts that abnormally extend the life of activated rhodopsin or increase opsin concentration result in delayed ERG

recovery kinetics¹⁹⁻²² and have been identified as one possible cause of retinal degeneration^{23, 24}. Since, GARP interacts with peripherin-2/rom-1 oligomer, CNGA1, and PDE6^{25, 26}, GARP may influence visual cycle proteins involved in recovery, such as the deactivating proteins of R* and T α -GTP-PDE6 complex. Thus, we have analyzed changes in the ERG b-wave recovery and flicker response in order to assess rod and cone function over the first 4-months of life in a *Cngb1-x1* knockout mouse. Our data suggest that rod function in the knockout mice is severely impaired and cone function begins to deteriorate within the first couple of months. Furthermore, these deficits and their progression do not affect the threshold cone-driven flicker response (CFF). Thus, CFF is a more sensitive measure of cone function in the knockout mice.

Materials and Methods

Generation of Cngb1-x1 Knockout Mice

Generation of Cngb1-x1 knockout mice was done by inGenious Targeting Laboratory, Inc. (inGenious Targeting Laboratory, Inc., Stony Brook, NY) and has been described in detail (Zhang et al, 2009¹⁸). Briefly, a targeting vector pCngb1-KO containing neomycin resistance (Neo) cassette flanked by Cngb1 sequence replaced a fragment including exons 1 & 2 and the predicted proximal promoter region. Knockout mice were produced on hybrid backgrounds of C57BL6 and 129SvEv, using a standard homologous recombination technique. Mice were maintained in compliance with National Institutes of Health guidelines, as approved by the Institutional Animal Care and Use Committees of the University of Alabama at Birmingham and conform to the ARVO guidelines for the use and care of animals.

Basic ERG Response Recording

All mice used in ERG experiments were littermates from heterozygous parents. ERGs were recorded monthly for each mouse, until 4 month's of age. Animals were dark-adapted overnight and anesthetized by intra-peritoneal injection with Avertin 300 µg/g body weight. Both eyes received topical

anesthesia (0.5% proparacaine Bausch & Lomb, Tampa, FL). The left eye, which received light stimuli was dilated with 2.5% phenylephrine (OCuSOFT, Inc., Richmond, TX) and 1% tropicamide (Alcon Laboratories, Inc., Fort Worth, TX). During recordings the mouse was placed on a 39°C heating pad (Model 39 DP, Braintree Scientific, Inc., Braintree, MA) inside of a Faraday cage. Head position was stabilized by a bite-bar. Goniosol (Ciba Vision Corp., Duluth, GA) was applied to the corneal platinum wire-electrodes. Corneal electrodes were gently placed on the eyes under dim red illumination. The recording electrode was placed on the left eye and reference electrode was placed on the right eye. A dedicated optical bench focused light from a 100 watt tungsten halogen source onto a fiber optic cable that delivered the light to a 2.2-mm diameter translucent adaptor into which a platinum wire electrode was embedded²⁷. A 10 ms stimulus of 505 nm light was attenuated in discreet steps by a set of six inconel neutral density (ND) filters. A second optical channel delivered light from a camera flash unit that delivered approximately 5.63×10^4 R*/rod. Data was digitized and recorded with National Instrument hardware and software. Total recording time was about 30 minutes. At each intensity 3-20 repeated responses were averaged. Interstimulus interval (ISI) ranged between 2.2 to 15.2s. Light intensities were measured in photons/ μm^2 and calculated as $\log R^*$ ²⁸. Results were analyzed by t-test.

Isolated Cone ERG Under Light-Adapted Conditions

Rod photoreceptors were saturated by 30s exposure to a 505-nm green conditioning light (bandwidth 35 nm) producing approximately 7300 R*/rod photoisomerizations per s. A bright white camera flash producing 5.63×10^4 R*/rod was delivered on this background in order to elicit the maximal cone ERG. Luminance of the 505-nm background light was 3 cd/m^2 , which is comparable to the amount of white light ($20\text{-}40 \text{ cd/m}^2$) used in other studies^{29, 30}.

Sensitivity of ERG Rod b-wave

There are two methods for calculating b-wave sensitivity. The first method is to calculate the threshold intensity (I) required to evoke a ($15\mu\text{V}$) criterion response. Since, our optical bench produced discrete steps of intensity, we assumed linearity and used dim flash responses to calculate sensitivity in $\mu\text{V}/(\text{R}^*$ or incident photons).

Sensitivity can also be defined as the light intensity required to evoke a half-maximal b-wave ($I_{1/2}$). $I_{1/2}$ was calculated by fitting an intensity response series with a Naka-Rushton function, $R/R_{\text{max}} = I^n/(I^n+k^n)$ ^{31, 32}, where $k = I_{1/2}$. We measured b-wave amplitude from the trough of the a-wave to the peak of the b-wave. Response amplitude was plotted over a 6 orders of magnitude intensity range. $I_{1/2}$ was determined for wild type (WT, n = 12), heterozygote (HT, n = 12) and knockout (KO, n = 11) in 1- and 2-month-old mice.

The maximum rod b-wave was computed for each mouse by subtracting the light-adapted b-wave from the maximum mixed response (Rmax). Rmax was recorded using our bright white camera flash.

Recovery of ERG b-wave by Multiple Flashes

Recovery of the b-wave was determined with respect to the interstimulus interval between flashes. Three 505-nm flashes (bandwidth 35 nm) flashes photoisomerizing 1.7×10^4 R*/rod each were presented in series. The following ISIs were tested: 32, 16, 8, 4, 2 s. We waited 3-minutes between flash trains, so the total recording time was about 15 min.

Responses to the second and third flash were averaged, since they were very similar. Recovery was expressed as a percentage ratio by comparing the latter flashes to the response from the first flash for each interval tested. Mice were divided into three groups, wild type (WT, n = 16), heterozygote (HZ, n = 17) and knockout (KO, n = 15) for 1-month-old ERG recovery experiments and four animals in each group for the 4 month-old experiments. Subsets of these animals were tested at 2- and 3-months old.

Flicker assessment of rod and cone function

CFF was determined for Cngb1-x1 knockout mice in comparison to WT mice in order to assess rod and cone function. ERG recordings were made postnatal (PN) at PN32 (n = 3), PN75 (n = 3), and at PN91 (n = 3). The Flicker ERG protocol has been described in detail previously³³. Briefly, a shutter with 6-

mm aperture (Uniblitz; Vincent Associates, Rochester, NY) set stimulation duration for 6 seconds. A second ferro-electric liquid crystal shutter LV050 (Displaytech, Longmont, CO) produced flicker by sinusoidally modulating the stimulus. The amplifier (Astro-med CP122W; Grass Telefactor, W. Warwick, RI) was set to DC. Responses were amplified 2000X and low-pass filtered at 300 Hz. An optical power meter (Graseby Optronics, Orlando, FL) was used to measure the energy output on every experimental day. Average Michelson contrast was 0.86, StDev = $\pm .017$

Experimental runs for any tested temporal frequency represent 5 seconds of light exposure containing between 5 and 200 repeated cycles of the sinusoidally modulated stimulus. The following stimulus frequencies were used: 1, 2, 4, 5, 10, 16, 20, 25, 32, and 40 Hz. The response was approximately sinusoidal mirroring the stimulus. Amplitude of an average one or two cycle response was measured. The \log_{10} of these response amplitudes were plotted, and CFF was extrapolated to be the stimulus frequency that produced a 3 μV criterion response amplitude³⁴.

Results

Dark adapted ERGs were recorded in *Cngb1-X1* KO (n=11), WT (n=12), and HT (n=12) mice. Figure 15a shows an intensity response series recorded at PN30 for a single KO mouse compared to a WT mouse. The maximum b-wave was only 50% that of the WT mouse and the a-wave was less than 20% that of the WT mouse. Table 2 shows mean Rmax values for the dark- and light-adapted (7300 R*/rod/second) b-wave at PN30. On average the dark-adapted b-wave in KO mice measured 50% of the amplitude in WT animals', meanwhile a-wave amplitude was only 12% of WT mice. Implicit time was significantly longer for both dark-adapted a- and b-waves. Light-adapted b-wave amplitude was unaffected, however the light-adapted b-wave's implicit time was significantly longer. The light-adapted a-wave in KO was just 15% of that found in WT mice.

Sensitivity ($I_{1/2}$) was determined for each mouse by fitting an intensity response series (Fig. 15B) to a Naka-Rushton function. As shown in Table 3, the b-wave was 27-times less sensitive ($P < 0.001$) in KO than WT mice. Average threshold response sensitivity was 800 times less in KO mice than WT litter-mates.

Over the next three months ERG response amplitudes decline further in *Cngb1-x1* knockout mouse. Since the a-wave becomes difficult to measure as these knockout mice age, the relatively larger b-wave was chosen as a metric for gauging retinal degeneration. Figure 16a shows the relative changes to dark-

adapted b-wave amplitudes over time for *Cngb-x1* knockout (KO) mice (grey filled triangles) compared to wild type (WT, filled circles) and heterozygote (HZ, open squares) mice. Values were normalized with respect to their genotype's average value at 1-month. Table 4 lists the voltages of these responses; for WT and HZ b-wave R_{max} increased from about 950 μV at 1-month to about 1200 μV by 3- and 4 months. Over the same time period the KO mouse b-wave amplitude decreased from about 500 μV to 140 μV , about a 3-fold reduction from its initial value. Figures 16b and 16c show representative ERG waveforms at 1 and 3 months for the dark-adapted condition. KO mice (grey trace) exhibit a conspicuous decline in b-wave amplitudes, while b-wave amplitudes for WT and HZ mice remain stable. Light-adapted a- and b-waves were both significantly reduced by 2-months old. Declines in the light-adapted b-wave amplitude over time are shown in Figure 16d; Figures 16e and 16f show representative ERG waveforms at 1 and 3 months for the light-adapted condition. Again, the WT b-wave amplitude grew about 25% while in the KO mice it declined to only 35% of its initial value. Table 5 gives values of the light adapted b-wave amplitudes.

There is a rapid and significant loss of both the light- and dark-adapted b-wave amplitudes over the first four months of life. However, it is difficult to appreciate whether the rod- or cone-driven b-wave amplitudes decreased faster. In order to compare the losses to rod- versus cone-driven signals we calculated the ratio of light- over dark-adapted b-wave amplitudes, plotting them as a function of age (Fig. 17). The magnitude of the cone component was relatively large in the KO mice. The light/dark ratio for KO mice at one month was 48%,

compared to WT and HZ values of only 26%. The Light/Dark ratio steadily increases over time in the KO mice, while remaining stable in both WT and HZ mice, suggesting that rod-driven function declines at a greater rate than cone driven function.

Recovery kinetics were investigated by examining the percentage recovery to repeated flashes. A series of three flashes were presented with an interstimulus interval (ISI) of 32-s, then 16-s, 8-s, 4-s, and finally three flashes at 2-s ISI. There was a 3-minute interval between presentations of flash trains in order to prevent light adaptation. Figure 18 shows the first (black line), second (dashed line) and third (grey line) responses of wild type and knockout mice to flashes delivered with 32-s ISI (right) and 8-s ISI (left). The average recovery of the b-wave is plotted vs. the ISI in Figure 18b. The similar responses to the second and third flash were averaged and then normalized as a percentage of the first flash. Recovery was close to 95% at 32-s ISI for all genotypes. However, at shorter ISI, the KO mice had recovered more (87.2%) than the wild types (81.4%) or heterozygotes (78.9%). A similar finding was observed with 4 month-old KO mice (data not shown).

The Flicker ERG also depends on recovery kinetics; and depending on background light levels it can isolate rod- from cone-driven responses. The Critical Flicker Frequency (CFF) was determined over a broad range of light intensities in wild type and knockout mice. Figure 19a shows the CFF vs. intensity functions for six mice, three WT (filled circles) and three KO (open circles). The results were very consistent from animal to animal within a

genotype, but the KO mice were dramatically less sensitive; they did not generate measurable responses over the lowest three log units of the range tested, consistent with the ERG results. However, at the upper end of our intensity range the cone-driven CFF of KO mice approached the 40Hz value seen in WT mice. The CFF function for the KO mice was remarkably stable. Figure 19b shows that the CFF results for PN32 (open circles), PN75 (filled squares), and PN91 (open triangles) are virtually indistinguishable. In fact, for the upper most log-unit of our stimuli, the knockout CFF falls within the range of the wild type values shown in Fig 19b, where the grey area represents the mean \pm one standard deviation. In summary, dark-adapted b-waves were abnormally low at the outset and rapidly declined, whereas light-adapted b-waves amplitudes were initially normal and then declined slowly. The b-wave had a delayed implicit time and its sensitivity was reduced. ERG CFF was lower at scotopic intensities, near normal at photopic intensities, and did not decline during the 4 months of testing.

Discussion

Rod photoreceptors in *Cngb1-x1* mice are functional, despite the significant reduction in the amount of the α -subunit. The threshold ERG response was raised by 2.8 log units in *Cngb1* KO mouse, which is 100-fold better than threshold in the rodless rhodopsin knockout mouse³⁵. The dark-adapted a-wave was about 2.5 times larger than the light-adapted a-wave. The difference between these two measures reflects a rod contribution to the ERG under dark-adapted conditions. The dark-adapted a-wave's implicit time in KO mice is significantly longer than in WT mice. Meanwhile, the timing of the light-adapted a-wave was not significantly different. Since, the amplitude of the light-adapted a-wave is significantly smaller, one could speculate that a smaller cone input in our KO mouse results in the longer implicit times seen under dark-adapted conditions. More likely, the mechanics of the transduction cascade are adversely affected in our KO mouse. These results indicate that functional rod photoreceptors are consistent with the reduced sensitivity observed in single cell recordings made from rods of one-month old KO mice¹⁸.

Dark-adapted b-wave sensitivity ($I_{1/2}$) was calculated for one-month old mice by fitting an intensity-response series with a Naka-Rushton function. KO mice are 26 fold less sensitive than WT mice. Interestingly, this result mirrors the loss of sensitivity seen in single rod photoreceptor recordings (34 fold). Modeling rod

photoreceptor sensitivity using the ERG has several advantages over single cell recording. The ERG is an easier technique and recordings can be made longitudinally in the same animal. Since, the ERG reflects massed activity over the entire retina, it may represent the average change in sensitivity better than single cell recordings.

The maximum dark-adapted b-wave represents a mixed rod and cone response, while the light-adapted b-wave reflects isolated cone activity. Thus, the ratio of the light- to dark-adapted b-wave amplitudes indicates the relative strengths of the rod- and cone-driven input. Following this ratio during retinal degeneration indicates which system or circuit is more significantly affected. In the model tested here both systems are declining. However, the rod-driven function is deteriorating at a faster rate, as demonstrated by the increase in Light/Dark adapted b-wave ratio over the 4-month period. The greater percentage recovery to repeated flashes in the KO mouse may reflect the proportionally larger cone signal, since cones recover faster.

It is remarkable that the KO mouse CFF curve is stable over the first four months of life while over the same time period the dark-adapted maximum b-wave amplitude decreases by over 50%. The light-adapted b-wave, which represents cone-driven retinal function, declines by nearly half (42%), yet the CFF is not only stable, it remains within the range of wild type CFF values for the brightest lights tested. One explanation for this apparent contradiction is that the two tests are measuring different functional aspects of the cone pathways in the retina. The bright flash on a rod-saturating background tests the maximum cone-

driven transretinal voltage achievable, while the CFF measures threshold; asking “What is the maximum frequency the cone-driven circuitry can follow while generating a minimally detectable trans-retinal voltage?” The criterion voltage selected was 3 μ V. If the behaviorally relevant voltage for flicker detection is more like 30 or 50 μ V then a more pronounced behavioral deficit might be found. The important point to emphasize is that ERG tests of maximum amplitude or maximum current may tell you something very different about the retinal integrity than threshold measures testing the same retinal circuits.

We have demonstrated impaired rod function in our Cngb1-GARP knockout mouse. The dark- and light-adapted ERG responses decline over time in a manner typical of RP. Although the scotopic flicker response was reduced, we did not measure any significant changes to the photopic ERG CFF over the course of our study. This finding was especially remarkable where the light adapted b-wave declined 65% in amplitude while CFF was stable. Maximum response amplitudes better reflect degenerative changes, however the relative maintenance of CFF, suggests that preservation of threshold responses may be functionally more important than the maximum response. Thus, CFF may be a better measure of absolute cone function remaining in retina degenerative disease.

References

1. Kaupp UB, Seifert R. Cyclic nucleotide-gated ion channels. *Physiol Rev* 2002;82:769-824.
2. Molday RS. Photoreceptor membrane proteins, phototransduction, and retinal degenerative diseases. The Friedenwald Lecture. *Invest Ophthalmol Vis Sci* 1998;39:2491-2513.
3. Barnes S. After transduction: response shaping and control of transmission by ion channels of the photoreceptor inner segments. *Neuroscience* 1994;58:447-459.
4. Penn RD, Hagins WA. Signal transmission along retinal rods and the origin of the electroretinographic a-wave. *Nature* 1969;223:201-204.
5. Hagins WA, Penn RD, Yoshikami S. Dark current and photocurrent in retinal rods. *Biophys J* 1970;10:380-412.
6. Gurevich L, Slaughter MM. Comparison of the waveforms of the ON bipolar neuron and the b-wave of the electroretinogram. *Vision Res* 1993;33:2431-2435.
7. Hood DC, Birch DG. Beta wave of the scotopic (rod) electroretinogram as a measure of the activity of human on-bipolar cells. *J Opt Soc Am A Opt Image Sci Vis* 1996;13:623-633.
8. Robson JG, Frishman LJ. Response linearity and kinetics of the cat retina: the bipolar cell component of the dark-adapted electroretinogram. *Vis Neurosci* 1995;12:837-850.
9. Weitz D, Ficek N, Kremmer E, Bauer PJ, Kaupp UB. Subunit stoichiometry of the CNG channel of rod photoreceptors. *Neuron* 2002;36:881-889.

10. Zhong H, Molday LL, Molday RS, Yau KW. The heteromeric cyclic nucleotide-gated channel adopts a 3A:1B stoichiometry. *Nature* 2002;420:193-198.
11. Zheng J, Trudeau MC, Zagotta WN. Rod cyclic nucleotide-gated channels have a stoichiometry of three CNGA1 subunits and one CNGB1 subunit. *Neuron* 2002;36:891-896.
12. Korschen HG, Illing M, Seifert R, et al. A 240 kDa protein represents the complete beta subunit of the cyclic nucleotide-gated channel from rod photoreceptor. *Neuron* 1995;15:627-636.
13. Chen TY, Peng YW, Dhallan RS, Ahamed B, Reed RR, Yau KW. A new subunit of the cyclic nucleotide-gated cation channel in retinal rods. *Nature* 1993;362:764-767.
14. Kaupp UB, Niidome T, Tanabe T, et al. Primary structure and functional expression from complementary DNA of the rod photoreceptor cyclic GMP-gated channel. *Nature* 1989;342:762-766.
15. Dhallan RS, Macke JP, Eddy RL, et al. Human rod photoreceptor cGMP-gated channel: amino acid sequence, gene structure, and functional expression. *J Neurosci* 1992;12:3248-3256.
16. Chen TY, Illing M, Molday LL, Hsu YT, Yau KW, Molday RS. Subunit 2 (or beta) of retinal rod cGMP-gated cation channel is a component of the 240-kDa channel-associated protein and mediates Ca²⁺-calmodulin modulation. *Proc Natl Acad Sci U S A* 1994;91:11757-11761.
17. Huttl S, Michalakis S, Seeliger M, et al. Impaired channel targeting and retinal degeneration in mice lacking the cyclic nucleotide-gated channel subunit CNGB1. *J Neurosci* 2005;25:130-138.
18. Zhang Y, Molday LL, Molday RS, et al. Knockout of cGMP-gated channel b-subunit and GARPs disrupts disk morphogenesis and rod outer segment structural integrity. *Journal of Cell Science* 2008.
19. Lyubarsky AL, Chen C, Simon MI, Pugh EN, Jr. Mice lacking G-protein receptor kinase 1 have profoundly slowed recovery of cone-driven retinal responses. *J Neurosci* 2000;20:2209-2217.

20. Chen CK, Burns ME, Spencer M, et al. Abnormal photoresponses and light-induced apoptosis in rods lacking rhodopsin kinase. *Proc Natl Acad Sci U S A* 1999;96:3718-3722.
21. Nusinowitz S, Nguyen L, Radu R, Kashani Z, Farber D, Danciger M. Electroretinographic evidence for altered phototransduction gain and slowed recovery from photobleaches in albino mice with a MET450 variant in RPE65. *Exp Eye Res* 2003;77:627-638.
22. Birch DG, Peters AY, Locke KL, Spencer R, Megarity CF, Travis GH. Visual function in patients with cone-rod dystrophy (CRD) associated with mutations in the ABCA4(ABCR) gene. *Exp Eye Res* 2001;73:877-886.
23. Fain GL, Lisman JE. Light, Ca²⁺, and photoreceptor death: new evidence for the equivalent-light hypothesis from arrestin knockout mice. *Invest Ophthalmol Vis Sci* 1999;40:2770-2772.
24. Frasson M, Sahel JA, Fabre M, Simonutti M, Dreyfus H, Picaud S. Retinitis pigmentosa: rod photoreceptor rescue by a calcium-channel blocker in the rd mouse. *Nat Med* 1999;5:1183-1187.
25. Korschen HG, Beyermann M, Muller F, et al. Interaction of glutamic-acid-rich proteins with the cGMP signalling pathway in rod photoreceptors. *Nature* 1999;400:761-766.
26. Poetsch A, Molday LL, Molday RS. The cGMP-gated channel and related glutamic acid-rich proteins interact with peripherin-2 at the rim region of rod photoreceptor disc membranes. *J Biol Chem* 2001;276:48009-48016.
27. Lyubarsky AL, Pugh EN, Jr. Recovery phase of the murine rod photoresponse reconstructed from electroretinographic recordings. *J Neurosci* 1996;16:563-571.
28. Lyubarsky AL, Daniele LL, Pugh EN, Jr. From candelas to photoisomerizations in the mouse eye by rhodopsin bleaching in situ and the light-rearing dependence of the major components of the mouse ERG. *Vision Res* 2004;44:3235-3251.

29. Peachey NS, Alexander KR, Fishman GA. The luminance-response function of the dark-adapted human electroretinogram. *Vision Res* 1989;29:263-270.
30. Peachey NS, Goto Y, al-Ubaidi MR, Naash MI. Properties of the mouse cone-mediated electroretinogram during light adaptation. *Neurosci Lett* 1993;162:9-11.
31. Birch DG, Fish GE. Rod ERGs in retinitis pigmentosa and cone-rod degeneration. *Invest Ophthalmol Vis Sci* 1987;28:140-150.
32. Hood DC, Birch DG. A quantitative measure of the electrical activity of human rod photoreceptors using electroretinography. *Vis Neurosci* 1990;5:379-387.
33. Rubin GR, Loop MS, Kraft TW. Flicker assessment of rod and cone function in a model of retinal degeneration. *Doc Ophthalmol* 2007;Pending:Pending.
34. Pinilla I, Lund RD, Sauve Y. Cone function studied with flicker electroretinogram during progressive retinal degeneration in RCS rats. *Exp Eye Res* 2005;80:51-59.
35. Toda K, Bush RA, Humphries P, Sieving PA. The electroretinogram of the rhodopsin knockout mouse. *Vis Neurosci* 1999;16:391-398.

a

1 Month Old Dark-adapted ERG

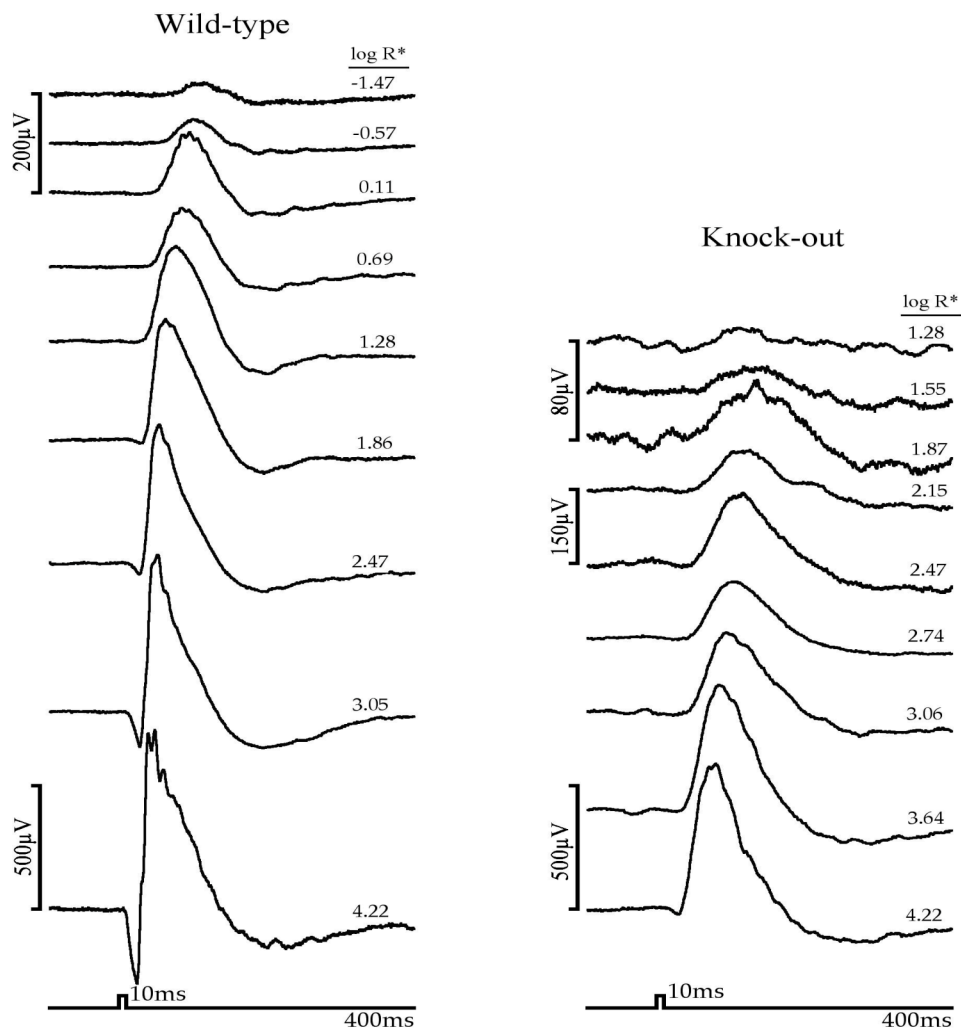


Figure 15. ERG intensity-response series at PN 30 for *Cngb1* Knockout and Wild Type Mice. **(a)** Dark-adapted flash ERGs recorded to 505 nm 10 ms flashes. Flash intensity increases vertically from dimmest (top trace) to brightest (bottom trace). Each trace was the average of 3-20 sweeps. Light intensities are indicated beside each trace as Log R* (see methods).

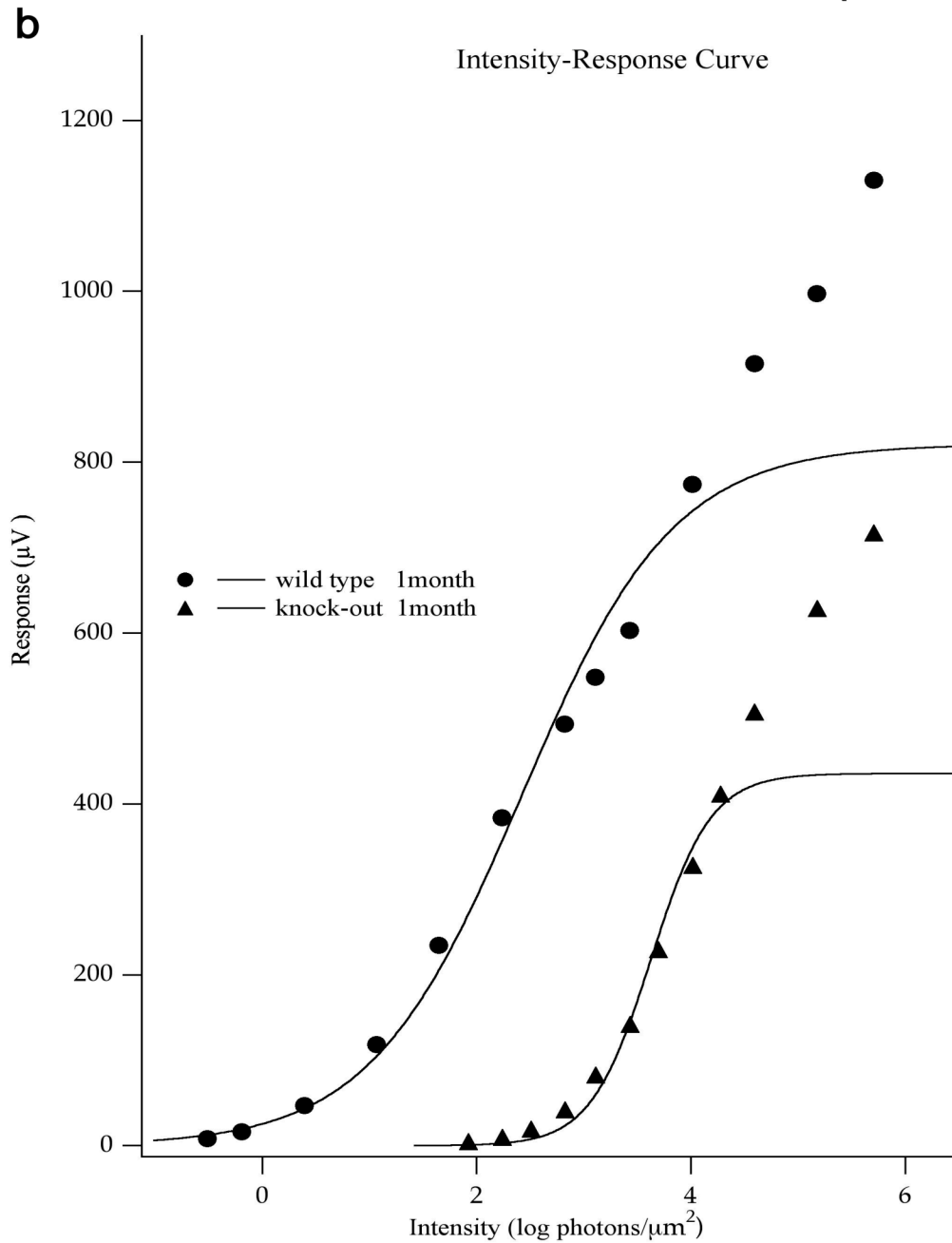


Figure 15. (b) The amplitude of each response (total b-wave) was plotted against stimulus intensity ($\log \text{photons}/\mu\text{m}^2$). Filled circles represent WT response; filled triangles represent knock-out mouse response. Curves were fitted using the Naka-Rushton function.

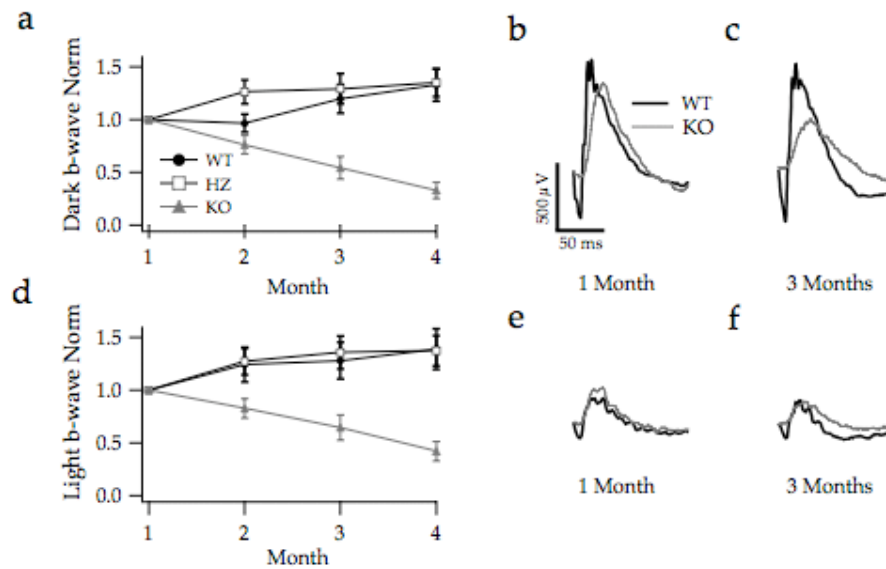


Figure 16. Dark- and light-adapted b-wave amplitudes plotted as a function of age. **(a)** Normalized dark-adapted b-wave amplitudes elicited by bright white flashes ($5.63 \times 10^4 R^*$) recorded up to 4 months postnatal in knock out (KO; $n=11$, filled grey triangles), wild type (WT; $n=12$, filled circles) and heterozygous (HZ; $n=12$, open squares) mice [Error bars = Mean \pm SEM]. **(b, c)** Dark-adapted ERGs at 1 and 3 months postnatal for WT (black trace) and KO (grey trace) mice. **(d)** Normalized light-adapted b-wave amplitudes elicited by bright white flashes recorded up to 4 months postnatal. 505 nm background light was set at an intensity necessary to produce 7300 R^*/s per rod. **(e, f)** Light-adapted ERGs at 1 and 3 months postnatal for WT and KO mice.

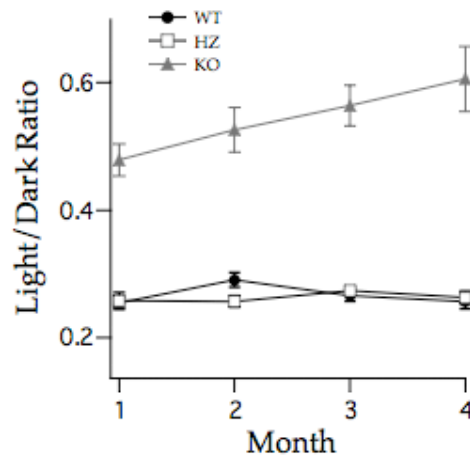


Figure 17. Ratio of light- to dark-adapted b-wave amplitudes plotted as a function of age for: knock out (KO; n=11, filled grey triangles), wild type (WT; n=12, filled circles) and heterozygous (HZ; n=12, open squares) mice [Error bars = Mean \pm SEM; where bars are absent error falls within symbol].

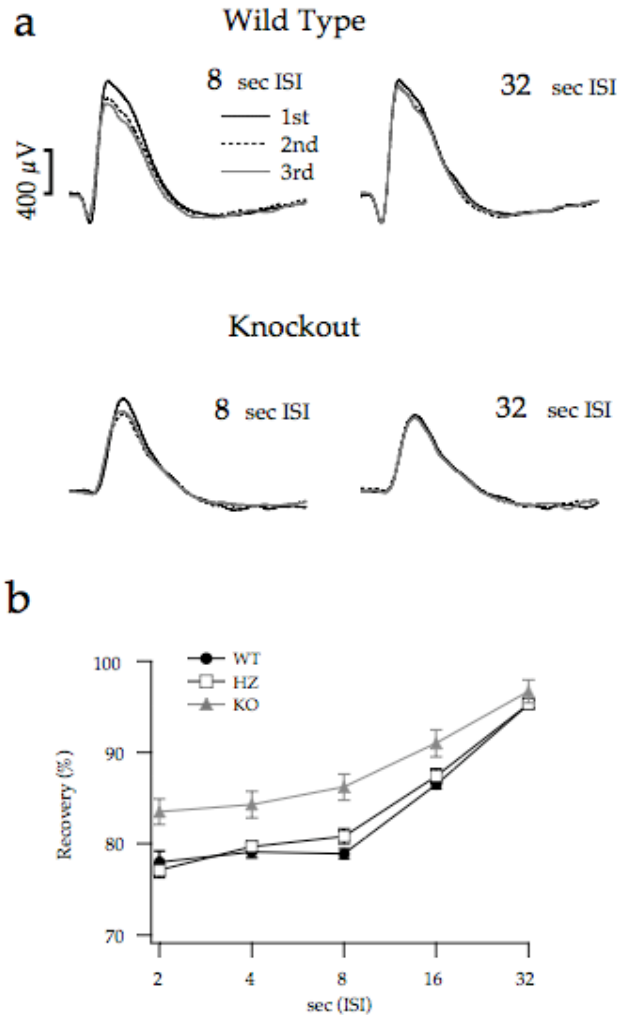


Figure 18. PN30 b-wave recovery in WT and KO mice. Recovery was determined by varying the interstimulus interval (ISI) between trains of three bright 505 nm flashes ($1.7 \times 10^4 R^*$). The series of interstimulus interval (ISI) values tested were 32, 16, 8, 4, and 2 s. **(a)** Examples of 8- and 32-s ISI are shown. **(b)** Dark-adapted b-wave recovery values as a function of ISI. Mice were divided into three groups, wild type (WT, $n=16$), heterozygote (HZ, $n=17$), and knockout (KO, $n=15$). Percentage recovery increased gradually over the range of ISI values. At the longest ISI of 32-s, recovery was close to 95% for all

three genotypes. However, recovery in KO mice was significantly greater ($P < 0.01$) for all other ISIs tested. There was no statistical difference between WT and HZ for these interval values ($p > 0.05$) [Error bars = Mean \pm SEM; where bars are absent error falls within symbol].

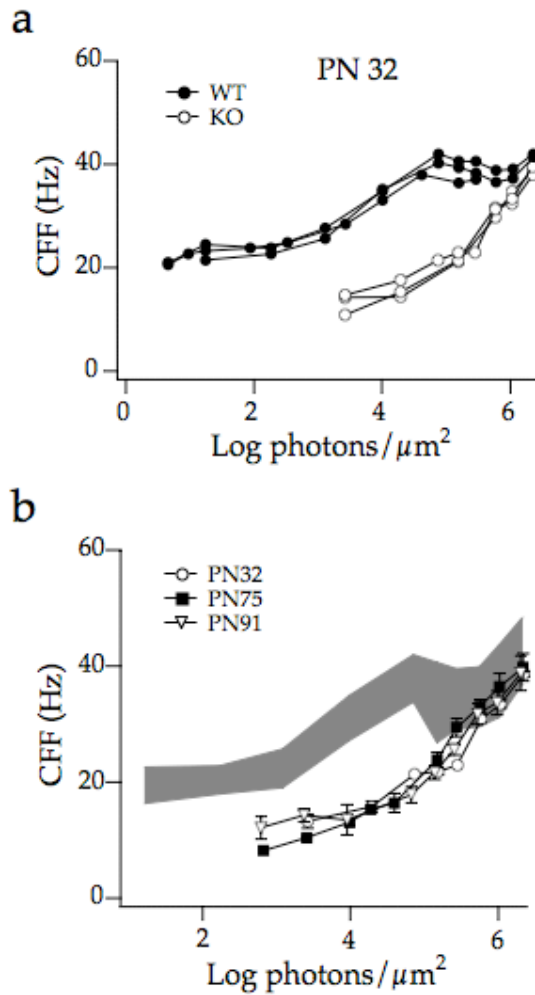


Figure 19. Comparison of CFF curves between WT and KO mice. (a) PN32 KO mice (open circles) did not respond over the lowest 3 log unit range of stimulus intensities, but at higher intensities compared favorably with the CFF of WT mice (filled circles). (b) KO mice CFF curves at three ages: PN32 (n=3, open circles), PN75 (n=3, filled squares), and PN91 (n=3, open inverted triangles). The grey region shows the range of WT CFF values (Mean \pm StDev; n=9, 3 animals, each tested 3 times) [Error bars = Mean \pm SEM; where bars are absent error falls within symbol].

Table 2. **ERG analysis of PN30 wild type and *Cngb1-X1* knockout mice**

	Implicit Time (ms)			Amplitude (μ V)		
	WT (n=12)	HT (n=12)	KO (n=11)	WT (n=12)	HT (n=12)	KO (n=11)
Dark adapted						
b-wave	35.2 \pm 1.8	34.9 \pm 1.7	58.0 \pm 5.3 P<0.001	964 \pm 295	955 \pm 402	485 \pm 194 P<0.001
a-wave	13.4 \pm 1.3	13.1 \pm 0.8	14.9 \pm 1.7 P<0.05	341 \pm 141	338 \pm 141	40 \pm 19 P<0.001
Light adapted						
b-wave	38.6 \pm 7.2	38.3 \pm 6.0	46.5 \pm 5.7 P<0.01	247 \pm 80	238 \pm 91 ns	229 \pm 97 ns
a-wave	13.2 \pm 1.1	13.3 \pm 1.5	13.2 \pm 2.3 ns	97 \pm 42	84 \pm 38 ns	15 \pm 9 P<0.001

ns=not significant

Table 3. **The rod $I_{1/2}$ of ERG b-wave amplitude**

	$I_{1/2}$ (R*/rod)
WT (n=12)	20.3 ± 5.9
HT (n=12)	27.5 ± 15.5
KO (n=11)	548 ± 283 **

The half-maximal stimulus intensity ($I_{1/2}$) for the three genotypes investigated.

** p < 0.001

Table 4. 1- to 4-Month-Old b-wave Amplitudes Under Dark-Adapted Conditions

		1 Mon	2 Mon	3 Mon	4 Mon
WT (n = 12)	μV	964 ± 85	910 ± 92	1090 ± 100	1190 ± 100
HZ (n = 12)	μV	955 ± 116	1120 ± 110	1170 ± 140	1170 ± 98
KO (n = 11)	μV	485 ± 59	340 ± 32	234 ± 34	139 ± 26*

Note: WT, HZ, and KO mice b-wave responses elicited by bright white flash under dark-adapted conditions are shown here. *, n = 9. The value of each cell in the table is average ± SEM. Flash intensity = $5.63 \times 10^4 R^*$ per rod.

Table 5**Table 5. 1- to 4-Month-Old b-wave Amplitudes Under Light-Adapted Conditions**

		1 Mon	2 Mon	3 Mon	4 Mon
WT (n = 12)	μV	247 ± 23	260 ± 23	288 ± 26	314 ± 36
HZ (n = 12)	μV	238 ± 26	285 ± 28	317 ± 36	311 ± 31
KO (n = 11)	μV	229 ± 29	177 ± 19	133 ± 21	81 ± 14*

Note: WT, HZ, and KO mice b-wave responses elicited by bright white flash under light-adapted conditions are shown here. *, n = 9. The value of each cell in the table is average ± SEM. Flash intensity = 5.63×10^4 R* per rod, background intensity = 7300 R*/s per rod.

Comparisons Between ERG and Behavioral CFF in a Light Damaged Albino Rat

by

GLEN R. RUBIN, YUQUAN WEN, MICHAEL S. LOOP, TIMOTHY W. KRAFT

Submitted to Investigative Ophthalmology and Visual Science

Format adapted for dissertation

Abstract

Purpose: The full-field corneal ERG is frequently used to estimate rod- or cone-driven function in rodent models of retinal degeneration. However, the relationship between ERG response amplitudes and visually guided behavior has been little studied. A longitudinal comparison of ERG to behavioral responses in a light-damage model of retinal degeneration allows us to better understand the functional implications of electrophysiological changes.

Methods: All animals were handled according to the principles of the ARVO Statement for the Use of Animals in Vision Research. Flicker-ERG and behavioral responses to flicker were used to determine the critical flicker frequency (CFF) of albino rats under scotopic and photopic conditions. Behavioral CFF was determined by two alternative forced choice tests in a water maze. Dark- and light-adapted flash ERG responses were also analyzed before and after a 10-day period of low-intensity (280 lux) light-damage. Control animals underwent sham light damage, but were maintained under regular cyclic lighting.

Results: Dark- and light adapted ERG responses were significantly reduced after light damage. The a-wave was permanently reduced, while b-wave amplitude recovered over 80% by R20. There was a small, but significant dip in scotopic ERG CFF at R6. Photopic behavioral CFF was slightly lower following light damage.

Conclusions: Flash ERG b-wave amplitudes were severely reduced after light damage, but recovered over time. In marked contrast, the CFF as measured by ERG or behavior remains remarkably stable. The recovery of b-wave amplitude and flicker sensitivity demonstrates a plasticity of retinal circuits following injury.

Introduction

The full-field electroretinogram (ERG) reveals the summed electrical activity of retinal neurons in response to light stimuli. It is a non-invasive technique commonly used to quantify retinal function in humans ¹ as well as rodent models ² of retinal degeneration. Abnormal ERG recordings can assist in the early detection of photoreceptor degenerations such as Retinitis Pigmentosa (RP). RP is a genetically heterogeneous group of retinal degenerations affecting one in every 4000 individuals world-wide ³. Degeneration is characterized by initial rod apoptosis followed by cone loss, suggesting a dependence of cone receptors survival upon rods ⁴. Cone ERGs are often used clinically to monitor disease progression, due to an early loss of the rod signal ⁵. The rod ERG signal may become more clinically relevant if therapeutic advances ^{4,6,7} and/or retinal plasticity ⁸ repairs rod mediated activity. Regardless, it is not clear whether improvements to an ERG signal, such as a larger a-wave, b-wave, or flicker response can be directly correlated to improvement in visual function (behavior).

Continuous exposure to low-intensity light in rats causes photoreceptor apoptosis, especially in albino animals ^{9,10,11}. Using this type of light damage as a model for RP has distinct advantages. There are no confounding genetic factors and the extent of degeneration is controllable. Anatomical studies have determined that a greater percentage of cones survive light damage over rods.

LaVail demonstrated relative sparing of cones exposed to light damage over rods in albino rats exposed to 700 lux for 54 days¹². Cones represented 60% of total photoreceptors after 178 days exposure.

Cicerone also found evidence that the photopic system was relatively spared after continuous exposure to light. ERG measures of the dark adaptation curve in albino rats exposed to 1080 lux for up to 24 hours showed a significantly elevated rod branch, whereas the cone branch of the adaptation curve was unaltered.

The characterization of rods as a more vulnerable to light damage is not consistent throughout the literature. Sugawara, Sieving & Bush showed significant reductions to the dark- and light adapted ERG in albino rats exposed to 1000-3000 lux for up to 48 hours¹³. Williams et al. determined significant deficits to visual function by behavioral testing of CFF in albino rats exposed to 500 lux for 8 days¹⁴. The CFF curve was suppressed over an intensity range covering six orders of magnitude. The largest decrease in CFF values (Hz) occurred in the photopic range of vision.

In the present study we monitor rod and cone function for a 90-day recovery period after 10-days continuous exposure to 280-lux fluorescent light. We measured the ERG response to dark- and light- adapted flashes and sinusoidal flicker. Psychophysical measures of CFF were made in a water maze. Histological measures of outer and inner nuclear layer thickness were taken at the end of our study. Differences between the effect of light induced retinal degeneration on threshold measures versus maximum responses were

observed. Strong parallels were noted between behavior and ERG measures of threshold. The light damage model demonstrates significant recovery of the flash ERG over the course of the experiment, however CFF thresholds were minimally disturbed by the 30% loss of photoreceptors over many weeks

Methods

Sprague Dawley Albino Rats were housed in a room under cyclic 12-hour light/dark conditions (57-140 lux). Animals were trained on a behavioral task for 65 days, prior to Light Damage. During light damage animals were exposed for 10-days to 280 lux light from a 32 watt fluorescent bulb (2950 lumens, Color Rendering Index 85, Correlated Color Temperature 3000k). All animals were handled according to the principles of the ARVO Statement for the Use of Animals in Ophthalmic and Vision Research.

Electroretinography

ERG recordings were made prior to light damage and regularly during the 90-day recovery period. Rats were dark-adapted over-night before ERG recordings. They were sedated with 3% isoflurane in a chamber and then anesthetized via intraperitoneal injection of xylazine (9.09 mg/kg) and ketamine (90.9 mg/kg). Corneas were anesthetized with proparacaine (0.5%) and pupils dilated with topical phenylephrine HCl (2.5%) and tropicamide (1%).

During recordings the rat was placed in a Faraday cage with its head fixed by a bite-bar and body temperature maintained at 38°C by a heating pad (Braintree Scientific, Braintree, MA). The light source was a 100-W tungsten-halogen lamp focused onto one end of a fiber optic.

Full-field ERGs were recorded using a 2 mm diameter sized recording electrode¹⁵. The electrode consisted of a platinum wire loop embedded in the tapered end of a hollow Plexiglas rod. The fiber optic serving as a light pipe from the optical bench, was secured onto the non tapered end, ensuring a constant distance between the fiber optic and the eye. The tapered end acted as a diffusing element, yielding an isotropic plane of illumination at the pupil¹⁵. The reference electrode was a second platinum loop gently placed on the non-stimulated right eye. Methylcellulose (Goniosol, CIBA Vision Corp, Duluth, GA) was applied to both eyes as well as to the recording and reference corneal electrodes, in order to maintain good electrical contact.

Responses were amplified 2000X (Astro-med CP122W; Grass Telefactor, W. Warwick, RI) and low-pass filtered at 300 Hz. The ERG voltage and stimulus-monitor signals were digitized with hardware (MIO16) and software (LabView) from National Instruments (Austin, TX). Stimulus intensity was controlled by a set of calibrated inconel neutral-density filters that allowed attenuation in steps of approximately 0.3 log units up to a maximum of 6.9 log units attenuation. Light intensity was calibrated each day by an optical power meter (Graseby Optronics, Orlando, FL) in units of photons/ μm^2 . Stimulus duration was controlled by a 6-mm aperture shutter (Uniblitz; Vincent Associates, Rochester, NY). A three-cavity interference filter (Andover Co., Salem, NH) set the wavelength of the stimulus at 505 nm (40 nm bandwidth). The data were analyzed and figures generated using IGOR PRO software (Wavemetrics Inc, Lake Oswego, OR).

Flash ERG

Flash ERGs were recorded with high pass AC 0.1 S filtering. ERG responses were sampled for 1 second at a rate of 0.5 ms/pt. An intensity response (IR) series was generated by progressively increasing the intensity of the 10 ms flash. Average responses were obtained using 3 to 20 repeats of the same stimulus. The inter-stimulus interval (ISI) ranged from 2.2 seconds up to 30 seconds to allow full recovery from bleaching. An intensity-response function was generated for both a- and b-waves by fitting plotted data with a modified Michaelis function of the form:

$$R = R_{\max} * (i) / (i + k) + \text{base}$$

Where R = response, Rmax = maximum response, i= log intensity, and k= $I_{1/2}$ (log intensity necessary to produce a half maximal response).

A bright camera flash filtered by 530 nm (10 nm bandwidth) interference filter was used to evoke maximum responses. Under dark-adapted conditions these bright flashes were delivered at an ISI of 120 seconds. Light-adapted ERGs to the same bright flash were recorded against a 505 nm saturating rod adapting field ($3.66E+4$ photons $\mu\text{m}^{-2}\text{s}^{-1}$) incident upon the cornea. Under light-adapted conditions flashes were delivered at an ISI of 60 seconds.

Flicker ERG

Sinusoidal flicker was produced by a ferro-electric liquid crystal shutter

(LV050; Displaytech, Longmont, CO), which modulated the stimulus. The amplifier (Astro-med CP122W; Grass Telefactor, W. Warwick, RI) was set to DC while recording flicker. Average Michelson contrast of the flicker stimulus was 0.86.

Experimental runs for each temporal frequency contained a total of 24,000 points, at a sampling rate of 0.25 ms/pt representing 6 seconds of recording time. The shutter was closed during the initial and final 500 ms of data collection. Thus 5 seconds of light exposure containing between 5 and 200 cycles of the sinusoidal stimulus drove the retinal response. The following stimulus frequencies were tested: 1, 2, 4, 5, 10, 16, 20, 25, 32, and 40 Hz. Light intensity was incrementally raised after each presentation of this temporal series.

The initial on-transient response was ignored in the analysis. The remaining 4.5 seconds of data was collected and averaged into a one or two cycle wave. The average response amplitude (μV) was fit by a sine wave. At lower frequencies the contribution of a second harmonic to the total response sometimes resulted in a response that was not a perfect sinusoid. In these cases we measured the peak to trough amplitude of this averaged response. The \log_{10} of the response amplitudes for each intensity were plotted and fit with a line starting from the peak of the monotonic decline, which typically occurred at 1 or 2 Hz. A $3\mu\text{V}$ criterion voltage was used to determine electrophysiological CFF¹⁶.

Behavior

Behavioral CFF was determined by two alternative forced choice testing in a water maze, which relied upon the animal's desire to escape from a pool of water and onto a hidden platform^{17, 18}. A trial began when an animal was released at the narrow end of a grey acrylic trapezoidal- shaped pool of water (~22° C, 15 cm deep). At the opposite wider end of the pool were two, side-by-side, displays positioned just above the water's surface. A centered divider (40cm x 40cm) separated the two displays. Typically the rats swam the length of the maze (140 cm) in 3 seconds. A display would be either flickering or steady. A hidden platform was always placed underneath the steady display.

The two displays were constructed by placing a translucent acrylic sheet (ca 17 cm square) in front of a bank of green LEDs. The bank of LEDs was enclosed in a funnel, which had a highly reflective mylar coating. The opening at the end of the funnel (1 ¾ cm) sat flush against the acrylic sheet. Inserting neutral density filters between the funnel and acrylic sheet attenuated light intensity.

A specially fabricated circuit drove one display at an adjustable flickering frequency (5-80 hz) and the other at a steady fixed high frequency (180 hz). The position (left/right) of the steady vs flickering displays could be switched and were matched in time-averaged luminance.

Behavioral testing was accomplished in 3 phases¹⁷. Initially, the rat was introduced into the pool a few inches in front of the steady (correct) stimulus and platform. After finding the platform the rat was allowed to remain on it for a few

seconds before being returned to its holding cage. The position of the steady (correct) stimulus and platform were moved from side to side and the rat was placed each time a few inches in front of the platform/steady light. Starting distance was increased when the rat reliably swam directly to the platform.

During the next training phase the rat learned to discriminate between the steady (correct) and flickering (incorrect ~ 6 Hz) stimuli. The rat was placed in the water maze and sequestered behind a clear starting gate. The gate was lifted and the rat was required to locate the platform in front of the correct stimulus before being removed from the maze. If the rat initially swam past the divider towards the incorrect flickering stimulus then the trial was recorded as an error. This training phase continued until the rat consistently (+ 80%, ~ 40 trials) selected the steady (correct) stimulus.

CFF was determined in the final testing phase by increasing the temporal frequency of the incorrect flickering stimulus and determining the animal's accuracy at discriminating it from the correct steady stimulus following a method of limits staircase procedure¹⁹. This procedure had the advantage of keeping the stimulus near threshold. Testing began similarly to the training phase. On the first trial the rat had to discriminate between the slow (incorrect) flickering stimulus (~6 Hz) and the steady (correct) stimulus. On subsequent trials the frequency of the incorrect flickering stimulus was raised in 5 Hz increments. In the event of two consecutive incorrect responses the frequency of the flickering stimulus was lowered by 10 Hz. Thereafter, every consecutive incorrect discrimination resulted in lowering the flickering stimulus by 5 Hz increments until correct discrimination.

Upon correct discrimination the stimulus frequency was increased (5 Hz) until two consecutive incorrect responses. This procedure continued until 3-5 reversals were made. Threshold was taken as the temporal frequency corresponding to 75% correct.

The position of the correct stimulus, except in very early training, followed a Gellerman series²⁰, which contains all possible left/right sequences under constraints such that 1) the correct stimulus appears on each side an equal number of times, 2) never more than three successive times on the same side and 3) positional strategies of single or double alternation yield 50% correct. In the event that an animal developed a position preference (going to the same side on four consecutive trials) the correct stimulus was retained on the non-preferred side until a correct response was made after which the left/right Gellerman sequence continued.

Rats were tested in groups in a session of ~25 trials with no more than 2 sessions per day. A CFF frequency-of-seeing curve was generated in 2 to 3 days based upon about 80 trials. Two luminance levels were tested (scotopic $6.5 \text{ E}+3 \mu\text{m}^{-2}\text{s}^{-1}$ photons, photopic $6.38\text{E}+6 \mu\text{m}^{-2}\text{s}^{-1}$ photons).

Light Damage

Light damage was conducted in a separate room from behavioral testing. Transparent cages were split along the long axis by means of a central divider. Rats were placed individually in these compartments. Minimum bedding and food were placed in the cages. Water was provided *ad libitum*. The cages were

cleaned every other day.

A fluorescent light bulb (T8, Phillips, 48 inch, 32 W, 2950 lumens, color rendering 85, correlated color temperature 3000K) was placed above the animal cages. The light bulb height and angle were adjusted to ensure average illuminance measured at 280 ± 20 lux. Illumination was sampled from six different locations in the cage. Illuminance levels were measured at the cage floor by a Digital Photometer/Radiometer J-6511 (Tektronix Corporation, Richardson, TX) immediately before and after each light-damage session. The animals were dark-adapted overnight before the light damage began. The exposure started around $12\text{PM} \pm 2\text{hrs}$. Following the light-damage treatment experimental rats were placed back into cyclic lighting at the animal housing facility where the mean luminance of the cage during the 12 hour light cycle was 57-140 lux.

Histology

Rats were euthanized by CO₂ asphyxiation. Whole eyes were harvested by enucleation along the conjunctiva and severing of the optic nerve. Extra-ocular muscle and conjunctival tissues were trimmed from the orbit in L-15 medium. The left eye was refrigerated overnight in fixative (2.5% glutaraldehyde, 1% paraformaldehyde).

Fixative was replaced by PBS and shaken (Junior Orbit Shaker; Lab-Line, Melrose Park, Illinois) for 2 X 15 minute washes. Tissue was dehydrated by immersion and shaking for 30-minute periods in increasingly concentrated ethanol (50%, 70%, 2 X 95%, & 2X 100%). Infiltration was initiated by 2 X 30

minute shakings in a solution made from equal parts 100% ethanol and JB-4A. Eyes were then refrigerated overnight in 100% JB-4A. The following day eyes were aligned in molds and embedded in JB-4 (glycol methacrylate) embedding medium (JB-4 Embedding Kit, Polysciences, Warrington, PA).

Radial sections, 5 μM thick, were cut using a Leica RM2065 microtome (Leica Microsystems, Germany). Sections were collected in deionized H_2O at 500 μM intervals and then transferred onto glass slides. Slides were stained overnight in Harris Hematoxylin (Fisher Scientific, Pittsburgh, PA). Staining was completed the next day by immersion in Bluing Reagent (Fisher Scientific, Pittsburgh, PA) followed by Eosin Y staining (Fisher Scientific, Pittsburgh, PA). Slides were soaked in Citrisolv (Decon Labs, King of Prussia, PA) before coverslips were mounted with Hitomount (National Diagnostics, Atlanta, GA). Retinal Sections were imaged on an axioskop optical microscope (Zeiss, West Germany) and captured with Retiga EXi Fast 1394 camera. Measures of outer nuclear layer (ONL) and inner nuclear layer (INL) thickness were taken at 450 μM increments starting from the optic nerve head (ONH) in both inferior and superior hemispheres. A small number of areas to be sampled were not available on the optimal retinal section. Consequently, in these cases ONL/INL area was calculated for a contiguous piece of retina that contained all corresponding data points (sections) for every animal. This piece of tissue ranged between 0.9-4.9 mm superior and 0.9-3.6 mm inferior to the ONH. Only animals surviving 48 days past light, or sham, damage were considered in the statistical analysis of histological data.

Statistical Analysis

Between-group significance for ERG data collected at specific experimental time-points (R6, R20, R48, etc...) was calculated by 2-tailed 2-sample t-test equal variance assumed. Within-subjects comparisons were made by paired t-test.

Flicker analysis and comparisons between ERG and behavioral CFF were made by repeated measures ANOVA. Histological analysis was made by 2-tailed 2-sample t-test equal variance assumed.

Results

Light damage treatment led to a loss of visual function represented by declines of the dark-adapted flash ERG responses; figure 20a illustrates the reductions of the maximum a- and b-wave amplitudes (R_{\max}) in an albino rat six days after a 10-day period of continuous exposure to 280-lux light. Before light damage (Pre-LD; solid trace) this animal had a- and b-wave of 375 μ V and 1730 μ V R_{\max} respectively. Six days after (R6, dashed trace) light damage, a- and b-wave R_{\max} values were reduced to 220 μ V and 1045 μ V respectively. Although both a- and b-wave R_{\max} were reduced by about a 40% in this animal, light damage did not significantly alter response kinetics as measured by AC coupled ERG.

Dark-adapted flash ERG a- and b-wave R_{\max} were lower across all experimental days following light damage. Figure 20b, 20c shows a- and b-wave R_{\max} values measured before light damage and on Recovery Day (R) 6, 20, 48, and 90 in groups of control (filled circles) and test animals (open squares). Each animal's response was normalized to its pre-light damage value. On R6, a- and b-wave R_{\max} responses for light damaged animals (n=9) were a 1/3 lower than pre-light damage responses. By R20 the b-wave recovered over 80% of its original amplitude, whereas the loss of a-wave was permanent. Table 6 compares control and light-damaged dark-adapted a- and b-wave maximum response amplitudes. The light damaged a-wave measured significantly lower on

R6 and R48 ($p < .001$). There was no significant difference between the a-wave amplitudes of the light damage and control groups at R90. Interestingly, b-wave amplitudes were affected very little by the loss of a-wave, there was no decrement in control animals and in addition the 33% loss of a-wave in LD group results in only a 19% decrement of b-wave in these animals at R90.

Cone ERG responses to bright flashes were measured on a 505 nm rod saturating background ($3.66E+4$ photons $\mu\text{m}^{-2}\text{s}^{-1}$) (figure 21). Rmax values of the light-adapted a- and b-wave were stable in control animals over the course of the investigation. However, the light damage group exhibited a progressively declining a-wave. On R6 the light damage group's a-wave measured 17% less than pre-light damage (Pre-LD) and steadily declined thereafter. By R90 the a-wave had declined to only 64% of Pre-LD value. In contrast, the b-wave showed an initial decline of 30%, but thereafter recovered to 85-90% of its pre-light damage amplitude.

An intensity response function was used to determine sensitivity ($I_{1/2}$) of a- and b-waves. Figure 22 shows the calculated $I_{1/2}$ of a- and b-waves at Pre-LD, R6, R20, and R34. The a-wave became more sensitive after light damage. At R6 a half maximal a-wave could be elicited with 1.7 fold less light than pre-light damage ($p < 0.05$). The a-wave sensitivity was not significantly different at R34. The relationship between light damage and b-wave sensitivity was less clear. Although $I_{1/2}$ values of the b-wave varied over the experimental period, there were no significant differences compared to Pre-LD $I_{1/2}$ b-wave values.

Oscillatory potentials (OP) were isolated by band-pass filtering the ERG

signal between 34 and 300 Hz²¹. OP power was determined by fast Fourier transform (FFT) of the first 65 ms of the ERG response. Total OP power was quantified by integrating the power spectrum from 75 to 165 Hz. Figure 23 shows differences between the OP power spectrum for control (n=3) and experimental (n=5) animals at Pre-LD, R6, R34, R90. The area under the OP power spectrum was significantly reduced (75%) on R6. In contrast, the area for the control animal's (6%) slightly increased. Light damaged OP power spectrum gradually recovered. These results parallel the changes seen in b-wave amplitude. At R90 OP power for both groups showed no significant difference between them.

ERG recordings to sinusoidal flicker and behavioral thresholds to flicker were measured in order to determine CFF. ERG CFF was determined by fitting a line to the log of response amplitude vs frequency plot and extrapolating to the frequency, which produced a 3 μV criterion response. In parallel behavioral CFF was determined by 2 alternative forced choice psychophysical testing in a water maze. CFF was tested under both scotopic (ERG = 3,800 photons $\mu\text{m}^{-2}\text{s}^{-1}$; water maze = 6,500 photons $\mu\text{m}^{-2}\text{s}^{-1}$) and photopic (ERG = 3.36 E+06 photons $\mu\text{m}^{-2}\text{s}^{-1}$ and water-maze = 6.4 E+06 photons $\mu\text{m}^{-2}\text{s}^{-1}$) conditions. Figure 24 shows ERG and behavioral CFF at Pre-LD, R6, R20 R48, and R90. ERG CFF values were generally higher than behavioral ones. In control animals, scotopic ERG CFF (24d) measured 24.7 Hz, while behavioral CFF (24b) measured 20.3 Hz. On R6 scotopic ERG CFF (24d) was significantly ($p < 0.01$) reduced in light-damaged animals. However, light-damaged animals did not exhibit significant behavioral differences under scotopic conditions. In control animals, photopic

ERG CFF (24c) measured 47.8 Hz, while behavioral CFF (24a) measured 40.8 Hz. Photopic behavioral CFF was significantly depressed ($p < 0.001$) for the recovery period until R90. The ERG measures showed no detectable difference between photopic CFF in control vs light damaged animals (24a). A comparison of ERG CFF to behavioral CFF in control animals showed ERG CFF to be statistically higher ($p=.002$) than behavioral CFF under scotopic conditions. Under photopic conditions in control-animals there was not a significant difference between ERG CFF and behavioral CFF. Light damaged animals exhibited significant differences between ERG CFF and behavioral CFF in both scotopic ($p < 0.05$) and photopic ($p < 0.01$) conditions.

Photoreceptor loss was quantified by comparing outer (ONL) and inner (INL) nuclear layer thickness of light damaged versus control animals. Figure 25 (pg 132) shows representative photographs from a section of retina approximately 1.3 mm inferior to the ONH in a (25a) light damaged and (25b) control animal. In figure 26, ONL and INL thickness are plotted as a function of distance from the ONH, for control ($n=3$; filled circles) and light damaged ($n=7$; open squares). The calculated area of the ONL for a 6.75 mm section of retina from light damaged animals was $324 \mu\text{M}^2$, significantly less ($p < .01$) than the matched area of ONL in control animals ($417 \mu\text{M}^2$). INL areas were also compared in light damaged animals to controls, however the difference was not statistically significant ($p = .16$).

Discussion

Our albino rats exposed to low-intensity light for 10-days showed transient changes in b-wave amplitude, a-wave sensitivity, CFF values, and the integrated power of the oscillatory potentials. These changes were markedly different from results we obtained previously detailing the permanent loss of the rod- and cone-driven ERG flicker signal in aging RCS rats²². In that study we found significant decrements to the flicker signals in RCS as early as PN23. Scotopic ERG CFF was reduced by 34% ($p < 0.001$) while photopic ERG CFF was reduced 16% ($p < 0.05$). At PN22 the dark-adapted b-wave amplitude is attenuated by about 40% compared to non-dystrophic congenic animals²³. This correlates well to losses seen in ONL thickness (~ 40%) adjacent the optic nerve head in RCS at this age^{24, 25}.

In the present study we measured a 33% loss of dark-adapted b-wave amplitude in albino rats six days after light damage. At the end of our study ONL thickness showed a 22% loss, but the b-wave had recovered. Considering the similar loss of b-wave amplitude in both RCS (PN23) and light damaged albino rats (R6), we expected to see greater reductions to ERG CFF in the light damaged rats. Scotopic ERG CFF was reduced 11% after light damage, while there were no changes in photopic ERG CFF.

The relatively greater deficit to RCS flicker function may be due to

pathophysiological stress. In RCS, degeneration stems from the inability of RPE cells to properly phagocytose shed rod outer segments owing to a defect in Mertk tyrosine kinase receptor gene²⁶. The build-up of these shed disks in the subretinal space leads to the formation of a debris zone and ensuing photoreceptor apoptosis²⁷. The exact mechanism of cell death is unclear²⁸⁻³⁰. The debris zone may interfere³¹ with diffusion of metabolites³² or oxygen³³. The lower CFF in RCS rat may be a product of the retina's chronic unmet metabolic demand or some associated degenerative stresses. In contrast, photoreceptor apoptosis caused by light damage³⁴ is the result of a temporary insult. The threshold flicker function may be robust in the face of this transitory stress, so as to fully recover six days after the exposure period. While the retina in the RCS rats has no time to recover, a plastic adjustment in gain along the rod-bipolar pathway in light damaged retina may partially compensate and maintain b-wave amplitude. We have also tested flicker function in a β subunit knockout (KO) mouse model (*Cngb1-x1*) (Zhang et al. 2009³⁵). In this genetic model of RP, CFF curves were suppressed over the scotopic range of intensities. Similarly, human testing has shown an earlier loss of the rod driven flicker signal over photopic CFF in RP patients³⁶. Further flicker ERG testing in rodent rescue models, which exhibit decrements to CFF would help clarify how flicker function is related to the degenerative condition.

A 3 μ V criterion of response was used for determining ERG CFF, since it is near the root mean squared noise in our averaged flicker ERG recordings. Other studies have also used a 3 μ V criterion amplitude for flicker ERG

analysis^{16, 22}. At the beginning of this study it was unclear how this ERG criterion would correspond to the behavioral detection of a flicker signal in albino rat. Behavioral threshold for seeing flicker (CFF) was calculated as 75% choice of the correct stimulus in our 2-alternative forced choice testing. Overall, there was a fair correspondence between ERG and behaviorally determined CFF values. The scotopic ERG CFF compared by repeated measures ANOVA to scotopic behavioral CFF values was significantly lower (24.7 vs 20.3 Hz) in control animals. Light-damaged animals exhibited significant differences between the ERG criterion and behavioral threshold CFF under both scotopic and photopic conditions. This interesting result suggests that after light damage a larger ERG signal is required in order to mediate the behavioral detection of a threshold flicker signal for cone driven visual function. Perhaps indicating a temporary perturbation in cone response effectiveness as seen by ganglion cells. We also tested an alternative ERG criterion of 5 μ V in order to find an electrophysiological criterion, which better represented psychophysical threshold. Using the 5 μ V criterion eliminated any statistical difference between ERG and behavioral measures of CFF in either control or light-damaged animals.

A single study by Coile, Pollitz, & Smith, has reported behavioral CFF exceeding ERG CFF measures in dog³⁷. However, our results agree with the majority of previous studies in primate showing ERG measures of CFF to be comparable or higher than those obtained psychophysically³⁸⁻⁴⁰, suggesting that the visual system is sensitive to nearly threshold temporal responses in the retina.

There was a significant dip in scotopic ERG CFF after light damage at R6. This temporary deficit may be the result of the phenomenon of photostasis⁴¹, in which the length of the rod outer-segments shortens with respect to the quantal photon catch per day. We did not find reductions to behavioral CFF due to light damage of the same magnitude described by Williams et al.¹⁴. Williams et al. tested CFF in albino rats exposed rats for eight days to a relatively higher intensity light (500 lux) resulting in a loss of 90% ONL thickness. Our model of partial damage (22% loss) did not exhibit significant functional deficits. Thus, the threshold for significant and permanent behavioral deficits lies somewhere in between these damage levels.

After light damage there was a relatively small decrease in the light-adapted a-wave at R6. Over time, however, the light adapted a-wave progressively decreases, so that R90 is the only statistically significant difference. This raises the interesting possibility that cone receptors continue to degenerate after light damage, which may also help explain the apparent greater disparity between the ERG and behavioral criterion. Several studies have documented long-term apoptosis in ONL after exposure to high-intensity light^{9, 42-45}. The b-wave and flicker responses may not reflect this loss due to their greater plasticity.

The generators of the oscillatory potential have not been clearly identified, but are thought to originate from inner retina⁴⁶. Hancock and Kraft showed there was a linear relationship between OP amplitude and b-wave amplitude^{21, 47}. We found a deficit to total OP power that persisted beyond the significant reductions

to b-wave. OP power spectra were not significantly different from control animals at R90. However, in both control and light damaged groups total OP power was significantly lower than at the beginning of the study. The decrease to OP power in normal rats maybe the result of normal aging or some underlying degeneration ongoing in the control group. Ye, et al. also saw decreased OP power in aged rats ⁴⁸.

Our study showed that CFF was less affected by light damage than the ERG b-wave. The relatively minor changes to CFF exhibit the preservation of threshold responses that mediate behavior despite significant photoreceptor degeneration. The CFF was not significantly different from control animals at the end of our study. These findings suggest that successfully treated retinal degeneration will benefit visual function over the long term.

References

1. Fishman GA. *Electrophysiologic testing in disorders of the retina, optic nerve, and visual pathway*. 2nd ed. San Francisco, CA: Foundation of the American Academy of Ophthalmology; 2001:xvi, 308 p.
2. Weymouth AE, Vingrys AJ. Rodent electroretinography: methods for extraction and interpretation of rod and cone responses. *Prog Retin Eye Res* 2008;27:1-44.
3. Hartong DT, Berson EL, Dryja TP. Retinitis pigmentosa. *Lancet* 2006;368:1795-1809.
4. Delyfer MN, Leveillard T, Mohand-Said S, Hicks D, Picaud S, Sahel JA. Inherited retinal degenerations: therapeutic prospects. *Biol Cell* 2004;96:261-269.
5. Birch DG, Fish GE. Rod ERGs in retinitis pigmentosa and cone-rod degeneration. *Invest Ophthalmol Vis Sci* 1987;28:140-150.
6. Margalit E, Maia M, Weiland JD, et al. Retinal prosthesis for the blind. *Surv Ophthalmol* 2002;47:335-356.
7. Humayun MS, Weiland JD, Fujii GY, et al. Visual perception in a blind subject with a chronic microelectronic retinal prosthesis. *Vision Res* 2003;43:2573-2581.
8. Richards A, Emondi AA, Rohrer B. Long-term ERG analysis in the partially light-damaged mouse retina reveals regressive and compensatory changes. *Vis Neurosci* 2006;23:91-97.
9. Noell WK, Walker VS, Kang BS, Berman S. Retinal damage by light in rats. *Invest Ophthalmol* 1966;5:450-473.

10. Noell WK. *Different Kinds of Retinal Light Damage in the Retina*. New York: Plenum Press; 1980:3-29.
11. Rapp LM, Williams TP. Damage to the albino rat retina produced by low intensity light. *Photochem Photobiol* 1979;29:731-733.
12. La Vail MM. Survival of some photoreceptor cells in albino rats following long-term exposure to continuous light. *Invest Ophthalmol* 1976;15:64-70.
13. Sugawara T, Sieving PA, Bush RA. Quantitative relationship of the scotopic and photopic ERG to photoreceptor cell loss in light damaged rats. *Exp Eye Res* 2000;70:693-705.
14. Williams RA, Pollitz CH, Smith JC, Williams TP. Flicker detection in the albino rat following light-induced retinal damage. *Physiol Behav* 1985;34:259-266.
15. Lyubarsky AL, Daniele LL, Pugh EN, Jr. From candelas to photoisomerizations in the mouse eye by rhodopsin bleaching in situ and the light-rearing dependence of the major components of the mouse ERG. *Vision Res* 2004;44:3235-3251.
16. Pinilla I, Lund RD, Sauve Y. Cone function studied with flicker electroretinogram during progressive retinal degeneration in RCS rats. *Exp Eye Res* 2005;80:51-59.
17. Prusky GT, West PW, Douglas RM. Behavioral assessment of visual acuity in mice and rats. *Vision Res* 2000;40:2201-2209.
18. McGill TJ, Douglas RM, Lund RD, Prusky GT. Quantification of spatial vision in the Royal College of Surgeons rat. *Invest Ophthalmol Vis Sci* 2004;45:932-936.
19. Cornsweet T. The Staircase Method in Psychophysics. *American Journal of Psychology* 1962;75:485-491.
20. Gellerman LW. Chance orders of alternating stimuli in visual discrimination experiments. *Journal of Genetic Psychology* 1933;206-208.

21. Hancock HA, Kraft TW. Oscillatory potential analysis and ERGs of normal and diabetic rats. *Invest Ophthalmol Vis Sci* 2004;45:1002-1008.
22. Rubin GR, Kraft TW. Flicker assessment of rod and cone function in a model of retinal degeneration. *Doc Ophthalmol* 2007;115:165-172.
23. Pinilla I, Lund RD, Sauve Y. Contribution of rod and cone pathways to the dark-adapted electroretinogram (ERG) b-wave following retinal degeneration in RCS rats. *Vision Res* 2004;44:2467-2474.
24. Jolly C, Jeanny JC, Behar-Cohen F, Laugier P, Saied A. High-resolution ultrasonography of subretinal structure and assessment of retina degeneration in rat. *Exp Eye Res* 2005;81:592-601.
25. Morimoto T, Fujikado T, Choi JS, et al. Transcorneal electrical stimulation promotes the survival of photoreceptors and preserves retinal function in royal college of surgeons rats. *Invest Ophthalmol Vis Sci* 2007;48:4725-4732.
26. Vollrath D, Feng W, Duncan JL, et al. Correction of the retinal dystrophy phenotype of the RCS rat by viral gene transfer of Mertk. *Proc Natl Acad Sci U S A* 2001;98:12584-12589.
27. Tso MO, Zhang C, Abler AS, et al. Apoptosis leads to photoreceptor degeneration in inherited retinal dystrophy of RCS rats. *Invest Ophthalmol Vis Sci* 1994;35:2693-2699.
28. Katai N, Kikuchi T, Shibuki H, et al. Caspase-like proteases activated in apoptotic photoreceptors of Royal College of Surgeons rats. *Invest Ophthalmol Vis Sci* 1999;40:1802-1807.
29. Perche O, Doly M, Ranchon-Cole I. Transient protective effect of caspase inhibitors in RCS rat. *Exp Eye Res* 2008;86:519-527.
30. Sheedlo HJ, Srinivasan B, Brun-Zinkernagel AM, et al. Expression of p75(NTR) in photoreceptor cells of dystrophic rat retinas. *Brain Res Mol Brain Res* 2002;103:71-79.
31. LaVail MM, Pinto LH, Yasumura D. The interphotoreceptor matrix in rats with inherited retinal dystrophy. *Invest Ophthalmol Vis Sci* 1981;21:658-668.

32. Herron WL, Jr., Riegel BW, Brennan E, Rubin ML. Retinal dystrophy in the pigmented rat. *Invest Ophthalmol* 1974;13:87-94.
33. Valter K, Maslim J, Bowers F, Stone J. Photoreceptor dystrophy in the RCS rat: roles of oxygen, debris, and bFGF. *Invest Ophthalmol Vis Sci* 1998;39:2427-2442.
34. Perche O, Doly M, Ranchon-Cole I. Caspase-dependent apoptosis in light-induced retinal degeneration. *Invest Ophthalmol Vis Sci* 2007;48:2753-2759.
35. Zhang Y, Molday LL, Molday RS, et al. Knockout of cGMP-gated channel β -subunit and GARPs disrupts disk morphogenesis and rod outer segment structural integrity. *Journal of Cell Science* 2009;122.
36. Scholl HP, Langrova H, Weber BH, Zrenner E, Apfelstedt-Sylla E. Clinical electrophysiology of two rod pathways: normative values and clinical application. *Graefes Arch Clin Exp Ophthalmol* 2001;39:71-80.
37. Coile DC, Pollitz CH, Smith JC. Behavioral determination of critical flicker fusion in dogs. *Physiol Behav* 1989;45:1087-1092.
38. Lee BB, Martin PR, Valberg A. Sensitivity of macaque retinal ganglion cells to chromatic and luminance flicker. *J Physiol* 1989;414:223-243.
39. Sokol S, Riggs LA. Electrical and psychophysical responses of the human visual system to periodic variation of luminance. *Invest Ophthalmol* 1971;10:171-180.
40. Van Der Tweel L. Relation between psychophysics and electrophysiology of flicker. *Documenta ophthalmologica* 1964;18:287-304.
41. Schremser JL, Williams TP. Rod outer segment (ROS) renewal as a mechanism for adaptation to a new intensity environment. I. Rhodopsin levels and ROS length. *Exp Eye Res* 1995;61:17-23.
42. Specht S, Organisciak DT, Darrow RM, Leffak M. Continuing damage to rat retinal DNA during darkness following light exposure. *Photochem Photobiol* 2000;71:559-566.

43. Noell WK, Organisciak DT, Ando H, Braniecki MA, Durlin C. Ascorbate and dietary protective mechanisms in retinal light damage of rats: electrophysiological, histological and DNA measurements. *Prog Clin Biol Res* 1987;247:469-483.
44. Hafezi F, Steinbach JP, Marti A, et al. The absence of c-fos prevents light-induced apoptotic cell death of photoreceptors in retinal degeneration in vivo. *Nat Med* 1997;3:346-349.
45. Delmelle M, Noell WK, Organisciak DT. Hereditary retinal dystrophy in the rat: rhodopsin, retinol, vitamin A deficiency. *Exp Eye Res* 1975;21:369-380.
46. Wachtmeister L. Oscillatory potentials in the retina: what do they reveal. *Prog Retin Eye Res* 1998;17:485-521.
47. Layton CJ, Safa R, Osborne NN. Oscillatory potentials and the b-Wave: partial masking and interdependence in dark adaptation and diabetes in the rat. *Graefes Arch Clin Exp Ophthalmol* 2007;245:1335-1345.
48. Ye H, Liu X, Tie H, Sun Y, Li P. Electroretinographic oscillatory potentials in different aged rats: an analysis in the domains of time and frequency. *Yan Ke Xue Bao* 1998;14:27-29.
49. Shankar H, Pesudovs K. Critical flicker fusion test of potential vision. *J Cataract Refract Surg* 2007;33:232-239.

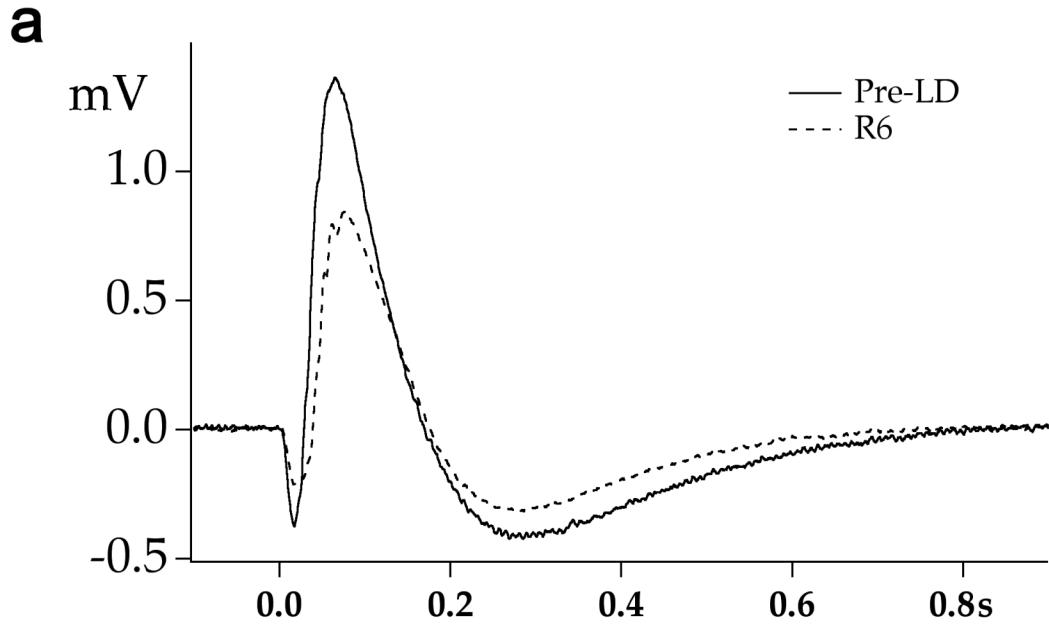


Fig. 20a Dark-adapted ERG response to bright camera flashes before (solid line) and 6 days after (R6 dashed line) a 10-day period of 280 lux constant light. Each trace represents the average of three responses with an inter-stimulus interval of 120 seconds.

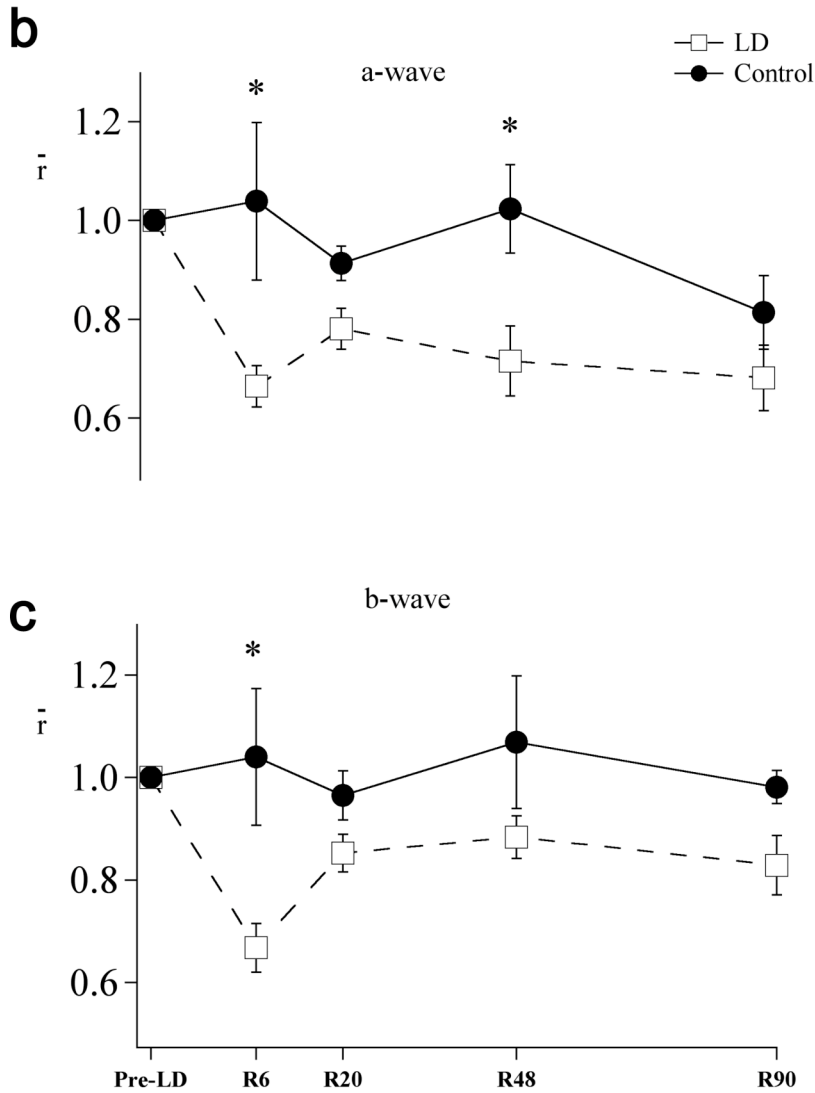


Fig. 20b, 1c Comparison of the dark-adapted flash ERG (Rmax) between light-damaged and control animals for (b) a- and (c) b-waves. Recordings were made before light damage and on Recovery Day (R) 6, 20, 48, and 90. Each animal's response was normalized to its pre-light damage value. Filled circles connected by solid lines show results for control animals (n = 3 to 6). Open squares connected by dashed lines show results for light damaged animals (n = 5 to 10). Error Bars = \pm SEM

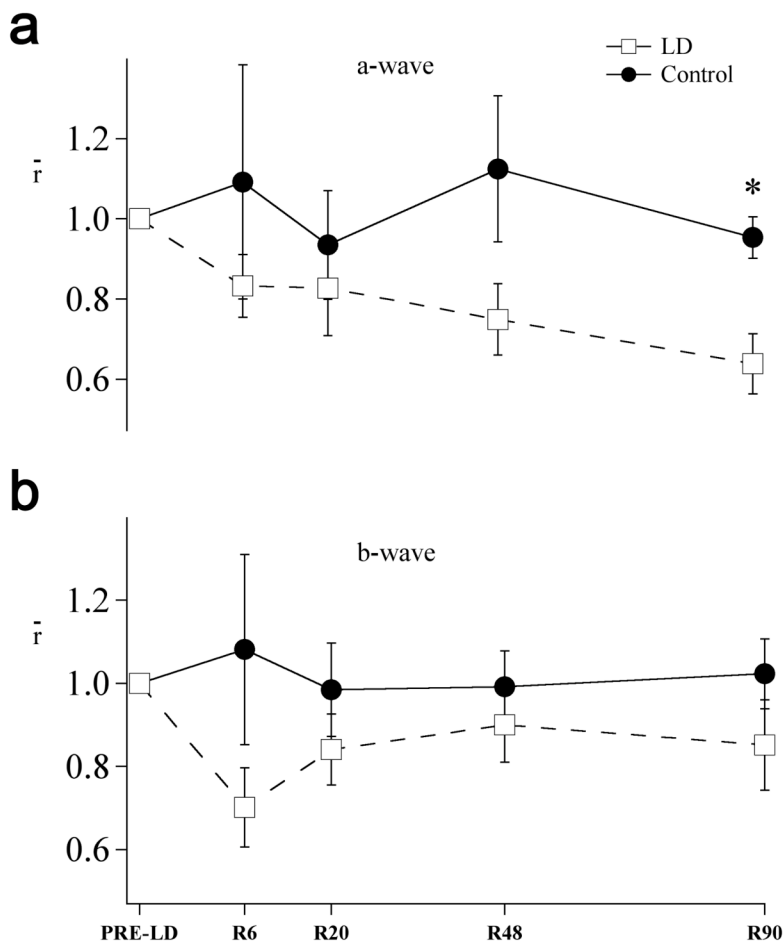


Fig. 21 Light-adapted ERG responses to bright camera flashes on a rod saturating background ($1.691\text{E}+4 \text{ photons } \mu\text{m}^{-2}\text{s}^{-1}$). Recordings were made before light damage and on Recovery Day (R) 6, 20, 48, and 90. Each animal's response was normalized to its pre-light damage value for (a) a-waves and (b) b-waves. Filled circles connected by solid lines show results for control animals ($n = 3$ to 6). Open squares connected by dashed lines show results for light damaged animals ($n = 5$ to 10). Error Bars = \pm SEM

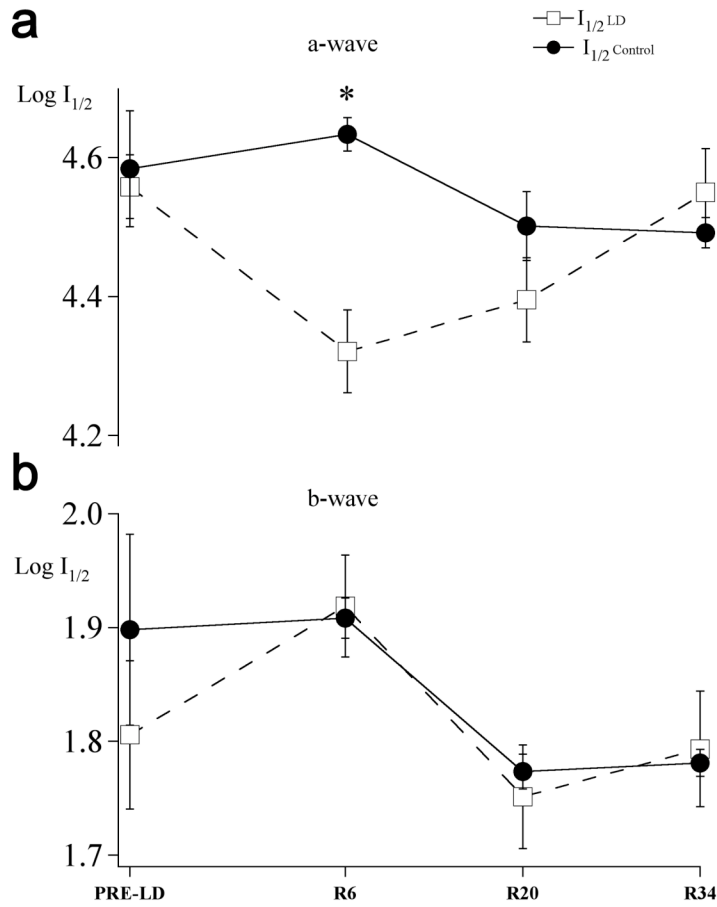


Fig 22. An Intensity Response (IR) series was recorded by progressively increasing flash intensity. Resulting curves were fit by a modified Michaelis function. Sensitivity (Log $I_{1/2}$) for (a) a- and (b) b-waves were calculated before light damage and on R6, R20, and R34. Open squares connected by dashed lines show results for light damaged animals (n = 6 to 10). Filled circles connected by solid lines show results for control animals (n = 3 to 6) Error Bars = \pm SEM

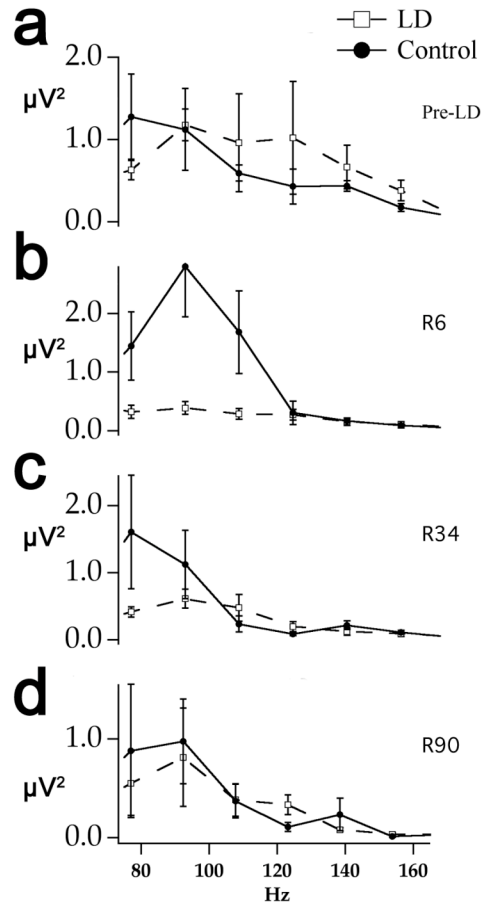


Fig 23. Oscillatory Potential (OP) power spectrum over the 75-165 Hz frequency domain. Traces represent the power from an averaged OP for control (filled circles) and light-damaged (open squares) animals Pre-LD (a) and on R6 (b), R34 (c), and R90 (d). Filled circles connected by solid lines show results for control animals (n = 3 to 6). Open squares connected by dashed lines show results for light damaged animals (n = 5 to 10). Error Bars = \pm SEM

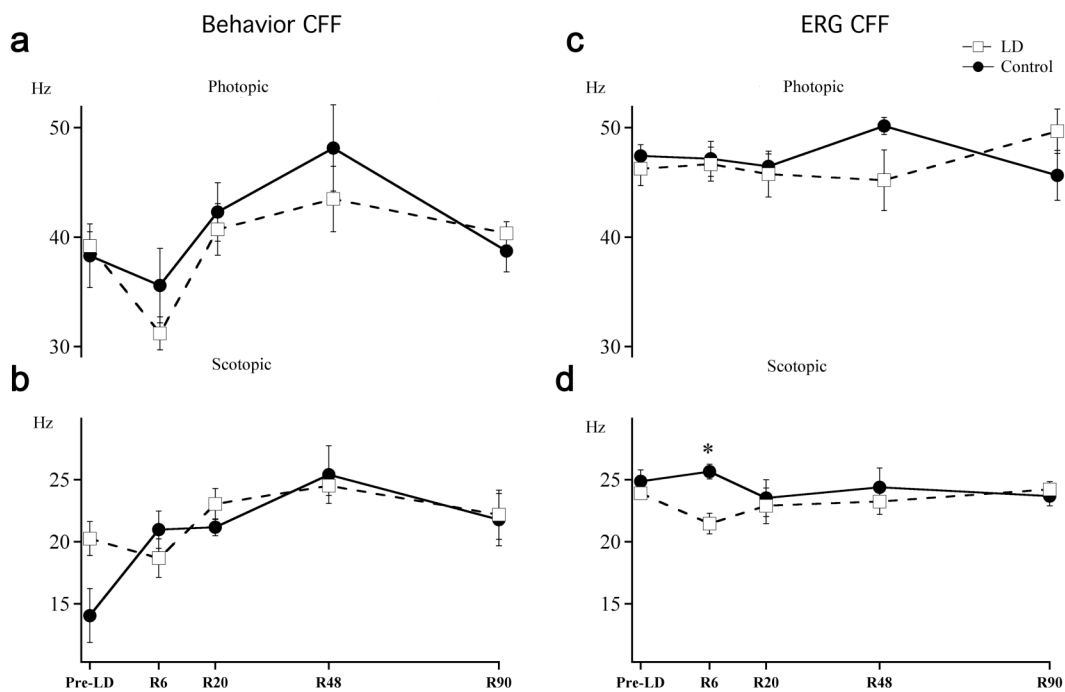


Fig. 24a, 24b Behavior CFF measured by (a) photopic flicker with a time averaged mean intensity of $6.4E+06$ photon/ $\mu\text{m}^2/\text{sec}$. The light source was attenuated by 3 log units of neutral density filtering for (b) scotopic testing. Fig. 24c, 24d ERG CFF for (c) photopic and (d) scotopic intensities were tested on background lights of $3.32E+06$ and $3.81E+03$ photon/ $\mu\text{m}^2/\text{sec}$ incident on the cornea, respectively. Filled circles connected by solid lines show CFF results for control animals ($n = 3$ to 6). Open squares connected by dashed lines show CFF results for light damaged animals ($n = 5$ to 10). All animal's were tested before light damage and on R6, R20, R48, and R90. Error Bars = \pm SEM

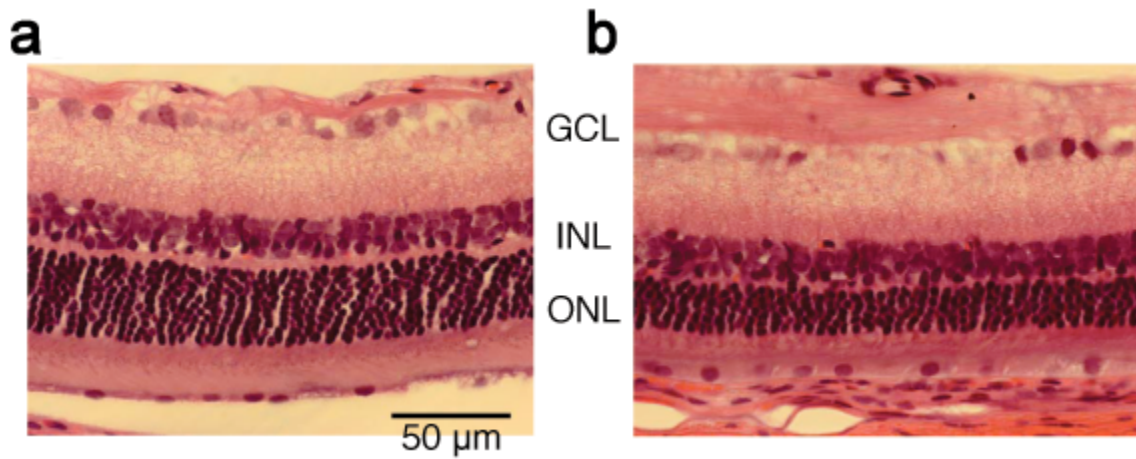


Figure 25 Photographs from a section of retina approximately 1.3 mm inferior to the ONH in a (25a) light damaged and (25b) control animal. Cell body layers labeled from the top of images; GCL (ganglion cell layer), (INL) inner nuclear layer, and ONL (outer nuclear layer).

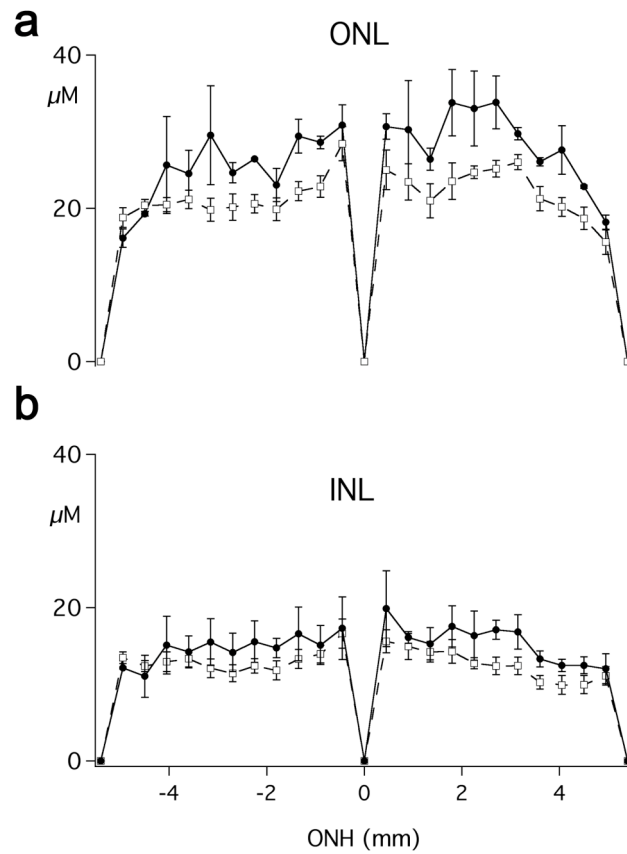


Fig 26. The μM thickness of (a) outer and (b) inner nuclear layers plotted as a function of distance from the ONH. Measures were made within 2-mm superior and inferior from the ONH.

Table 6 Comparison of Dark-Adapted ERG Responses (μV) for Control and Light Damaged Animals; Mean \pm SEM (n).

Animal	<u>a-wave</u>		<u>b-wave</u>	
	Control	LD	Control	LD
Pre-LD	367 \pm 19 (5)	354 \pm 7 (10)	1440 \pm 123(5)	1450 \pm 78 (10)
R6	363 \pm 42 (4)	236 \pm 15 (9)	1420 \pm 144 (4)	930 \pm 64 (9)
R20	313 \pm 9 (3)	277 \pm 20 (7)	1230 \pm 55 (3)	1200 \pm 57 (7)
R48	349 \pm 9 (3)	250 \pm 30 (5)	1350 \pm 49 (3)	1250 \pm 74 (5)
R90	278 \pm 16 (3) (p = 0.15)	237 \pm 5 (5) (p < 0.01)	1260 \pm 126 (3) (p = 0.62)	1180 \pm 95 (5) (p < 0.05)

2-tailed paired t-test: Pre-LD vs R90 (n=3 WT, n=5 LD)

DISCUSSION

Rod versus Cone- driven Flicker Response

Aim

Our goal was to investigate the fidelity of retinal circuits that encode temporal resolution as measured by CFF during a period of retinal degeneration. We expected to observe declines in function and possibly evidence of compensatory mechanisms in the retinal response. The ERG response to high frequency photopic flicker is routinely used for isolating the cone response. Studies in RCS and P23H RP model rats by Pinilla et al.^{138, 194} showed relatively early changes to ERG CFF compared to traditional flash ERG measures. Advantages of using CFF as a metric of retinal function is that it can be obtained from both psychophysical and electrophysiological techniques and it separates rod- versus cone-driven function. We measured CFF in three animal models of retinal degeneration: a traditional model of RP with rapid loss of rods and cones, a knockout mouse where rods fail to develop normally and cones are relatively spared, and a transient insult model that affects primarily rods.

Retinal Function in RCS Rat

Significant deficits to ERG CFF were found in all three animal models. The most dramatic losses we saw were in RCS rats. RCS rats present with retinal

degeneration typical of RP, wherein cones degenerate secondarily to rods. RCS rats exhibit an abnormal ERG response to flashes of light as early as PN18^{121, 133, 134, 136-138}, yet the cone ERG remains normal until PN42¹³⁷. Pinilla et al. were able to detect an early deficit to cone function by measuring the ERG response to photopic flicker. In their study CFF was determined by presenting white flashes (luminance of $1.37 \log \text{ cd s m}^{-2}$) of increasing frequency on a ganzfeld with a background luminance of 29.8 cd m^{-2} . Pinilla et al. found that CFF in RCS rats was significantly reduced (75.5%) at PN28 and declined further thereafter¹³⁸. They did not find a significant reduction in CFF at PN21 their next earliest experimental time point. Pinilla et al. did not measure the ERG response to scotopic flicker. Scotopic CFF is lower than photopic CFF due to slower rod temporal resolution. We were interested in expanding the study of CFF in RCS rat by measuring ERG CFF at both scotopic and photopic intensities in RCS rat.

We measured ERG CFF in RCS rat over a broad range of light intensities at PN23, PN44, and PN64. CFF was reduced across the entire intensity range examined. At PN23 photopic CFF in RCS rat was significantly lower ($p < 0.05$) than in LER rats. This result demonstrates a measurable reduction in CFF before the deficit found by Pinilla et al. In their study of RCS, CFF was reduced compared to control animals at PN21, but was not statistically significant. The significant difference we found at PN23 may be the earliest point that a deficit in RCS cone function can be detected. Scotopic ERG CFF in RCS rats was also significantly reduced at PN23. At a dim scotopic intensity ERG CFF in RCS rat

measured only 66% of control animals. The isolated rod b-wave in RCS animals at this age typically measures about 50% of normal¹³⁷.

At PN44 there was a loss of the lowest 1.5 log units of the rod flicker response intensity range. At this age ERG CFF was reduced to about 50% of normal and there was no longer a clearly discernable rod-cone break. The disappearance of the rod-cone break at PN44 suggests a single generator of the flicker response. Recordings from single rod photoreceptor cells in RCS rat at this age exhibit a reduced sensitivity and an accelerated recovery. The reduction in sensitivity probably accounts for the truncated flicker response at the lower scotopic intensity range. An accelerated recovery may boost temporal resolution, yielding increases to CFF. One could therefore argue that remaining CFF after PN44 is being mediated by rod. However, this seems unlikely since the light adapted b-wave is relatively normal until PN42, so there is no reason to suspect that cone function is impaired. However, there is evidence to suggest that the maximum b-wave and threshold flicker responses are not directly correlated to one another as we will discuss next.

Retinal Function in Cngb1 GARP Knockout Mouse

A recently created Cngb1-x1 knockout mouse by Zhang et al. lacks both β subunits of the CNG channel and GARP proteins^{184-186, 195}. This transgenic model differs from a separately reported β subunit knockout mouse (Cngb1-x26) that targeted only the channel like region, but does not effect GARP expression. In Cngb1-x26 the retina exhibits a slow RP-like degeneration. In single cell

recordings the vast majority of rod photoreceptors did not respond to light. ERG recordings also indicated an extinguished rod response. The *Cngb1-x1* knockout mouse also presents with slow RP type degeneration. However, *Cngb1-x1* rod photoreceptors have a reduced but measurable rod response in single cell recordings. We further characterized the *Cngb1-x1* knockout mouse by recording the ERG response to flash and flicker stimuli over the first four months of life and we extended the investigation to the cone-driven system.

We evaluated rod function in *Cngb* knockout mice by measuring b-wave sensitivity. Threshold for generating an ERG b-wave response in *Cngb* knockout mice is raised by 2.8 log units. Although severely reduced, this response is 100-fold better than threshold in the rodless, rhodopsin knockout mouse¹⁹⁶, indicating a significant amount of remaining rod function, however this rod-driven retinal function declines over time. Dark-adapted b-wave sensitivity ($I_{1/2}$) was also determined by fitting an intensity-response series with a Naka-Rushton function. *Cngb* knockout mice are 26-fold less sensitive than wild type litter-mates. This result is consistent with a 34-fold loss of sensitivity measured in one-month old *Cngb* knockout mice in single cell recordings¹⁹⁷.

We tracked the b-wave response under dark- and light adapted conditions in *Cngb* knockout mice over the first 4 months of life. At PN30 the maximum dark-adapted b-wave was 50% of wild type mice, while the maximum light-adapted b-wave was not significantly different. The implicit time of the b-wave was also significantly longer under both dark- and light- adapted conditions. Over the next 4 months there is a rapid and significant loss to both dark-and

light- adapted b-wave. The dark-adapted b-wave declines to about 10% of wild type by 4 months old, while the light-adapted b-wave amplitude declines to about 25% of wild type. The changes to b-wave amplitude, sensitivity, and implicit times in Cngb1 knockout mice confirm a progressive RP degeneration with initial rod loss followed by cone loss.

Cngb1 knockout mice also exhibit conspicuous reductions to CFF over the scotopic intensity range at all ages. ERG CFF was determined over a broad range of intensities in Cngb1 knockout and wild type mice at PN32, PN75, and PN91. There was no detectable flicker response over the lowest three log units tested, which was similar to our result in RCS at PN64. In both RCS rats and Cngb1 knockout mice the sensitivity of b-wave is reduced and implicit times are longer. This decrease in sensitivity means that a greater stimulus intensity is required in order to produce a half maximal or threshold response. The reductions in sensitivity may therefore be due to the loss of the flicker response over the lower end of the scotopic range in both Cngb1 knockout mice and RCS rats. In contrast, the light damage model did not show significant changes in b-wave sensitivity or implicit time. In this light damage model there was no truncation of the flicker response range, but light damage was mild (<30%) compared to rod loss late in the life of RCS rat or Cngb1 knockout mouse.

ERG CFF measured significantly lower in the scotopic range, reflecting the physiological result that remaining rod function in Cngb1 knockout mice is impaired. At the upper end of our intensity range the cone-driven ERG CFF in knockout mice falls within the range of the wild type mice. Over the course of 3

months testing, there was no significant decline in cone ERG CFF. This is surprising considering the progressive loss of light-adapted b-wave amplitude. One explanation for this apparent contradiction is that the two tests are measuring different functional aspects of the cone pathways in the retina. Thresholds may play a more important role in mediating visual function, while maximum responses are a better indicator the degenerative condition.

ERG Measures of Retinal Function in a Light Damaged Albino Rat

Retinal degeneration is produced in freely roaming albino rats by continuous light exposure. The magnitude of effect depends on stimulus intensity, wavelength, and duration of exposure. Our aim was to produce partial retinal degeneration using 10-days of continuous exposure to white fluorescent light. This model may help inform us of how the visual system responds to a temporary and damaging insult. Similar partial damage might occur if retinal degeneration was successfully constrained by treatment. Furthermore, it is unclear whether rod- or cone-driven function is more vulnerable to light damage. Anatomical studies suggest that there is greater rod loss, however impaired photopic function has also been demonstrated.

We measured the ERG response in light damaged albino rats to flashes of light under dark- and light-adapted conditions. There was about a 30% permanent loss to the dark-adapted a-wave. However, the light adapted a-wave amplitude measured 83% of pre-damage levels immediately after light damage, but it declined to only 64% of Pre-LD value by the end of our study. At the same

time the light-adapted a-wave in control animals also declined to 84% of pre-sham damage value. This apparent delayed decline in cone function in both groups may be caused by degeneration stemming from the background illumination provided in our animal housing room or may be the result of normal ageing. Alternatively, the larger decline in the experimental group may also be due to the light damage exposure period, since delayed photoreceptor loss has been reported after exposure to high intensity light^{158, 198-202}. If there is delayed cone loss unique to light damage then the deficit measured might be proportional to the interval of time following damage. This may bias longer-term studies toward a conclusion that cones are more vulnerable to light damage. TUNEL staining for apoptotic markers in ONL could help to confirm delayed photoreceptor loss.

Dark- and light- adapted b-wave amplitudes were reduced about 30% immediately after light damage, however both recovered to over 80%. The b-wave's recovery following light damage necessarily depends on an increased photoreceptor input or response gain. The a-wave losses discussed earlier contradict the idea of a larger photoreceptor input. This suggests gain in the response of the bipolar cells or at the site of rod-bipolar synapse. Also, it is known that the bipolar cells have a highly non-linear synaptic gain in responses to contrast²⁰³. The bipolar cell response gain may be mediated by the sprouting of new bipolar cell dendrites. Sprouting of bipolar cell dendrites has been previously reported as a possible compensatory mechanism in rodents during

normal aging and RP^{204, 205}. Staining for bipolar cells after low-intensity light damage could identify morphological changes to the cell's dendritic structure.

Measuring the intensity response series showed increased a-wave sensitivity ($I_{1/2}$) until R34. The change in sensitivity indicates that a half maximal response could be evoked by a less intense stimulus following light damage. Since this gain in sensitivity is not apparent in single cell recordings in light damage animals (Wen, Y 2008), it could possibly be due to unmasking of the a-wave due to delays in the b-wave implicit time.

ERG CFF has not been previously measured in light damaged albino rats. There was a small, but significant decline in scotopic ERG CFF immediately following light damage. The scotopic ERG CFF recovered by our next experimental time point, 14 days later. There was no measurable change in photopic ERG CFF at anytime. We expected to see larger reductions to CFF in this model given the reductions in b-wave amplitude. The reduction in scotopic ERG CFF was relatively small and transitory. The relative maintenance of a near threshold flicker signal compared to the maximum response suggests that different mechanisms are responsible for mediating threshold and maximum responses.

Summary of ERG Findings

We hypothesized that ERG CFF would be a sensitive indicator of rod- versus cone-driven visual function. We tested this by measuring scotopic and photopic CFF in three rodent models of retinal degeneration. The results from these

animal models are contradictory and surprising. We expected to see progressive declines of CFF in RCS rats and Cngb mice. In these two genetic models there is a progressive loss of dark- and light-adapted b-wave amplitudes. However, dramatic and progressive losses to CFF were only formed in RCS rats. In Cngb knockout mice scotopic CFF was greatly reduced, but CFF was stable. In the light damage model there was significant reductions to both dark- and light-adapted b-waves. However there was no change in photopic CFF and only minor and transitory reduction in scotopic ERG CFF. Overall, these results suggest that maximum responses are a more sensitive way of detecting retinal degeneration. And that threshold measures may be more important for visual function, which we will discuss further in the next section. These threshold responses may be vulnerable only under special pathological conditions. In RCS rat, for example, there is a debris zone, which may interfere with the diffusion of metabolites ¹²⁷. The lower CFF may therefore be a product of the retina's chronic unmet metabolic demand. In contrast, RPE and associated metabolic pathways are relatively preserved in Cngb knockout mouse and low intensity light damaged rat models.

Behavioral Versus ERG CFF

Another goal of our research was to compare ERG and behavioral measures of CFF. RCS rat and Cngb knockout mouse contain a genetic form of retinal degeneration. In such a model training on a behavioral task would have been complicated by ongoing degeneration. We therefore chose to investigate

the relationship between ERG and behavior in an albino rat light damage model of retinal degeneration. Albino rats were trained to discriminate steady from flickering light in a water maze before receiving 10-days continuous exposure to 280-lux fluorescent light. Preliminary data suggested that this level of exposure would lead to a 30% reduction in ONL thickness in freely roaming animals.

Measures of ERG and behavioral CFF were made before the exposure period and at regular intervals over a 90-day recovery period. Overall we found no change in scotopic CFF following light damage. The small decline in scotopic ERG CFF found at R6 was transient and recovered by our next experimental time point. There was no measurable change in photopic ERG CFF. Scotopic behavioral CFF in light-damaged animals was not significantly different than controls. Photopic behavioral CFF measured slightly, but significantly lower after light damage until R90.

A previous study by Williams et al. of behavior in light damaged rat showed apparently greater deficit to photopic over scotopic visual function. In this study 3-month old albino rats were exposed for eight days to 700-lux light. A psychophysical technique was used to measure behavioral CFF. Rats were tested for 1-month following light damage. Williams et al. found pronounced downward shift in the CFF curve over the 6-log unit intensity range tested. The largest differences were found at photopic intensities. These losses were permanent and histology showed a 90% loss of photoreceptor layer.

In our light damaged animals we did not find the conspicuous losses to behavioral CFF reported by Williams et al. There was no measurable deficit in

scotopic CFF. Photopic CFFs were slightly lower on average than in control animals. This result although not pronounced seems to confirm the greater reduction to photopic CFF after light damage. Surprisingly, this is contrary to the changes we found to ERG CFF, which was temporarily lower after light damage only at the scotopic intensity. The transitory losses to scotopic ERG CFF may be due to the phenomenon of photostasis²⁰⁶, in which the length of the rod outer-segments shortens with respect to the quantal photon catch per day. Williams et al. found a reduction in ONL thickness of 90%. By comparison in our study the ONL was only reduced by 22%. It seems the threshold for causing significant and permanent damage to visual function is at a middling intensity between these two studies. The next experiment should test 50% loss of rods.

We compared a 3 μ V criterion of response used for determining ERG CFF, with our behavioral criterion of 75% correct in the 2-alternative forced choice testing. ERG CFF measured slightly higher on average than behavioral CFF. Similar results have been reported in primates^{115, 207}.

In control animals scotopic ERG CFF measured significantly higher than scotopic behavioral CFF. In light damaged animals both scotopic and photopic ERG CFF was significantly higher than in controls. This suggests that after light damage a larger ERG signal is required in order to mediate the behavioral detection of a threshold flicker signal for cone driven visual function. We also tested an alternative ERG criterion of 5 μ V in order to find an electrophysiological criterion, which better represented psychophysical threshold. There was no statistical difference between electrophysiological and behavioral CFF in either

control or light-damaged animals, with respect to this higher 5 μ V criterion amplitude. This finding indicates that there is a fair correspondence between behavioral and ERG thresholds. It is difficult to predict how the behavioral threshold may change if there was a larger reduction to ERG CFF. Unfortunately, the exposure period we used did not produce the expected deficit.

Contrary to our expectations the ERG thresholds were better preserved than ERG maximum amplitudes. These findings depict a visual system that is able to detect near threshold physiological responses in spite of significant neurological loss or cell death. In fact, the visual system seems weighted towards the preservation of the threshold sensitivity at the expense of the maximum response. In general, the maximum response may be a better indicator of retinal degeneration. However, the CFF can inform us of when visual function is impaired. The goal in treating retinal degeneration is to preserve or restore visual function. Understanding the relationship between the maximum and threshold responses may inform us of the likely outcome from an attempt at therapeutic rescue. This information would thus prove valuable in the clinic.

References

1. Buttery RG, Hinrichsen CF, Weller WL, Haight JR. How thick should a retina be? A comparative study of mammalian species with and without intraretinal vasculature. *Vision Res* 1991;31:169-187.
2. Massey SC. Functional Anatomy of the Mammalian Retina. In: Ryan SJ (ed), *Retina*: MOSBY; 2006:43-82.
3. Wassle H, Boycott BB. Functional architecture of the mammalian retina. *Physiol Rev* 1991;71:447-480.
4. Massey SC, O'Brien JJ, Trexler EB, et al. Multiple neuronal connexins in the mammalian retina. *Cell Commun Adhes* 2003;10:425-430.
5. Bowmaker JK. Evolution of vertebrate visual pigments. *Vision Res* 2008;48:2022-2041.
6. Fu Y, Yau KW. Phototransduction in mouse rods and cones. *Pflugers Arch* 2007;454:805-819.
7. Arshavsky V. Like night and day: rods and cones have different pigment regeneration pathways. *Neuron* 2002;36:1-3.
8. Kawamura S, Tachibanaki S. Rod and cone photoreceptors: molecular basis of the difference in their physiology. *Comp Biochem Physiol A Mol Integr Physiol* 2008;150:369-377.
9. Cajal SRy. Figure of the Retina. In: retina.png (ed): Wikipedia.
10. Hargrave PA, McDowell JH. Rhodopsin and phototransduction: a model system for G protein-linked receptors. *Faseb J* 1992;6:2323-2331.

11. Zigmond MJ. *Fundamental neuroscience*. San Diego: Academic Press; 1999:xvi, 1600 p.
12. Kwok-Keung Fung B, Stryer L. Photolyzed rhodopsin catalyzes the exchange of GTP for bound GDP in retinal rod outer segments. *Proc Natl Acad Sci U S A* 1980;77:2500-2504.
13. Grant JE, Guo LW, Vestling MM, Martemyanov KA, Arshavsky VY, Ruoho AE. The N terminus of GTP gamma S-activated transducin alpha-subunit interacts with the C terminus of the cGMP phosphodiesterase gamma-subunit. *J Biol Chem* 2006;281:6194-6202.
14. Stryer L. Cyclic GMP cascade of vision. *Annu Rev Neurosci* 1986;9:87-119.
15. Baehr PAP, K. Vertebrate phototransduction. *Trends in Neurosciences* 1996;19:547-554.
16. Schmitz Y, Witkovsky P. Glutamate release by the intact light-responsive photoreceptor layer of the *Xenopus* retina. *J Neurosci Methods* 1996;68:55-60.
17. Copenhagen DR, Jahr CE. Release of endogenous excitatory amino acids from turtle photoreceptors. *Nature* 1989;341:536-539.
18. Winkler BS. Glycolytic and oxidative metabolism in relation to retinal function. *J Gen Physiol* 1981;77:667-692.
19. Strauss O. The retinal pigment epithelium in visual function. *Physiol Rev* 2005;85:845-881.
20. Steinberg RH. Interactions between the retinal pigment epithelium and the neural retina. *Doc Ophthalmol* 1985;60:327-346.
21. Bok D. The retinal pigment epithelium: a versatile partner in vision. *J Cell Sci Suppl* 1993;17:189-195.
22. Hartong DT, Berson EL, Dryja TP. Retinitis pigmentosa. *Lancet* 2006;368:1795-1809.

23. Wang DY, Chan WM, Tam PO, et al. Gene mutations in retinitis pigmentosa and their clinical implications
Perspective on genes and mutations causing retinitis pigmentosa. *Clin Chim Acta* 2005;351:5-16.
24. Daiger SP, Bowne SJ, Sullivan LS. Perspective on genes and mutations causing retinitis pigmentosa. *Arch Ophthalmol* 2007;125:151-158.
25. Rebello G, Ramesar R, Vorster A, et al. Apoptosis-inducing signal sequence mutation in carbonic anhydrase IV identified in patients with the RP17 form of retinitis pigmentosa. *Proc Natl Acad Sci U S A* 2004;101:6617-6622.
26. Gal A, Li Y, Thompson DA, et al. Mutations in MERTK, the human orthologue of the RCS rat retinal dystrophy gene, cause retinitis pigmentosa. *Nat Genet* 2000;26:270-271.
27. Mohand-Said S, Hicks D, Leveillard T, Picaud S, Porto F, Sahel JA. Rod-cone interactions: developmental and clinical significance. *Prog Retin Eye Res* 2001;20:451-467.
28. Delyfer MN, Leveillard T, Mohand-Said S, Hicks D, Picaud S, Sahel JA. Inherited retinal degenerations: therapeutic prospects. *Biol Cell* 2004;96:261-269.
29. Hamel CP. Cone rod dystrophies. *Orphanet J Rare Dis* 2007;2:7.
30. Milam AH, Li ZY, Fariss RN. Histopathology of the human retina in retinitis pigmentosa. *Prog Retin Eye Res* 1998;17:175-205.
31. Sahel JA, Mohand-Said S, Leveillard T, Hicks D, Picaud S, Dreyfus H. Rod-cone interdependence: implications for therapy of photoreceptor cell diseases. *Prog Brain Res* 2001;131:649-661.
32. Lorentz O, Sahel J, Mohand-Said S, Leveillard T. Cone Survival: Identification of RdCVF. *Retinal Degenerative Diseases*; 2006:315.
33. Lorentz O, Sahel J, Mohand-Said S, Leveillard T. Cone survival: identification of RdCVF. *Adv Exp Med Biol* 2006;572:315-319.

34. Sahel JA. Saving cone cells in hereditary rod diseases: a possible role for rod-derived cone viability factor (RdCVF) therapy. *Retina* 2005;25:S38-S39.
35. Mohand-Said S, Hicks D, Simonutti M, et al. Photoreceptor transplants increase host cone survival in the retinal degeneration (rd) mouse. *Ophthalmic Res* 1997;29:290-297.
36. Mohand-Said S, Deudon-Combe A, Hicks D, et al. Normal retina releases a diffusible factor stimulating cone survival in the retinal degeneration mouse. *Proc Natl Acad Sci U S A* 1998;95:8357-8362.
37. Fintz AC, Audo I, Hicks D, Mohand-Said S, Leveillard T, Sahel J. Partial characterization of retina-derived cone neuroprotection in two culture models of photoreceptor degeneration. *Invest Ophthalmol Vis Sci* 2003;44:818-825.
38. Chalmel F, Leveillard T, Jaillard C, et al. Rod-derived Cone Viability Factor-2 is a novel bifunctional-thioredoxin-like protein with therapeutic potential. *BMC Mol Biol* 2007;8:74.
39. Murakami Y, Ikeda Y, Yonemitsu Y, et al. Inhibition of nuclear translocation of apoptosis-inducing factor is an essential mechanism of the neuroprotective activity of pigment epithelium-derived factor in a rat model of retinal degeneration. *Am J Pathol* 2008;173:1326-1338.
40. Cao W, Tombran-Tink J, Elias R, Sezate S, Mrazek D, McGinnis JF. In vivo protection of photoreceptors from light damage by pigment epithelium-derived factor. *Invest Ophthalmol Vis Sci* 2001;42:1646-1652.
41. Miyazaki M, Ikeda Y, Yonemitsu Y, et al. Synergistic neuroprotective effect via simian lentiviral vector-mediated simultaneous gene transfer of human pigment epithelium-derived factor and human fibroblast growth factor-2 in rodent models of retinitis pigmentosa. *J Gene Med* 2008.
42. Perry J, Du J, Kjeldbye H, Gouras P. The effects of bFGF on RCS rat eyes. *Curr Eye Res* 1995;14:585-592.
43. Cayouette M, Gravel C. Adenovirus-mediated gene transfer of ciliary neurotrophic factor can prevent photoreceptor degeneration in the retinal degeneration (rd) mouse. *Hum Gene Ther* 1997;8:423-430.

44. LaVail MM, Yasumura D, Matthes MT, et al. Protection of mouse photoreceptors by survival factors in retinal degenerations. *Invest Ophthalmol Vis Sci* 1998;39:592-602.
45. Liang FQ, Dejneka NS, Cohen DR, et al. AAV-mediated delivery of ciliary neurotrophic factor prolongs photoreceptor survival in the rhodopsin knockout mouse. *Mol Ther* 2001;3:241-248.
46. Bok D, Yasumura D, Matthes MT, et al. Effects of adeno-associated virus-vectored ciliary neurotrophic factor on retinal structure and function in mice with a P216L rds/peripherin mutation. *Exp Eye Res* 2002;74:719-735.
47. Frasson M, Picaud S, Leveillard T, et al. Glial cell line-derived neurotrophic factor induces histologic and functional protection of rod photoreceptors in the rd/rd mouse. *Invest Ophthalmol Vis Sci* 1999;40:2724-2734.
48. Buch PK, MacLaren RE, Duran Y, et al. In contrast to AAV-mediated Cntf expression, AAV-mediated Gdnf expression enhances gene replacement therapy in rodent models of retinal degeneration. *Mol Ther* 2006;14:700-709.
49. Leveillard T, Mohand-Said S, Lorentz O, et al. Identification and characterization of rod-derived cone viability factor. *Nat Genet* 2004;36:755-759.
50. McGill TJ, Prusky GT, Douglas RM, et al. Intraocular CNTF reduces vision in normal rats in a dose-dependent manner. *Invest Ophthalmol Vis Sci* 2007;48:5756-5766.
51. Beltran WA, Wen R, Acland GM, Aguirre GD. Intravitreal injection of ciliary neurotrophic factor (CNTF) causes peripheral remodeling and does not prevent photoreceptor loss in canine RPGR mutant retina. *Exp Eye Res* 2007;84:753-771.
52. Kent TL, Glybina IV, Abrams GW, Iezzi R. Chronic intravitreal infusion of ciliary neurotrophic factor modulates electrical retinal stimulation thresholds in the RCS rat. *Invest Ophthalmol Vis Sci* 2008;49:372-379.
53. Beltran WA. On the role of CNTF as a potential therapy for retinal degeneration: Dr. Jekyll or Mr. Hyde? *Adv Exp Med Biol* 2008;613:45-51.

54. Granit R, Riddell LA. The electrical responses of light- and dark-adapted frogs' eyes to rhythmic and continuous stimuli. *J Physiol* 1934;81:1-28.
55. Granit R. *Sensory mechanisms of the retina, with an appendix on electroretinography*. New York: Hafner; 1963:xxiii, 412 p.
56. Hood DC, Birch DG. Human cone receptor activity: the leading edge of the a-wave and models of receptor activity. *Vis Neurosci* 1993;10:857-871.
57. Hood DC, Birch DG. Light adaptation of human rod receptors: the leading edge of the human a-wave and models of rod receptor activity. *Vision Res* 1993;33:1605-1618.
58. Hood DC, Birch DG. A quantitative measure of the electrical activity of human rod photoreceptors using electroretinography. *Vis Neurosci* 1990;5:379-387.
59. Hood DC, Birch DG. The A-wave of the human electroretinogram and rod receptor function. *Invest Ophthalmol Vis Sci* 1990;31:2070-2081.
60. Robson JG, Frishman LJ. Response linearity and kinetics of the cat retina: the bipolar cell component of the dark-adapted electroretinogram. *Vis Neurosci* 1995;12:837-850.
61. Hood DC, Birch DG. Beta wave of the scotopic (rod) electroretinogram as a measure of the activity of human on-bipolar cells. *J Opt Soc Am A Opt Image Sci Vis* 1996;13:623-633.
62. Xu X, Karwoski C. Current source density analysis of the electroretinographic d wave of frog retina. *J Neurophysiol* 1995;73:2459-2469.
63. Sieving PA, Murayama K, Naarendorp F. Push-pull model of the primate photopic electroretinogram: a role for hyperpolarizing neurons in shaping the b-wave. *Vis Neurosci* 1994;11:519-532.
64. Oakley B, 2nd, Green DG. Correlation of light-induced changes in retinal extracellular potassium concentration with c-wave of the electroretinogram. *J Neurophysiol* 1976;39:1117-1133.

65. Xu X, Karwoski CJ. Current source density analysis of retinal field potentials. II. Pharmacological analysis of the b-wave and M-wave. *J Neurophysiol* 1994;72:96-105.
66. Steinberg RH, Linsenmeier RA, Griff ER. Retinal pigment epithelial cell contributions to the electroretinogram. *Progress in retinal research* 1985;4:33-66.
67. Kofuji P, Ceelen P, Zahs KR, Surbeck LW, Lester HA, Newman EA. Genetic inactivation of an inwardly rectifying potassium channel (Kir4.1 subunit) in mice: phenotypic impact in retina. *J Neurosci* 2000;20:5733-5740.
68. Wachtmeister L. Oscillatory potentials in the retina: what do they reveal. *Prog Retin Eye Res* 1998;17:485-521.
69. Dong CJ, Agey P, Hare WA. Origins of the electroretinogram oscillatory potentials in the rabbit retina. *Vis Neurosci* 2004;21:533-543.
70. Wachtmeister L, Dowling JE. The oscillatory potentials of the mudpuppy retina. *Invest Ophthalmol Vis Sci* 1978;17:1176-1188.
71. Ogden TE. The oscillatory waves of the primate electroretinogram. *Vision Res* 1973;13:1059-1074.
72. Layton CJ, Safa R, Osborne NN. Oscillatory potentials and the b-Wave: partial masking and interdependence in dark adaptation and diabetes in the rat. *Graefes Arch Clin Exp Ophthalmol* 2007;245:1335-1345.
73. Takahashi T, Machida S, Masuda T, Mukaida Y, Tazawa Y. Functional changes in rod and cone pathways after photoreceptor loss in light-damaged rats. *Curr Eye Res* 2005;30:703-713.
74. Yu M, Peachey NS. Attenuation of oscillatory potentials in nob2 mice. *Doc Ophthalmol* 2007;115:173-186.
75. Heckenlively JR, Martin DA, Rosenbaum AL. Loss of electroretinographic oscillatory potentials, optic atrophy, and dysplasia in congenital stationary night blindness. *Am J Ophthalmol* 1983;96:526-534.

76. Akula JD, Mocko JA, Moskowitz A, Hansen RM, Fulton AB. The oscillatory potentials of the dark-adapted electroretinogram in retinopathy of prematurity. *Invest Ophthalmol Vis Sci* 2007;48:5788-5797.
77. Liu K, Akula JD, Hansen RM, Moskowitz A, Kleinman MS, Fulton AB. Development of the electroretinographic oscillatory potentials in normal and ROP rats. *Invest Ophthalmol Vis Sci* 2006;47:5447-5452.
78. Ponte F, Anastasi M, Lauricella MR. Retinitis pigmentosa and inner retina. Functional study by means of oscillatory potentials of the electroretinogram. *Doc Ophthalmol* 1989;73:337-346.
79. Wu X. [Oscillatory potentials in retinitis pigmentosa with TCM treatment]. *Zhongguo Yi Xue Ke Xue Yuan Xue Bao* 1995;17:30-35.
80. Carleton KL, Spady TC, Cote RH. Rod and cone opsin families differ in spectral tuning domains but not signal transducing domains as judged by saturated evolutionary trace analysis. *J Mol Evol* 2005;61:75-89.
81. Sandberg MA, Miller S, Berson EL. Rod electroretinograms in an elevated cyclic guanosine monophosphate-type human retinal degeneration. Comparison with retinitis pigmentosa. *Invest Ophthalmol Vis Sci* 1990;31:2283-2287.
82. Bowmaker JK, Dartnall HJ. Visual pigments of rods and cones in a human retina. *J Physiol* 1980;298:501-511.
83. Verdon WA, Schneck ME, Haegerstrom-Portnoy G. A comparison of three techniques to estimate the human dark-adapted cone electroretinogram. *Vision Res* 2003;43:2089-2099.
84. Zrenner E, Nowicki J, Adamczyk R. Cone function and cone interaction in hereditary degenerations of the central retina. *Doc Ophthalmol* 1986;62:5-12.
85. Greenstein VC, Zaidi Q, Hood DC, Spehar B, Cideciyan AV, Jacobson SG. The enhanced S cone syndrome: an analysis of receptor and post-receptor changes. *Vision Res* 1996;36:3711-3722.
86. Neitz J, Jacobs GH. Reexamination of spectral mechanisms in the rat (*Rattus norvegicus*). *J Comp Psychol* 1986;100:21-29.

87. Hood DC, Birch DG. Phototransduction in human cones measured using the alpha-wave of the ERG. *Vision Res* 1995;35:2801-2810.
88. Pepperberg DR, Birch DG, Hood DC. Photoresponses of human rods in vivo derived from paired-flash electroretinograms. *Vis Neurosci* 1997;14:73-82.
89. Friedburg C, Allen CP, Mason PJ, Lamb TD. Contribution of cone photoreceptors and post-receptoral mechanisms to the human photopic electroretinogram. *J Physiol* 2004;556:819-834.
90. Bui BV, Fortune B. Origin of electroretinogram amplitude growth during light adaptation in pigmented rats. *Vis Neurosci* 2006;23:155-167.
91. Schnapf JL, Kraft TW, Nunn BJ, Baylor DA. Spectral sensitivity of primate photoreceptors. *Vis Neurosci* 1988;1:255-261.
92. Yau KW. Phototransduction mechanism in retinal rods and cones. The Friedenwald Lecture. *Invest Ophthalmol Vis Sci* 1994;35:9-32.
93. Marmor MF, Holder GE, Seeliger MW, Yamamoto S. Standard for clinical electroretinography (2004 update). *Doc Ophthalmol* 2004;108:107-114.
94. Bush RA, Sieving PA. Inner retinal contributions to the primate photopic fast flicker electroretinogram. *J Opt Soc Am A Opt Image Sci Vis* 1996;13:557-565.
95. Burns SA, Elsner AE, Kreitz MR. Analysis of nonlinearities in the flicker ERG. *Optom Vis Sci* 1992;69:95-105.
96. Odom JV, Reits D, Burgers N, Riemslag FC. Flicker electroretinograms: a systems analytic approach. *Optom Vis Sci* 1992;69:106-116.
97. Baron WS, Boynton RM. Response of primate cones to sinusoidally flickering homochromatic stimuli. *J Physiol* 1975;246:311-331.
98. Baron WS, Boynton RM, Hammon RW. Component analysis of the foveal local electroretinogram elicited with sinusoidal flicker. *Vision Res* 1979;19:479-490.

99. Baron WS, Boynton RM, van Norren D. Primate cone sensitivity to flicker during light and dark adaptation as indicated by the foveal local electroretinogram. *Vision Res* 1979;19:109-116.
100. Donovan WJ, Baron WS. Identification of the R-G-cone difference signal in the corneal electroretinogram of the primate. *J Opt Soc Am* 1982;72:1014-1020.
101. Abraham FA, Alpern M. Factors influencing threshold of the fundamental electrical response to sinusoidal excitation of human photoreceptors. *J Physiol* 1984;357:151-172.
102. Abraham FA, Alpern M, Kirk DB. Electroretinograms evoked by sinusoidal excitation of human cones. *J Physiol* 1985;363:135-150.
103. Slaughter MM, Miller RF. 2-amino-4-phosphonobutyric acid: a new pharmacological tool for retina research. *Science* 1981;211:182-185.
104. Slaughter MM, Miller RF. An excitatory amino acid antagonist blocks cone input to sign-conserving second-order retinal neurons. *Science* 1983;219:1230-1232.
105. Kondo M, Sieving PA. Primate photopic sine-wave flicker ERG: vector modeling analysis of component origins using glutamate analogs. *Invest Ophthalmol Vis Sci* 2001;42:305-312.
106. Krishna VR, Alexander KR, Peachey NS. Temporal properties of the mouse cone electroretinogram. *J Neurophysiol* 2002;87:42-48.
107. Viswanathan S, Frishman LJ, Robson JG. Inner-retinal contributions to the photopic sinusoidal flicker electroretinogram of macaques. Macaque photopic sinusoidal flicker ERG. *Doc Ophthalmol* 2002;105:223-242.
108. Stockman A, Sharpe LT, Zrenner E, Nordby K. Slow and fast pathways in the human rod visual system: electrophysiology and psychophysics. *J Opt Soc Am A* 1991;8:1657-1665.
109. Sharpe LT, Stockman A, MacLeod DI. Rod flicker perception: scotopic duality, phase lags and destructive interference. *Vision Res* 1989;29:1539-1559.

110. MacLeod DI. Rods cancel cones in flicker. *Nature* 1972;235:173-174.
111. Hecht S, Smith EL. Intermittent stimulation by light. VI. Area and the relation between critical frequency and intensity. *J Gen Physiol* 1936;19:979-991.
112. Corwin TR, Dunlap WP. The shape of the high frequency flicker sensitivity curve. *Vision Res* 1987;27:2119-2123.
113. Landis C. Determinants of the critical flicker-fusion threshold. *Physiol Rev* 1954;34:259-286.
114. Spekreijse H, van Norren D, van den Berg TJ. Flicker responses in monkey lateral geniculate nucleus and human perception of flicker. *Proc Natl Acad Sci U S A* 1971;68:2802-2805.
115. Sokol S, Riggs LA. Electrical and psychophysical responses of the human visual system to periodic variation of luminance. *Invest Ophthalmol* 1971;10:171-180.
116. Bourne MC, Campbell, D.A., & Tansley, K. Hereditary degenerations of the rat retina. *British Journal of Ophthalmology* 1938;22:608-612.
117. Herron WL, Riegel BW, Myers OE, Rubin ML. Retinal dystrophy in the rat—a pigment epithelial disease. *Invest Ophthalmol* 1969;8:595-604.
118. Mullen RJ, LaVail MM. Inherited retinal dystrophy: primary defect in pigment epithelium determined with experimental rat chimeras. *Science* 1976;192:799-801.
119. Bok D, Hall MO. The role of the pigment epithelium in the etiology of inherited retinal dystrophy in the rat. *J Cell Biol* 1971;49:664-682.
120. LaVail MM, Sidman RL, O'Neil D. Photoreceptor-pigment epithelial cell relationships in rats with inherited retinal degeneration. Radioautographic and electron microscope evidence for a dual source of extra lamellar material. *J Cell Biol* 1972;53:185-209.

121. Dowling JE, Sidman RL. Inherited retinal dystrophy in the rat. *J Cell Biol* 1962;14:73-109.
122. Tso MO, Zhang C, Abler AS, et al. Apoptosis leads to photoreceptor degeneration in inherited retinal dystrophy of RCS rats. *Invest Ophthalmol Vis Sci* 1994;35:2693-2699.
123. Katai N, Kikuchi T, Shibuki H, et al. Caspase-like proteases activated in apoptotic photoreceptors of Royal College of Surgeons rats. *Invest Ophthalmol Vis Sci* 1999;40:1802-1807.
124. Perche O, Doly M, Ranchon-Cole I. Transient protective effect of caspase inhibitors in RCS rat. *Exp Eye Res* 2008;86:519-527.
125. Sheedlo HJ, Srinivasan B, Brun-Zinkernagel AM, et al. Expression of p75(NTR) in photoreceptor cells of dystrophic rat retinas. *Brain Res Mol Brain Res* 2002;103:71-79.
126. LaVail MM, Pinto LH, Yasumura D. The interphotoreceptor matrix in rats with inherited retinal dystrophy. *Invest Ophthalmol Vis Sci* 1981;21:658-668.
127. Herron WL, Jr., Riegel BW, Brennan E, Rubin ML. Retinal dystrophy in the pigmented rat. *Invest Ophthalmol* 1974;13:87-94.
128. Valter K, Maslim J, Bowers F, Stone J. Photoreceptor dystrophy in the RCS rat: roles of oxygen, debris, and bFGF. *Invest Ophthalmol Vis Sci* 1998;39:2427-2442.
129. D'Cruz PM, Yasumura D, Weir J, et al. Mutation of the receptor tyrosine kinase gene *Mertk* in the retinal dystrophic RCS rat. *Hum Mol Genet* 2000;9:645-651.
130. Nandrot E, Dufour EM, Provost AC, et al. Homozygous deletion in the coding sequence of the *c-mer* gene in RCS rats unravels general mechanisms of physiological cell adhesion and apoptosis. *Neurobiol Dis* 2000;7:586-599.
131. Hall MO, Prieto AL, Obin MS, et al. Outer segment phagocytosis by cultured retinal pigment epithelial cells requires Gas6. *Exp Eye Res* 2001;73:509-520.

132. LaVail MM. Analysis of neurological mutants with inherited retinal degeneration. Friedenwald lecture. *Invest Ophthalmol Vis Sci* 1981;21:638-657.
133. Noell WK. Cellular Physiology of the Retina. *Journal of the Optical Society of America* 1963;53:36-48.
134. Bush RA, Hawks KW, Sieving PA. Preservation of inner retinal responses in the aged Royal College of Surgeons rat. Evidence against glutamate excitotoxicity in photoreceptor degeneration. *Invest Ophthalmol Vis Sci* 1995;36:2054-2062.
135. Kurylo DD, Hansen RM, Fulton AB. Dark adapted thresholds in young RCS rats. *Vision Res* 1991;31:637-642.
136. Birch DG, Hood DC, Nusinowitz S, Pepperberg DR. Abnormal activation and inactivation mechanisms of rod transduction in patients with autosomal dominant retinitis pigmentosa and the pro-23-his mutation. *Invest Ophthalmol Vis Sci* 1995;36:1603-1614.
137. Pinilla I, Lund RD, Sauve Y. Contribution of rod and cone pathways to the dark-adapted electroretinogram (ERG) b-wave following retinal degeneration in RCS rats. *Vision Res* 2004;44:2467-2474.
138. Pinilla I, Lund RD, Sauve Y. Cone function studied with flicker electroretinogram during progressive retinal degeneration in RCS rats. *Exp Eye Res* 2005;80:51-59.
139. LaVail MM, Sidman M, Rausin R, Sidman RL. Discrimination of light intensity by rats with inherited retinal degeneration: a behavioral and cytological study. *Vision Res* 1974;14:693-702.
140. Trejo LJ, Cicerone CM. Changes in visual sensitivity with age in rats with heredity retinal degeneration. *Vision Res* 1987;27:915-918.
141. Prusky GT, West PW, Douglas RM. Behavioral assessment of visual acuity in mice and rats. *Vision Res* 2000;40:2201-2209.
142. Masaki T, Nakajima S. Further evidence for conditioned taste aversion induced by forced swimming. *Physiol Behav* 2005;84:9-15.

143. DiLoreto DA, Jr., del Cerro C, Cox C, del Cerro M. Changes in visually guided behavior of Royal College of Surgeons rats as a function of age: a histologic, morphometric, and functional study. *Invest Ophthalmol Vis Sci* 1998;39:1058-1063.
144. Trejo LJ, Cicerone CM. Retinal sensitivity measured by the pupillary light reflex in RCS and albino rats. *Vision Res* 1982;22:1163-1171.
145. Hetherington L, Benn M, Coffey PJ, Lund RD. Sensory capacity of the royal college of surgeons rat. *Invest Ophthalmol Vis Sci* 2000;41:3979-3983.
146. Lawrence JM, Sauve Y, Keegan DJ, et al. Schwann cell grafting into the retina of the dystrophic RCS rat limits functional deterioration. Royal College of Surgeons. *Invest Ophthalmol Vis Sci* 2000;41:518-528.
147. McGill TJ, Douglas RM, Lund RD, Prusky GT. Quantification of spatial vision in the Royal College of Surgeons rat. *Invest Ophthalmol Vis Sci* 2004;45:932-936.
148. Reme C, Reinboth J, Clausen M, Hafezi F. Light damage revisited: converging evidence, diverging views? *Graefes Arch Clin Exp Ophthalmol* 1996;234:2-11.
149. Zigman S. Ocular light damage. *Photochem Photobiol* 1993;57:1060-1068.
150. Glickman RD. Phototoxicity to the retina: mechanisms of damage. *Int J Toxicol* 2002;21:473-490.
151. Wu J, Seregard S, Algvere PV. Photochemical damage of the retina. *Surv Ophthalmol* 2006;51:461-481.
152. Jones BW, Marc RE. Retinal remodeling during retinal degeneration. *Exp Eye Res* 2005;81:123-137.
153. Gorgels TG, van Norren D. Ultraviolet and green light cause different types of damage in rat retina. *Invest Ophthalmol Vis Sci* 1995;36:851-863.

154. Kremers JJ, van Norren D. Retinal damage in macaque after white light exposures lasting ten minutes to twelve hours. *Invest Ophthalmol Vis Sci* 1989;30:1032-1040.
155. Abramov I, Hainline L (eds). *Light and the Developing Visual System*. The Susceptible Visual Apparatus ed. Boca Raton: CRC Press, Inc; 1991:104-133.
156. Ham WT, Jr., Mueller HA. *The photopathology and nature of the blue light and near-UV retinal lesions produced by lasers and other optical sources*. New York: Plenum Press; 1989:191-246.
157. Ham WT, Jr., Ruffolo JJ, Jr., Mueller HA, Clarke AM, Moon ME. Histologic analysis of photochemical lesions produced in rhesus retina by short-wave-length light. *Invest Ophthalmol Vis Sci* 1978;17:1029-1035.
158. Noell WK, Walker VS, Kang BS, Berman S. Retinal damage by light in rats. *Invest Ophthalmol* 1966;5:450-473.
159. Noell WK. *Different Kinds of Retinal Light Damage in the Retina*. New York: Plenum Press; 1980:3-29.
160. Williams TP, Howell WL. Action spectrum of retinal light-damage in albino rats. *Invest Ophthalmol Vis Sci* 1983;24:285-287.
161. Grimm C, Wenzel A, Hafezi F, Yu S, Redmond TM, Reme CE. Protection of Rpe65-deficient mice identifies rhodopsin as a mediator of light-induced retinal degeneration. *Nat Genet* 2000;25:63-66.
162. Rapp LM, Williams TP. Damage to the albino rat retina produced by low intensity light. *Photochem Photobiol* 1979;29:731-733.
163. Seiler MJ, Liu OL, Cooper NG, Callahan TL, Petry HM, Aramant RB. Selective photoreceptor damage in albino rats using continuous blue light. A protocol useful for retinal degeneration and transplantation research. *Graefes Arch Clin Exp Ophthalmol* 2000;238:599-607.
164. Ballowitz L. Effects of blue and white light on infant (Gunn) rats and on lactating mother rats. Report 2. *Biol Neonate* 1971;19:409-425.

165. O'Steen WK, Anderson KV, Shear CR. Photoreceptor degeneration in albino rats: dependency on age. *Invest Ophthalmol* 1974;13:334-339.
166. Noell WK. Effects of environmental lighting and dietary vitamin A on the vulnerability of the retina to light damage. *Photochem Photobiol* 1979;29:717-723.
167. Penn JS, Naash MI, Anderson RE. Effect of light history on retinal antioxidants and light damage susceptibility in the rat. *Exp Eye Res* 1987;44:779-788.
168. Bennett MH, Dyer RF, Dunn JD. Light induced retinal degeneration: effect upon light-dark discrimination. *Exp Neurol* 1972;34:434-445.
169. Bennett MH, Dyer RF, Dunn JD. Visual dysfunction after long-term continuous light exposure. *Exp Neurol* 1973;40:652-660.
170. Bennett MH, Dyer RF, Dunn JD. Visual-deficit following long-term continuous light exposure. *Exp Neurol* 1973;38:80-89.
171. Anderson KV, O'Steen WK. Black-white and pattern discrimination in rats without photoreceptors. *Exp Neurol* 1972;34:446-454.
172. O'Steen WK, Anderson KV. Photically evoked responses in the visual system of rats exposed to continuous light. *Exp Neurol* 1971;30:525-534.
173. La Vail MM. Survival of some photoreceptor cells in albino rats following long-term exposure to continuous light. *Invest Ophthalmol* 1976;15:64-70.
174. Cicerone CM. Cones survive rods in the light-damaged eye of the albino rat. *Science* 1976;194:1183-1185.
175. Marshall J, Mellerio J, Palmer DA. Damage to pigeon retinae by commercial light sources operating at moderate levels. *Vision Res* 1971;11:1198-1199.
176. Marshall J, Mellerio J, Palmer DA. Damage to pigeon retinae by moderate illumination from fluorescent lamps. *Exp Eye Res* 1972;14:164-169.

177. Lawwill T, Crockett S, Currier G. Retinal damage secondary to chronic light exposure, thresholds and mechanisms. *Doc Ophthalmol* 1977;44:379-402.
178. Sykes SM, Robison WG, Jr., Waxler M, Kuwabara T. Damage to the monkey retina by broad-spectrum fluorescent light. *Invest Ophthalmol Vis Sci* 1981;20:425-434.
179. Williams RA, Pollitz CH, Smith JC, Williams TP. Flicker detection in the albino rat following light-induced retinal damage. *Physiol Behav* 1985;34:259-266.
180. Sugawara T, Sieving PA, Bush RA. Quantitative relationship of the scotopic and photopic ERG to photoreceptor cell loss in light damaged rats. *Exp Eye Res* 2000;70:693-705.
181. Birch DG, Jacobs GH. Light-induced damage to photopic and scotopic mechanisms in the rat depends on rearing conditions. *Exp Neurol* 1980;68:269-283.
182. Donning our fancy coats. *Nat Genet* 2005;37:1173.
183. Huttli S, Michalakis S, Seeliger M, et al. Impaired channel targeting and retinal degeneration in mice lacking the cyclic nucleotide-gated channel subunit CNGB1. *J Neurosci* 2005;25:130-138.
184. Zhang YP, SJ. Generation and Transcriptional Analysis of a Cngb1 Knockout Mouse. *ARVO: Invest Ophthalmol Vis Sci*; 2004.
185. Pittler S, Molday L, Molday R, Kraft T, Zhang Y. Structural and Functional Abnormalities Caused by Absence of Retinal Cngb1 Gene products. *ARVO: Invest Ophthalmol Vis Sci*; 2004.
186. Zhang Y, Molday LL, Molday RS, et al. Knockout of cGMP-gated channel b-subunit and GARPs disrupts disk morphogenesis and rod outer segment structural integrity. *Journal of Cell Science* 2009;122.
187. Zheng J, Trudeau MC, Zagotta WN. Rod cyclic nucleotide-gated channels have a stoichiometry of three CNGA1 subunits and one CNGB1 subunit. *Neuron* 2002;36:891-896.

188. Ardell MD, Bedsole DL, Schoborg RV, Pittler SJ. Genomic organization of the human rod photoreceptor cGMP-gated cation channel beta-subunit gene. *Gene* 2000;245:311-318.
189. Korschen HG, Illing M, Seifert R, et al. A 240 kDa protein represents the complete beta subunit of the cyclic nucleotide-gated channel from rod photoreceptor. *Neuron* 1995;15:627-636.
190. Sarfare S, Pittler SJ. Focus on molecules: rod photoreceptor cGMP-gated cation channel. *Exp Eye Res* 2007;85:173-174.
191. Pentia DC, Hosier S, Cote RH. The glutamic acid-rich protein-2 (GARP2) is a high affinity rod photoreceptor phosphodiesterase (PDE6)-binding protein that modulates its catalytic properties. *J Biol Chem* 2006;281:5500-5505.
192. Poetsch A, Molday LL, Molday RS. The cGMP-gated channel and related glutamic acid-rich proteins interact with peripherin-2 at the rim region of rod photoreceptor disc membranes. *J Biol Chem* 2001;276:48009-48016.
193. Rubin GR, Kraft TW. Flicker assessment of rod and cone function in a model of retinal degeneration. *Doc Ophthalmol* 2007;115:165-172.
194. Pinilla I, Lund RD, Sauve Y. Enhanced cone dysfunction in rats homozygous for the P23H rhodopsin mutation. *Neurosci Lett* 2005;382:16-21.
195. Zhang Y. **Characterization of a rod photoreceptor cGMP-gated cation channel beta-subunit knockout mouse.** *Vision Sciences*. Birmingham: University of Alabama at Birmingham; 2005.
196. Toda K, Bush RA, Humphries P, Sieving PA. The electroretinogram of the rhodopsin knockout mouse. *Vis Neurosci* 1999;16:391-398.
197. Zhang Y, Molday LL, Molday RS, et al. Knockout of cGMP-gated channel b-subunit and GARPs disrupts disk morphogenesis and rod outer segment structural integrity. *Journal of Cell Science* 2008.
198. Tanito M, Kaidzu S, Anderson RE. Delayed loss of cone and remaining rod photoreceptor cells due to impairment of choroidal circulation after acute light exposure in rats. *Invest Ophthalmol Vis Sci* 2007;48:1864-1872.

199. Specht S, Organisciak DT, Darrow RM, Leffak M. Continuing damage to rat retinal DNA during darkness following light exposure. *Photochem Photobiol* 2000;71:559-566.
200. Delmelle M, Noell WK, Organisciak DT. Hereditary retinal dystrophy in the rat: rhodopsin, retinol, vitamin A deficiency. *Exp Eye Res* 1975;21:369-380.
201. Hafezi F, Steinbach JP, Marti A, et al. The absence of c-fos prevents light-induced apoptotic cell death of photoreceptors in retinal degeneration in vivo. *Nat Med* 1997;3:346-349.
202. Noell WK, Organisciak DT, Ando H, Branietcki MA, Durlin C. Ascorbate and dietary protective mechanisms in retinal light damage of rats: electrophysiological, histological and DNA measurements. *Prog Clin Biol Res* 1987;247:469-483.
203. Burkhardt DA, Fahey PK. Contrast enhancement and distributed encoding by bipolar cells in the retina. *J Neurophysiol* 1998;80:1070-1081.
204. Cuenca N, Pinilla I, Sauve Y, Lund R. Early changes in synaptic connectivity following progressive photoreceptor degeneration in RCS rats. *Eur J Neurosci* 2005;22:1057-1072.
205. Liets LC, Eliasieh K, van der List DA, Chalupa LM. Dendrites of rod bipolar cells sprout in normal aging retina. *Proc Natl Acad Sci U S A* 2006;103:12156-12160.
206. Schremser JL, Williams TP. Rod outer segment (ROS) renewal as a mechanism for adaptation to a new intensity environment. I. Rhodopsin levels and ROS length. *Exp Eye Res* 1995;61:17-23.
207. Van Der Tweel L. Relation between psychophysics and electrophysiology of flicker. *Documenta ophthalmologica* 1964;18:287-304.

APPENDIX A
PERMISSION LETTERS

Figure 1

Re: image use
Anne Hanson [afhanson@spflrc.com]
Sent: Tuesday, February 24, 2009 12:08 PM
To:
Glen R Rubin
Attachments:
Dear Glen,

You have my permission to use my figure of a rat's eye for your PhD thesis.

Best,

Anne Hanson

Figure 3

Thank you for your Rightslink / Elsevier order
donotreply@copyright.com [donotreply@copyright.com]

This message was sent with High importance.

Sent: Tuesday, February 24, 2009 2:19 PM

To:

Glen R Rubin

Attachments:

Thank you for placing your order through Copyright Clearance Center's Rightslink service. Elsevier has partnered with Rightslink to license its content online. Note: Payee for this order is Copyright Clearance Center.

Your order details and publisher terms and conditions (including any credit line requirements) are available by clicking the link below:

http://s100.copyright.com/CustomerAdmin/PLF.jsp?IID=2009021_1235506741293

Order Details

Licensee: Glen R Rubin

License Date: Feb 24, 2009

License Number: 2135501141293

Publication: Experimental Eye Research

Title: Focus on Molecules: Rod photoreceptor cGMP-gated cation channel

Type Of Use: Thesis / Dissertation

Total: 0.00 USD

To access your account, please visit <https://myaccount.copyright.com>. Please note: Credit cards payments are charged immediately after order confirmation. Invoice payments are billed twice monthly.

Please take a moment to complete our customer satisfaction survey.

<http://www.surveymonkey.com/s.asp?u=500021004336>

If you have any comments or questions, please contact Rightslink:

Copyright Clearance Center

Rightslink

Tel (toll free): +1-877-622-5543

Tel: +1-978-646-2777

E-mail: <mailto:customercare@copyright.com>

Web: <http://www.copyright.com>

B.1:v4.2

Figure 4

Penny Ripka

From: Glen R Rubin [gimalive@uab.edu]
Sent: Tuesday, February 24, 2009 2:11 PM
To: Penny Ripka
Subject: dissertation image permission

Can I have permission to adapt fig1 from The Retinal Pigment Epithelium in Visual Function by Olaf Straussthe for my PhD disseration? Fast reply would be appreciated...thanks!!!

Glen Rubin

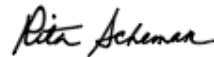
Journal info:
Physiol. Rev. 85: 845-881, 2005; doi:10.1152/physrev.00021.2004
0031-9333/05 \$18.00

<http://physrev.physiology.org/cgi/content/full/85/3/845>

APPROVED
By prjka at 1:46 pm, Feb 26, 2009

THE AMERICAN PHYSIOLOGICAL SOCIETY
9650 Rockville Pike, Bethesda, MD 20814-3991

Permission is granted for use of the material specified above, provided the publication is credited as the source, including the words "used with permission."



Publications Manager & Executive Editor

Figure 6

Re: permission to use image
Olle Holm [olle.holm@elmat.lth.se]
Sent: Wednesday, February 04, 2009 3:14 PM
To:
Glen R Rubin
Attachments:
Glen, use it and refer to the article writer, olle

--

Olle Holm MD, PhD
Associate professor of Ophthalmology, Inst of Technology, Lund University
postal address: Mellanvangsv.9, S-223 55 Lund, Sweden
phone +46708138871, FAX +46462602850
<http://www.lyyn.com>

Figure 9

Re: image use
RUP Permissions Dept. [permiss@mail.rockefeller.edu]
Sent: Tuesday, February 17, 2009 4:54 PM
To:
Glen R Rubin
Attachments:
Glen,

This reuse will be fine. Please note, our preferred citation style:

© Hecht and Smith, 1936. Originally published in The Journal of General Physiology. 19: 979–991.

Best wishes with your dissertation. Please let me know if you have any questions.

Sincerely,
Suzanne O'Donnell
RUP Permissions Department

Figure 10

Thank you for your Rightslink / Elsevier order
donotreply@copyright.com [donotreply@copyright.com]

This message was sent with High importance.

Sent: Tuesday, February 24, 2009 2:19 PM

To:

Glen R Rubin

Attachments:

Thank you for placing your order through Copyright Clearance Center's Rightslink service. Elsevier has partnered with Rightslink to license its content online. Note: Payee for this order is Copyright Clearance Center.

Your order details and publisher terms and conditions (including any credit line requirements) are available by clicking the link below:

http://s100.copyright.com/CustomerAdmin/PLF.jsp?IID=2009021_1235506741293

Order Details

Licensee: Glen R Rubin

License Date: Feb 24, 2009

License Number: 2135501141293

Publication: Experimental Eye Research

Title: Focus on Molecules: Rod photoreceptor cGMP-gated cation channel

Type Of Use: Thesis / Dissertation

Total: 0.00 USD

To access your account, please visit <https://myaccount.copyright.com>. Please note: Credit cards payments are charged immediately after order confirmation. Invoice payments are billed twice monthly.

Please take a moment to complete our customer satisfaction survey.

<http://www.surveymonkey.com/s.asp?u=500021004336>

If you have any comments or questions, please contact Rightslink:

Copyright Clearance Center

Rightslink

Tel (toll free): +1-877-622-5543

Tel: +1-978-646-2777

E-mail: <mailto:customer care@copyright.com>

Web: <http://www.copyright.com>

B.1:v4.2

APPENDIX B

INSTITUTIONAL ANIMAL CARE AND USE COMMITTEE APPROVAL FORM



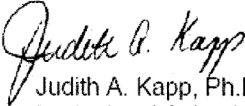
THE UNIVERSITY OF ALABAMA AT BIRMINGHAM

Institutional Animal Care and Use Committee (IACUC)

NOTICE OF APPROVAL

DATE: March 20, 2008

TO: Timothy Kraft, Ph.D.
 WORB 612 4390
 FAX: 934-5725

FROM: 
 Judith A. Kapp, Ph.D., Chair
 Institutional Animal Care and Use Committee

SUBJECT: Title: Studies of Retinal Electrophysiology
 Sponsor: Internal
 Animal Project Number: 080308096

On February 29, 2008, the University of Alabama at Birmingham Institutional Animal Care and Use Committee (IACUC) reviewed the animal use proposed in the above referenced application. It approved the use of the following species and numbers of animals:

Species	Use Category	Number in Category
Rats	A	90

Animal use is scheduled for review one year from March 2008. Approval from the IACUC must be obtained before implementing any changes or modifications in the approved animal use.

Please keep this record for your files, and forward the attached letter to the appropriate granting agency.

Refer to Animal Protocol Number (APN) 080308096 when ordering animals or in any correspondence with the IACUC or Animal Resources Program (ARP) offices regarding this study. If you have concerns or questions regarding this notice, please call the IACUC office at 934-7692.

Institutional Animal Care and Use Committee B10 Volker Hall 1670 University Boulevard 205.934.7692 FAX 205.934.1188	Mailing Address: VH B10 1530 3RD AVE S BIRMINGHAM AL 35294-0019
--	--